Republic of Iraq
Ministry of Higher Education
& Scientific Research
University of Kerbala
College of Science
Department of Physics

Theoretical investigation of electronic structure properties of doped zinc oxide nanosheet

A Thesis submitted to the College of Science University of Kerbala in Partial Fulfillment of Requirement for the Degree of Master of Science in Physics

By

Haneen Ali Rashed Alnasrawi

B.Sc. in physics University of Babylon 2016

Supervised by

Assistance Prof. Dr. Nibras Mossa Umran

2019 A. D. 1440 H. D.

ذَٰلِكَ فَضْلُ اللَّهِ يُؤْتِيهِ مَن يَشَاءُ ۚ وَاللَّهُ ذُو الْفَضْلِ الْعَظِيمِ

صدق الله العلي العظيم

سورة الجمعة:(الآية 4)

Supervisors Certificate

We certify that this thesis, entitled (***Theoretical investigation of electronic structure properties of doped zinc oxide nanosheet)*** has been prepared under our supervision, by ***(Haneen Ali Rashed Alnasrawi)*** at College of Science, University of Kerbala as a partial fulfillment of the requirement for the degree of Master of Science in Physics.

Signature:
Name: Dr. Nibras Mossa Umran
Title: Assistance prof.
Date: / /2019

In view of the available recommendation, I forward this thesis for debate by the examination committee.

Signature:
Name: Dr. Rajaa A. Madlool
Title: Professor
Head of Physics Department /College of Science / University of Kerbala
Date: / / 2019

Dedication

To…

My lord…The Prophet of mercy and the light of the Worlds …Prophet Mohammad (Peace Be Upon Him)… and AhlulBayt (Peace Be Upon Them) …

And to My Father the secret of my success and My Beloved Mother who paved the way for me to achieve my goal. And to all who stood by my side and supported me.

Haneen Ali

Acknowledgment

First and foremost, I thank Allah Almighty for providing me with the opportunity to reach this goal.

I would like to thank Dr. Nibras Mossa Umran for suggesting the topic of the thesis and for his endless guidance, support, motivation, encouragement and patient help during my study and you have given enough freedom during my research to encourage me becoming an independent thinker.

I would like to express my gratitude to all my professors at the Faculty of Science for their help. I want to thank all my friends especially Heba, Sara and Furqan for helping me through the difficult times, camaraderie, support and for all the encouragement. I owe my sincere gratitude to Dr. Adnan H. Al-Aarajiy and Dr. Hikmat Adnan, for his valuable advice and friendly help.

I am thankful to the Dean of the chairman Department of Physics and the College of Science for their help.

Last but not least, I would like to express my deepest appreciation to my parents, all my current and former colleagues, and my family for their patience and support.

Haneen Ali

Abstract

The thesis describes the structural and electronic properties of the ZnO nanosheet doped with B, C, N, Al, Si and P has been investigated by performing density functional theory calculations. The aim of this study is to identify the effects of substituting from one to six atoms of oxygen with different impurities in super cell of the ZnO nanosheet composed of 84 host atoms by taking into account the impurities sites and its effects on the structural and electronic properties of ZnONSs using SIESTA program. The electronic properties can be controlled certainly a most significant step in the development of electronic devices by doping. All systems under consideration have been fully optimized. bond length, and bond angle, binding energy/dopant atom, total and projected density of state, the total energy, electronic states, energy gap, some electronic variables (vertical ionization potential (VIP), vertical electron affinity (VAE), electronegativity (EN) and hardness (H)) have been calculated and compared with each other. The results show that B and P atom substitution expands the bond length with respect to pristine ZnONSs. Therefore, this density functional investigation shows that the high stability of ZnO nanosheet can be achieved for both dopants depending on the designed growth condition and type dopant. The configuration of B and Al atoms replacing O atoms is more stable than other doped. The HOMO and LUMO are slightly different and this suggests that according to the number, type and position dopant in structure play significant roles on electronic properties and improving the electron accepting ability. It has been found that the energy gap of ZnO nanosheets decreases gradually along with (B, C, N, Al, Si and P) ions. B_2 and C_2, N_3 and P_3, Al_4 and Si_4 occupying O sites as compound have energy gaps for

conductor materials. These results are potentially useful for spintronic applications. The results showed that, vertical ionization potential and vertical electron affinity for B and Al doping and has donor level at 3.3eV. On the other hand, for the N and P doped ZnO nanosheet has acceptor level at 4.0eV. The electronegativity increased for N and P doped and hardness decreased for B, C and Al doped that is shown more energetic favorable.

Table of Contents

CHAPTER 3: RESULTS AND DISCUSSION

CHAPTER 4: CONCLUSION

List of Figures

List of Tables

List of symbols and Abbreviations

χ_i	Basis function of each one-electron molecular orbital
BE	Binding energy
$\hat{V}_T$	Coulomb interaction
$v_{eff}(r)$	Effective potential
n(r)	Electron density
EN	Electronegativity
$\hat{T}_e$	Electronic kinetic energy operator
$E_{XC}[n(r)]$	Exchange-correlation energy
$V_{XC}[n(r)]$	Exchange-correlation potential
GGA	Generalized Gradient Approximation
H	Hamiltonian operator
H	Hardness
HOMO	Highest Occupied Molecular Orbital
LDA	Local density approximation
LUMO	Lowest Unoccupied Molecular Orbital
$\|\Psi_e\rangle$	N-electron ground state wavefunction
N	Normalization factor
$\hat{T}_n$	Nuclear kinetic energy operator
SIESTA	Spanish Initiative for Electronic Simulation with Thousands of Atoms
$\hat{V}_{n-e}$	The attractive interactions operator between nuclei and electrons

$E_X[n(r)]$	The Dirac exchange
$r_i r_j$	The distance between electrons i and j
$r_i R_\alpha$	The distance between nucleus α and electron i
$n(r)$	The electronic density of the system
$\varepsilon_{XC}[n(r)]$	The exchange –correlation energy per electron
$\mathrm{E_{XC}}[\mathrm{n}\uparrow, \mathrm{n}\downarrow]$	The exchange-correlation energy for the system with the two spin-densities
$V_{XC}(r)$	The exchange-correlation potential
$\hat{V}$,$V_{en}(r)$	The external potential
$V_H(r)$	The Hartree-potential
$\hat{U}_{ee}$	The interaction internal potential
$T[n(r)]$	The kinetic energy of non-interacting electrons system
M_α	The mass of atom α
$Z_\alpha Z_\beta$	The nucleic charge of atoms α and β
$\hat{V}_{e-e}$	The repulsive electron-electron interactions
$\hat{V}_{n-n}$	The repulsive interactions operator between the nuclei
$U_{ee}[n(r)]$	The term of electron-electron interaction
$\mathrm{E_{total}}$	Total energy
$E[\tilde{n}]$	Total energy functional
$\hat{H}$	Total Hamiltonian of the molecular system
$\hat{T}_T$	Total kinetic energy
VEA	Vertical electron affinity
VIP	Vertical ionization potential
ψ	Wavefunction

CHAPTER 1: INTRODUCTION AND LETERATURE REVIEW

1.1 Crystal structure of zinc oxide (ZnO)

The crystal structure of Zinc oxide consists of three types are wurtzite, zinc blende, and rock salt, as shown in (Figure 1.1). Among them, wurtzite structure is the most common ZnO phase at ambient pressure and temperature. Zincblende ZnO is stable only by growth on cubic structures. Rocksalt structure is a high-pressure metastable phase forming at ~10 GPa, and cannot be epitaxial stabilized[1]. The natural crystal structure of ZnO is the hexagonal wurtzite structure. Zn and O atoms are arranged into a hexagonal crystal structure with interpenetrating lattices where each Zn ion is surrounded by tetrahedral of O ions, and vice-versa[2]. The lattice parameters of the hexagonal unit cell measured by x-ray diffraction method under ambient conditions are a= 3.2495Å, c= 5.2069Å, the axial ratio c/a is 1.603, and the density is 5.605g/cm^3 [2-4]. The tetrahedral coordination between Zn^{+2} and O^{-2} ions is responsible for polar symmetry along the hexagonal axis. This polar structure is the reason behind numerous properties of ZnO, including its piezoelectricity and spontaneous polarization, and is also a vital feature in crystal growth, etching and defect generation. The Zn-O bond also has very strong ionic character, and consequently ZnO lies on the borderline between being classed as a covalent and ionic compound, with an ionicity of f_i =0.616 on the Phillips ionicity scale[5]. The four most common face terminations of wurtzite ZnO are the polar Zn terminated (0001) and O terminated $(000\bar{1})$ faces (c-axis oriented), and the nonpolar $(11\bar{2}0)$ (a-axis) and $(10\bar{1}0)$ faces[6]. These polar faces are known to possess slightly different Physical and chemical properties.

Most frequently, oppositely charged ions produce positively charged (0001)-Zn and negatively charged$(000\bar{1})$-O polar surfaces bring about a normal dipole moment and spontaneous polarization along the c-axis, along with a divergence in surface energy[7]. Thus while growth of ZnO, the structure grow in such a way that it tends to minimize the surface energy which leads to formation of diverse nanostructures. All the ZnO nanostructures synthesized in the present work demonstrate hexagonal wurtzite crystal structures.

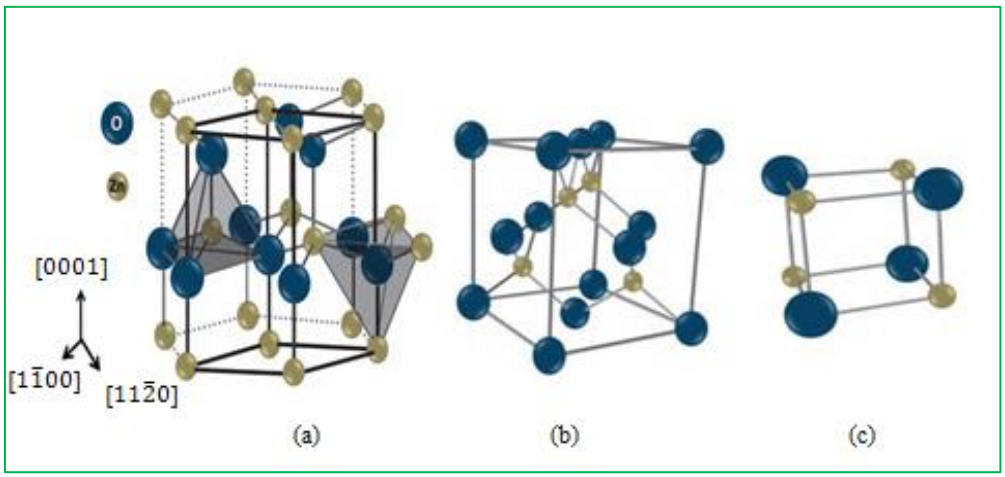

Figure 1.1:Unit cells of (a) hexagonal wurtzite, (b) zinc blend and (c) rocksalt phase of ZnO[6].

1.2 Electronic structure of ZnO

The ZnO binding in its crystal lattice involves sp^3 hybridization of the electron states, resulting in four equivalent orbitals. In the resulting ZnO crystal, the bonding sp^3 states create the valence band, while its antibonding states constitute the conduction band. The resulting energy gap is 3.37 eV [8, 9], which lies in the UV spectral range. Due to its wide band gap, pure ZnO is transparent in the visible region. Moreover, a large band gap results in higher breakdown voltages, electronic stability, lesser electronic noise and high power operation.

ZnO possesses a high exciton binding energy of ~60 meV[9]. Due to the native defects such as oxygen vacancies and zinc interstitials, ZnO naturally exhibits n-type semiconductor behavior. P-type doping of ZnO is still a problem that is hindering the possibility of a ZnO p-n homojunction devices. The electronic band structure of ZnO has been calculated by many groups [10, 11]. The band structure has been evaluated using the local density approximation (LDA) and incorporating atomic "self-interaction-corrected pseudo-potentials" (SIC-PP) to accurately account for the Zn 3d electrons, as shown in Figure 1.2 [12].

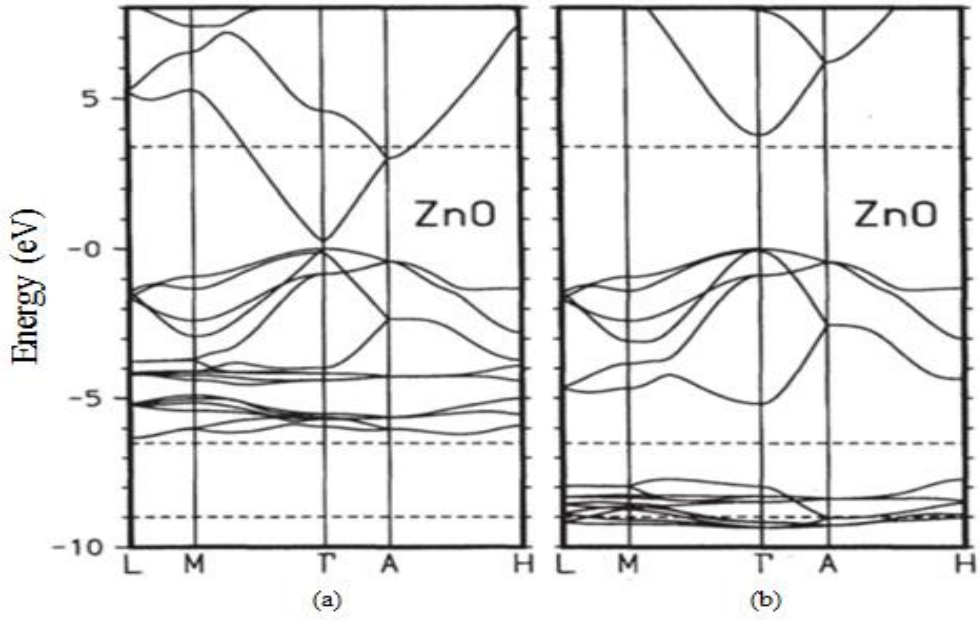

Figure 1.2:The LDA bond structure of bulk wurtzite ZnO calculated by using (a) a standard pseudopotential, and (b) SIC-PP[12].

Both the valence band maxima and the lowest conduction band minima occur at the Γ point k=0 indicating direct band gap nature of ZnO. The bottom 10 bands (occurring around -9 eV) are related to Zn 3d levels. Whereas, there are no bands in the bottom of the left panel of Figure(1.2) which is evaluated from conventional LDA method that does not account for the effect of Zn 3d levels. The next 6 bands from -5 eV to 0 eV correspond to O 2p bonding states[12, 13].

In SIC-PP incorporated LDA approximation, the bands are shifted down in energy noticeably and the band gap opening is clearly visible, as "modified LDA" method is 3.37 eV, which is in much better agreement with the experimentally evaluated value of 3.37 eV[12].

1.3 Physical properties of zinc oxide

Table 1.1 shows some of the basic physical parameters for wurtzite ZnO. However, investigation of the properties of individual ZnO nanostructures is essential for developing their nanoscale devices.

Table 1.1: Some basic physical parameters for ZnO[1, 5, 13].

Crystal structure (stable phase at 300 K)	Wurtzite (Hexagonal)
Energy gap	3.37eV. Direct
Lattice constants (T=300K)	a=3.2469Å, c=5.2069Å
Exciton Binding Energy	60meV
Electron effective mass	0.24
Refractive index	2.004
Electron mobility (at 300K)	200cm^2/V.sec.
Density	5.67g/cm^3
Relative dielectric constant	8.66
Melting point	2248K
Hole mobility (at 300K)	5-50 cm^2/V.sec.
Intrinsic carrier concentration	$<10^6$ /cm^{-3}
Ionicity	62%
Hole effective mass	0.59

1.4 Doping of zinc oxide

Doping means the introduction of impurities intentionally in a pure semiconductor. Chemical doping is the most widely used and most useful technique in terms of band gap engineering. It can be done in two ways: (i) by introducing foreign atoms or molecules on the surface of graphene which is called adsorption (ii) by replacing the Zn or O atoms of ZnO lattice by other atoms which is referred to as substitution and is most popular method to introduce a band gap in ZnO nanosheet without altering its structural properties drastically. Substitution doping is the primary method used in doping conventional semiconductors[14]. The main focus of ZnO is still on its optical and electrical properties. The dopant elements are introduced according to their effects on electrical properties in the following sections. Undoped ZnO shows intrinsic n-type conductivity, ZnO doped with group-III B, Al, Ga and In elements[15, 16]show n-type conductivity while Group V elements, N, P, As and Sb, are important for the realization of p-type ZnO. Al-doped ZnO nanostructure by substituting for Zn sites in the ZnO lattice, it turns out that a dopant working to increase conductivity of the material and get highly conductive transparent oxide[17]. Theoretically, B doped ZnO investigate the influence of intrinsic defects on the formation energy, crystal structure, electronic structure, and optical properties of BZO. Our results revealed that the formation energy of V_{Zn} is lowest under O-rich conditions and the formation energy of V_O is lowest under O-poor conditions. V_{Zn} defects in BZO may decrease carrier concentration as well as mobility, which increases transmittance in the visible light region but decreases transmittance in the UV region. V_O or Zn_i defects in BZO lead to the appearance of n-type conductive characteristics، increasing the optical band gap, and decreasing transmittance in the visible light

and UV regions. In addition, Zn_i defects increase the effective mass, which may consequently decrease the mobility and conductivity of BZO[18]. ZnO monolayer doped with Al, Ga and In observed that the band gap increases using higher than 12.5 wt% Al and Ga doping concentrations compared to the pristine ZnO monolayer. The absorption edge has a clear blue-shift to a shorter wavelength region with increasing doping concentrations after Al, Ga and In doping. When ZnO monolayer is doped with Al، Ga and In concentrations less than 12.5 wt% the average transmittance found reaches up 99% in the visible and UV regions. For the 18.75 wt% In doping concentration the average transmittance is around 99% in the visible and UV regions and above 95% in the IR region. As for the electrical conductivity a higher of the In doped ZnO monolayer in comparison with the ZnO monolayer doped with Al or Ga at 6.25 wt %[19, 20].When N doped ZnO nanosheets, it was observed that there is an automatic spontaneous polarization of N 2p state with a magnetic moment 1.0 μB/N, this electromagnetic coupling can be attributed to a strong p-d interaction between nitrogen and zinc atoms[21].The doped As tends to go on the Zn site found that a complex, As_{Zn}-$2V_{Zn}$, has a rather low formation energy to act as the acceptors in ZnO[22]. By using density functional theory (DFT), C, N, F and P atom doped of ZnO sheets. P atom substitution expands the bond length with respect to ZnO sheets and it is exothermic whereas C, N, and F atom doping is endothermic[23]. The binding energies of B_{Zn} and P_O codoped ZnO are more stable whereas the energy levels of some impurity appear above the valence band maximum, and that a pronounced absorption in low energy range[24].In addition, after doped ZnO nanowires with In are evolved into nanobelts[25]. Therefore, doping has taken a great path to change the microstructures and practical performance of ZnO.

1.5 Nanotechnology and nanomaterials

1.5.1 Nanotechnology and application

Nanotechnology is the creation and exploitation of nanomaterials with structural features in between those of atoms and their bulk materials. In order words, nanotechnology is a technology of design and applications of nanoscale materials with their fundamentally new properties and functions. When the dimensions of materials are in nanoscales the properties of the materials are significantly different from those of atoms as well as those of bulk materials. Moreover, when the size of materials is in the nanoscale regime the large surface area to volume ratio exhibited by nanomaterials, improves the high surface reactivity with the surrounding surface, which makes nanomaterials ideally suitable candidates for many types of sensor applications. Therefore, nanomaterials has opened up possibilities for new innovative functional devices and technologies[26]. The importance of nanotechnology was pointed out by Richard Feynman in his delivered lecture at an international forum in the meeting of the American Physical Society at California Institute of Technology (CalTech) entitled "There is plenty of room at the bottom"[27]. Currently, nanotechnology has been recognized as a revolutionary field of science and technology and has been applied in many applications, including environmental applications, medical applications, biomedical applications, healthcare and life sciences, agricultures, food safety, security, energy production and conversion applications, energy storage, consumer goods, infrastructure, building and construction sector and aerospace[28-30]. Moreover, the new nanotechnology applications provide very fast response, low-cost, long-life time, easy to use for unskilled users, and high efficiency of devices and it also provides a new approach to diagnosis and treatment

of diseases, effective environmental monitoring and alternative ways for substantial energy development for a better world. We can say that, nanotechnology is applied almost in every aspect of our modern world. In this regard, the development of new methods to synthesize nanomaterials have paved the way in creating new opportunities for the development of innovative nanostructures based devices. In particular, the ability to synthesize nanostructures materials with controllable shape, size and structure and enhance the properties of nanomaterials provides excellent prospects for designing nanotechnology based devices.

1.5.2 Classification and synthesis of nanomaterials

Over decades, the ability to tune surface morphologies and the structure of semiconductor materials with near atomic scale has led to further idealization of semiconductor structures: quantum wells, wires, and dots. These nanostructures have completely different density of electronic states predicted by simple particle in a box type model of quantum mechanics. According to their basic dimensions (X, Y and Z) in space, nanostructures of nanomaterials can be classified into zero-dimension (0-D), one-dimension (1-D), two-dimension (2-D) and three-dimension (3-D). While 0-D nanostructures refer to quantum dots or nanoparticles, 1-D nanostructures refer to nanowires, nanorods, nanofibres, nanobelts, and nanotubes, 2-D nanomaterials represent for nanosheets, nanowalls and nanoplates and 3-D nanomaterials are nanoflowers and other complex structures such as nanotetrapods[31-34]. Due to the quantum effects dominating most of the properties of the nanomaterials, its density of states of the nanomaterials are quite different from those of the bulk materials. The density of states which

describes the electronic states versus energy in the band diagram of the 0-D, 1-D, 2-D and bulk materials are shown in Figure 1.3.

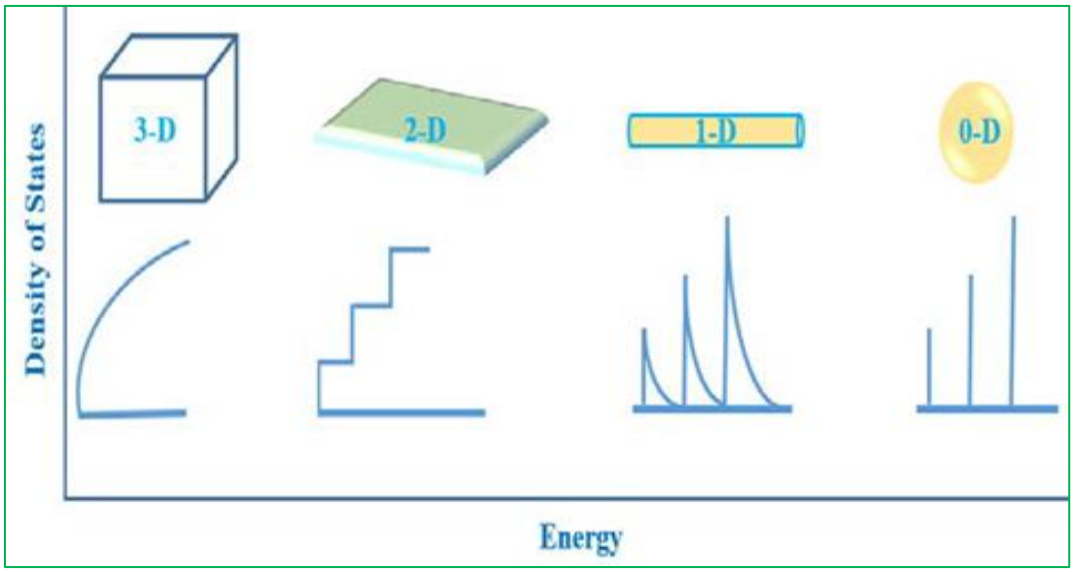

Figure 1.3:The electron density of states in bulk semiconductor and the electron density of states in quantum well (2-D), in quantum wire (1-D), and in quantum dot (0-D) nanomaterials (adopted from [31]).

Nanotechnology fields have extensive research focused on gaining control of particle size, shape and composition in different ways. However, syntheses of nanoscale materials are generally grouped into mainly two approaches: bottom-up and top-down approaches. The bottom up method is a method that builds nanomaterials from atomic or molecular precursors while top-down technique is a method that tearing down larger building blocks into finer pieces tills their constitution up to nanoscale level. The schematic diagram of these two approaches is presented in Figure 1. 4.

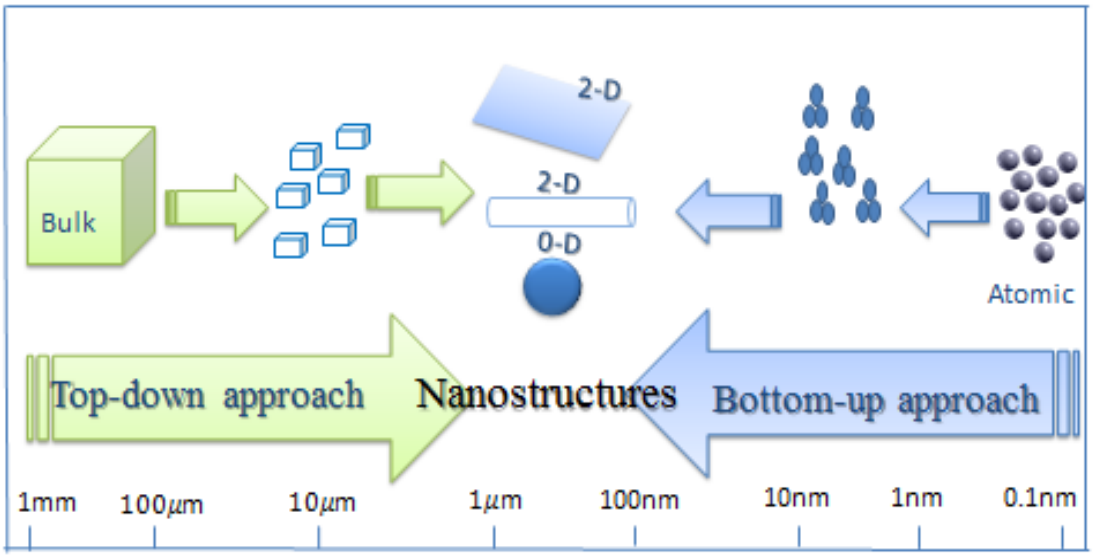

Figure 1. 4: Top-down and bottom-up approaches (adopted from [14]).

1.5.3 Two dimension nanosheet

Recently, in both experimental and theoretical areas had been explored different nanostructures such as nanosheets, nanowires and nanobelts due to their unique properties and novel applications[35, 36]. Among these nanostructures, two-dimensional systems show peculiar properties which are different from their bulk phases[37, 38].

A two-dimension material is defined as a material in which the bond strength and the atomic configuration along two dimensions and much stronger than along a third dimension[39]. by Sasaki et al. was first used name "nanosheets" on the two dimension to reflect the specific features of titanium oxide layers with a lateral size in the micrometer, a thickness of around ~1 nm and an extremely high 2D anisotropy[40]. Nanosheets in the ideal case consist of single monolayers, but they are often demonstrated as incompletely exfoliated flakes comprising a small number (<10) of stacked monolayers [41]. So, the planar ZnO monolayer can form a hexagonal honeycomb structure in which Zn and O atoms are arranged in planar 3-fold coordination. In addition to this will be for ZnO

monolayer more important advantages over graphene because of the large energy gap [42]. A number of groups have reported the synthesis of high-quality two-monolayer-thick ZnO (0001) nanosheet on Ag(111) substrate by pulsed laser deposition, had been experimentally achieved which provided a direct evidence for the presence of planar ZnO sheets[43]. Moreover, graphene structures of ZnO had been obtained which prepared on Pd(111)substrate[44]. In the bulk, hybridization is sp^3 while it is changed to sp^2 in the ZnO nanosheet structures, causing the valence and conduction bands to be near. Therefore, ZnO nanosheet can exhibit very different electronic properties, as compared with the bulks. Owing to the quantum confinement effect, chemically active exposed surface, high surface area, and confined thickness. It is expected that ZnO nanosheet attractive in a variety of applications from nanostructured electronic or photonic devices.

1.5.4 Application of ZnO nanosheet

Zinc oxide (ZnO) clearly distinguishes itself from other II-VI semiconductors. The rather unique characteristics, such as wide energy gap (~3.37eV), large exciton binding energy (60 meV), and extraordinary piezoelectric and optical properties[6], endow ZnO a wide range of technological applications in UV-light emitting diodes[45], solar cells[46], photocatalysts[47], etc. At the nanoscale, ZnO brings us more sweet surprises[48-50]. The versatile chemical bonding of ZnO leads to probably the richest family of nanostructures among all materials[5]; nanowires[51], nanotubes, nanobelts[52], nanorods[53], nanobridges/ nanonails[54], nanofilms[55] (14), and nanorings[56] have been successfully synthesized through a variety of experimental techniques. These low-dimensional structures have demonstrated

extraordinary electrical and optical performances compared with the bulk crystalline ZnO, and are promising candidates for many novel applications in transparent electronics، gas sensors, transducers, solar cells, and biomedical devices. This material is electrically very sensitive and exist n-type electrical conductivity hence used in vacuum fluorescent display and field emission display. By doping ZnO with suitable dopant, we can achieve p-type conductivity of the material. ZnO has large non-linear optical coefficient hence it is used in nonlinear optical devices. Highly sensitive and tunable electric conductivity make it suitable for transparent conductive oxide (TCO) application.

1.6 Literature review

C.W. Zhang, et al., in 2012[57] the electronic structure and magnetic properties have been investigated via first-principles calculations of the fully-hydrogenated ZnO nanosheet (ZnONSs) doped with B, C, N and F atoms using VASP package for the plane-wave basis set. When the dopant is replaced by O atoms, where they exhibited, that nonmagnetic states appears in case of n-type doping while p-type doping ZnONSs was exhibiting magnetic behaviors. The appearance doping of fully-hydrogenated ZnONSs related to Ferro-magnetism. As expected efficient route toward long-range ferromagnetism in 2D nanostructures.

F. Li, et al., in 2013[58]investigated the magnetic and optical properties of Cu-doped ZnO nanosheet by first-principles calculations based on DFT at the GGA+U level. Using the plane-wave pseudopotential method implemented VASP package, when two Zn atoms are substituted by two Cu dopants, they tend to form a cluster and ferromagnetic (FM) ordering becomes energetically more favorable. With increasing Cu

concentrations, both the imaginary part of dielectric function and the absorption spectrum exhibit a red-shift behavior.

X.Y. Feng, et al., in 2013[20]analyzed the changes in electronic and magnetic properties by doping of IIIA group (Al, Ga and In) atom to ZnONSs using the first-principles full-potential linearized augmented plane wave (FLAPW) method based on Density Functional Theory (DFT) with Generalized Gradient Approximation (GGA) as exchange-correlation in the WIEN2K package to calculated the formation energy, band gap, and magnetic for the configurations with IIIA ions replacing Zn atoms, that they are exhibited Al-ZnONSs is more stable than other doped, as well as band gap of ZnONSs increases gradually along with Al, Ga and In ions occupying Zn sites and O sites. The system shows half-metallic characteristics for Al, In-doped ZnONSs. Ga-doped ZnONSs shows metallic character with strong spin polarization.

J. Ren, et al., in 2013[59]investigated stable geometries, electronic structures and magnetic properties of the ZnONSs doped with 3d transition-metal (TM) (Sc, Ti, V, Cr, Mn, Fe, Co, Ni and Cu) atoms substituting the cation Zn have been investigated using first-principles pseudopotential plane wave method within DFT.

The results showed that the doping of Cr, Mn, Fe, Co, Ni and Cu atoms can induce magnetization, while no magnetism is observed when Sc, Ti and V atoms are doped into the ZnONSs. The formation energies calculated indicate that the doping is suitable, and the optimized structures show that TM atom substituting a Zn leads to a structural distortion around the TM impurity compared to the pure ZnONSs.

G. Qin, et al., in 2014[60] first-principles calculations based on DFT as implemented VASP package and the GGA are used with the projector-augmented plane wave potentials (PAW) studied the electronic and magnetic properties of ZnONSs with intrinsic defects. The results

showed that, the oxygen vacancy (V_O) of ZnONSs did not exhibit magnetism, while the ZnONSs with a single V_{Zn} was exhibiting the magnetic ground state that mainly originates from the unpaired O 2p electrons. Using the GGA and GGA+U calculated the spin-polarized of the perfect ZnONSs indicate is a kind of non-magnetic semiconductor and found band gap are 1.56 eV (GGA) and 2.4 eV (GGA + U).

Y.H. Zhang, et al., in 2014[61] studies the electronic and magnetic properties of g-ZnO upon chemical doping (with B, N and C) and CO adsorption by using first-principles calculations implemented in the(VASP)package. The g-ZnO with oxygen atom substituted by a C or N atom (one atom per supercell) are ferromagnetic (FM) half metal (HM), while that substituted by a B atom is an FM semiconductor. Furthermore, CO adsorption converts the N and C-doped g-ZnO to n-type semiconductor with nonmagnetic (NM) ground states, while B-doped g-ZnO becomes a ferromagnetic half metal (FM-HM).

H. Kökten and Ş. Erkoç, in 2015[23] studied the structural and electronic properties of doped ZnONSs by performing fully optimized first principles DFT calculations in the CRYSTAL03 package program. The substitution atom C, N, F and P atoms have been replaced on the O site in the neutral charge state and it repeated for different cell sizes. P atom substitution expanded the bond length with respect to pristine ZnONSs and C atom substitution yields relatively larger charge transfer from C to the lattice. The formation energies of C-doped are more stable of other dopant.

S. Datta, et al., in 2015[62] using DFT within pseudopotential plane wave method, as implemented in the VASP package performed electronic structure calculations to investigate the effects of morphological changes of the Bi-doped ZnO nanostructures with the impurity dopant atoms of the 3d late transition metals (Mn, Fe, Co, Ni

and Cu) on the magnetic properties and band gap variations of three different structures a 2D nanosheet, a 1D nanotube, and a finite cage-shaped nanocluster of the ZnO. The result showed, the pristine systems are nonmagnetic and the magnetic couplings in the most stable structures are mostly anti-ferromagnetic in case of doping in the sheet as well as cage morphologies, while the optimal ferromagnetic and anti-ferromagnetic couplings are almost degenerate for the Bi-doping in the tube morphology. Band gap shows overall a decreasing trend while moving along sheet → tube → cage structures.

D. Ma, et al., in 2015 [63] using first-principle investigated the electronic structure, structure stability, and catalytic of the Al-g-ZnO monolayer sheet. The substituted a Zn atom with an Al atom was highly exothermic and Al atoms can barrierlessly push out of Zn atoms and enter into the Zn sites. The Al-g-ZnO monolayer were promising materials for CO oxidation sensing at low temperature and also tune the electronic structure and chemical activity of the inert g-ZnO monolayer through sensing.

C. Tan, et al., in 2016 [64] by first-principles density functional theory based on the local density approximation plus Hubbard (LDA+U) approach, using CASTEP code investigated structure, electronic and optical properties of Cd-doped ZnO monolayer. Implying a stable substitution of Cd, the formation energy of the doped system is negative. The band gap of Cd-doped ZnONSs decrease with increasing Cd concentration which is attributed to the less ionic of the Cd-O bond. Cd doping ZnONSs produced a red shift of the absorption peaks, enhancing the visible light absorption.

D. Sun, et al., in 2017[19] using the first-principles calculation in combination with the Boltzmann transport theory investigated the electronic, optical, and electrical properties of ZnONSs doped with Al,

Ga and In. The calculations were performed with the CASTEP code 8.0, when one to three Zn atoms are replaced by Al, Ga and In atoms. Using high concentrations for Al and Ga doping the band gap increases compared to the pristine ZnONSs. When ZnONSs is doped with Al, the average transmittance reaches up 99% in the visible and UV regions. In addition, a higher electrical conductivity of the In doped ZnONSs in comparison with the ZnONSs doped with Al or Ga.

C. Supatutkul, et al., in 2017[65] the electrical and optical properties of these doping effects on ZnONSs were studied using Heyd-Scuseria-Ernzerhof (HSE) hybrid functional. The dopant ions were substituted on Zn sites in ZnONSs. The results showed that, for the p-type doping the Li-doped ZnONSs has the highest stability and the acceptor level exists under O-rich condition. While under O-poor condition, for the n-type doping, the Sn-doped ZnONSs is the highest stability and has the donor level occurs. Li-Ni co-doping ZnONSs did not stabilized.

S. A. Khan, et al., in 2017[66] using the first principle full-potential linear augmented plane wave (FP-LAPW) method, as implemented in WIEN2 K code, based on GGA for the exchange–correlation potential within the DFT were investigated the electronic structure and optical properties of Cd-doped ZnONSs. When replace one Zn atom in supercell by Cd exhibited a direct band gap of 1.5 eV compared to 1.7 eV of the pure ZnONSs. Due to effect of Cd doping and different contributions electronic transitions that occurred within ZnONS the absorption spectrum was found to be limited in energy region.

Z. Luan, et al., in 2017[67] by first principles density functional theory had been studied the effect of Be doping on the electronic structure and optical properties. Be doping increasing of band gap of ZnO monolayer compared with pristine ZnO monolayer. The negative formation energy of Be doping ZnO monolayer proposed. Imaginary parts of dielectric

function of Be doped ZnO monolayer stir toward bigger energy and the blue-shift of optical absorption edge was observed.

1.7 Aim of the Present Work

The aim of the present work is to investigate the structural and electronical properties of pure ZnO nanosheet. Doping is found to be an effective method to realize band gap engineering in ZnO. ZnO can be doped by many elements to meet the demands of different application. This work focuses on studying the effect of (B, C, N, Al, Si and P) substitutional doping in ZnO nanosheet on the structural and electronical properties using the density functional theory together with GGA.

1.8 Broad Outline of thesis

The thesis is divided into five chapters. Chapter one of the thesis contains introduction to the ZnO and their properties, information about the doped ZnO, and Literature review studies in this field of nanotechnology.

Chapter two of the thesis contains general discussion of the different methodologies, approximations and parameters used in simulations in context of the method used in present work. Density functional theory (DFT) based on *ab intio* have used for calculation. DFT is described in detail along with the brief detail of the SIESTA computational code.

Chapter three presents the results for pure and doped ZnO nanosheet studied. The optimized geometries of pure ZnO nanosheet and then studied their structure and electronic properties, and also by

considering different doping locations for the same concentration of dopants.

This Chapter consists of two groups, first group that we have presented the results for substitutional doping of (B, C and N) doping on structure and electronic properties of ZnO nanosheet are discussed. The obtained results are compared with pure ZnO nanosheet and other previous results. Second group, calculations regarding effects of individual (Al, Si and P) substituting doping on structure and electronic properties of ZnO nanosheet at varying concentrations are discussed.

Chapter five is a conclusion of the major findings in this study with some suggestions for the future research works.

CHAPTER 2: THEORETICAL METHODS

2.1 Introduction

The density functional theory is a standout amongst the most vital strategies in the quantum calculations of electronic structure of solids. It has likewise a wide use in the physics of dense issue and quantum chemistry. These theorists might manage the quantum mechanics strategies, which supplant the Hartree-Fock method. Llewellyn Thomas and Enrico Fermi have considered DFT as a created [68]. The genuine model depends on the contribution of Pierre Hohenberg, Walter Kohn and Lu Sham. This formalism is for the most part bound to model different systems with extended precision. The Hartree-Fock method shows a few issues calculation and requests a numerical exertion, particularly in the instance of transition metal materials including electronic correlations. This method constructs basically with respect to multi-electronic wavefunctions, while the DFT depends on the electron density, which supplanted the multi-electronic wavefunctions. This trademark is extremely valuable for calculations and modeling of different broad systems, including materials with rare earth elements. The DFT lessens the N-body system to another single or bi-body in the event that the spin problems consider. With quantum mechanics, the clarification of the many-body problem with interacting particles was the subject of a few inquiries about, especially with a correct depiction of the electronic structure of solids. The researchers have built up a few approaches for illuminating the Schrödinger equation for many-body problems which display challenges and have no systematic arrangements. In this part will talk about the methodological instruments that have utilized for my thesis.

2.2 The N-body system equation

A system of interacting particles (crystalline or molecular system) is described in non-relativistic quantum mechanics using the Schrodinger equation. The study of this formalism with many-body contribute to solve the Schrödinger equation which is independent of time (2.1) and that will be detailed and simplified by various approximations.

$$\widehat{H}\,\psi\left(\{r_i\},\{R_j\}\right) = E\,\psi(\{r_i\},\{R_j\}) \quad (2.1)$$

$\psi(\{r_i\},\{R_j\})$: Wavefunction of N-body system (multiple particles), $\{r_i\}$ stands for the term of the variables which describe the electrons, $\{R_j\}$ describes the nuclei.$\widehat{H}$ is the Hamiltonian of the system, and hence it can be written as[69, 70]

$$\widehat{H} = \sum_{i=1}^{n} \frac{-\hbar^2\nabla_i^2}{2m} + \sum_{\alpha=1}^{N} \frac{-\hbar^2\nabla_\alpha^2}{2M_\alpha} - \frac{1}{4\pi\varepsilon_0}\sum_{i=1}^{n}\sum_{\alpha=1}^{N}\frac{Z_\alpha e^2}{|r_i - R_\alpha|}$$

$$+\frac{1}{8\pi\varepsilon_0}\sum_{i,i\,\#\,j}\frac{e^2}{|r_i - r_j|} + \frac{1}{8\pi\varepsilon_0}\sum_{\propto\#\beta}\frac{Z_\alpha Z_\beta e^2}{|R_\alpha - R_\beta|} \quad (2.2)$$

The Hamiltonian operator describes a system that has multiple particles. The kinetic energy is shown in the first two terms. It describes also the electron-nuclei interaction, electron-electron interaction and the interaction energy of nuclei- nuclei. These interactions are described for N nuclei and n electrons. The Hamiltonian is expressed in the Coulomb interaction$\widehat{V}_T$ and total kinetic energy$\widehat{T}_T$, thus we can write:

$$\widehat{H} = \widehat{T}_T + \widehat{V}_T \quad (2.3)$$

With

$$\widehat{T}_T = \widehat{T}_n + \widehat{T}_e \; and \widehat{V}_T = \widehat{V}_{n-e} + \widehat{V}_{e-e} + \widehat{V}_{n-n} \quad (2.4)$$

The total kinetic energy corresponds to two kinetic energies, those of n electrons with mass m and the other of N nuclei with mass M, can then write:

Kinetic energy of electrons $\hat{T}_e = \sum_{i=1}^{n} \frac{-\hbar^2 \nabla_i^2}{2m}$ (2.4a)

Kinetic energy of nuclei $\hat{T}_n = \sum_{\alpha=1}^{N} \frac{-\hbar^2 \nabla_\alpha^2}{2M_\alpha}$ (2.4b)

The Coulomb interactions $\hat{V}_T$ may be expressed in the following expressions:

$$\hat{V}_{e-e} = \frac{1}{8\pi\varepsilon_0} \sum_{i\#j} \frac{ke^2}{|r_i - r_j|} \quad (2.4c)$$

$$\hat{V}_{n-e} = \frac{-1}{4\pi\varepsilon_0} \sum_{i=1}^{n} \frac{Z_\alpha e^2}{|r_i - R_\alpha|} \quad (2.4d)$$

$$\hat{V}_{n-n} = \frac{1}{8\pi\varepsilon_0} \sum_{\alpha\#\beta} \frac{Z_\alpha Z_\beta k e^2}{|R_\alpha - R_\beta|} \quad (2.4e)$$

The variables $i\ and\ j$ describe the electrons, $\alpha\ and\ \beta$ these variables describes the nuclei, those of $Z_\alpha e^2$ with charge of nuclei.

With the introduction of the Hamiltonian in the Schrodinger equation, the resolution is still relatively complicated and not possible. A solid with multiple particles (n + N), N nuclei and n electrons which are mutually interacting and moving in an electromagnetic field presents a problem in the solution of the system, hence the need to use different approximations. Among these approximations that may help to solve the equation of Schrödinger are the Born-Oppenheimer approximation, Hartree-Fock, DFT.

2.3 Born-Oppenheimer approximation

The Schrodinger equation for the multi-particle system (n + N), n nuclei and N electrons is still relatively complex and is not possible. So, it resorted to different approximations among these approximations the Born-Oppenheimer approximation[71], Hartree-Fock, and DFT. Knowing that the mass of electrons is strictly less comparable with that of the nuclei, the Born-Oppenheimer approximation therefore supposes

that the nuclei of system are fixed and the electrons are moving in a potential, which is created by the fixed nuclei. The ratio between the mass of electrons and that of the nuclei is always less than 10^{-5}; the movement of electrons is therefore faster as compared to that of nuclei. The kinetic energy of the nuclei can be considered equal to zero$T_n = 0$, the interaction energy of the nuclei (Coulomb energy caused by the repulsion between the nuclei) $V_{n-n} = ste$ is a constant value that can be also canceled[72]. Thus, this approximation presents a simplified formalism of Schrodinger equation from the resolution of (n + N) equation system to a system of n electrons. The electrons can be studied adiabatically, which means that the coupled terms are neglected. This approximation allows envisaging the decoupling of electronic and nuclear movement, which leads to write the electronic and nuclear variables separately.

The electronic Hamiltonian of the equation (2.2) can be written as:

$$\hat{H}_e = \hat{T}_e + \hat{V}_{n-e} + \hat{V}_{e-e} + \mathrm{C}^{ste}\left(\hat{V}_{n-n}\right) \quad (2.5)$$

Then we have

$$H = \sum_{i=1}^{n} \frac{-\hbar^2 \nabla_i^2}{2m} - \frac{1}{4\pi\varepsilon_0} \sum_{i=1}^{n} \sum_{\alpha=1}^{N} \frac{Z_\alpha e^2}{|r_i - R_\alpha|} + \frac{1}{8\pi\varepsilon_0} \sum_{i,i\,\#\,j} \frac{ke^2}{|r_i - r_j|} \quad (2.6)$$

The wavefunction is given by the following expression:

$$\psi\left(\{r_i, R_j\}\right) = \chi(R)\varphi\left(\{r_i, R_j\}\right) \quad (2.7)$$

R_j are the position of the nuclei that we supposed to be fixed. $\varphi(\{r, R\})$ is the electronic wavefunction and $\chi(R)$ is the nuclear wavefunction.

Now, it remains to solve the equation Schrödinger for $H = H_e$, and determine the electronic energy and the wavefunction corresponding to this system.

$$H_e \Psi = E_e \Psi \quad (2.8)$$

It is now necessary to say that with the Born-Oppenheimer approximation, the Schrödinger equation has become simplified, this adiabatic approximation is the first step for the resolution. The new form of Schrödinger equation (electronic equation) is still also system with many bodies, and the new wavefunction depends on electron coordinates in the system, those electrons are in mutual interaction which makes the problem much more difficult to solve. Therefore, other additional approximations are required for resolution.

2.4 Hartree-Fock approximation

The mutual interactions between electrons complicate the resolution of equation (2.8). The electrons are considered independent in the Hartree method[73]; each electron can move in a mean field generated by nuclei and other electrons. This method proposed by Hartree in 1927 allows the calculation of the wavefunctions for many body systems (poly-electronic) and making them as mono-electronic wavefunction products.

For each electron which corresponds to an electronic state, the total wavefunction is thus written as the product of mono-electronic wavefunctions:

$$\psi = \psi_1(r_1).\psi_2(r_2).\psi_3(r_3).\psi_4(r_4) \ldots \psi_N(r_N) \quad (2.9)$$

Fock showed in 1930 that the anti-symmetry principle of the wavefunction is not respected in the Hartree method. Certainly, according to the Pauli Exclusion Principle, two electrons cannot exist simultaneously in the same quantum state. Fock has replaced the wavefunction ψ ((r_1, $r_2 \ldots$ r_n) by a Slater determinant[72].

$$\psi(r_1, r_2, \dots, r_n) = \frac{1}{\sqrt{N!}} \begin{vmatrix} \psi_1(r_1)\psi_2(r_1) \dots & \psi_n(r_1) \\ \psi_1(r_2)\psi_1(r_1) & \dots \quad \psi_n(r_1) \\ \vdots \qquad\qquad \vdots & \ddots \qquad \vdots \\ \psi_1(r_N)\psi_1(r_N)\psi_n(r_N) & \end{vmatrix} \tag{2.10}$$

This method is considered as an approach which can solve the Schrödinger equation for a quantum system with n electrons and N nuclei.

2.5 Density functional theory

The theory of density functional (DFT) developed by Hohenberg, W. Kohn and L. Sham[74-80], have demonstrated two fundamental theorems on which the DFT is based. The theory allows determine the ground state properties of a many-body system and it is a positive function which depends on the space coordinates (x, y, and z). Density function theory is applied bulk materials and more complex structure such as bio-molecules and functionalized nanostructures. DFT has been summed up to manage numerous various systems: nuclei, spin-polarized systems, relativistic electrons, superconductors with electron pairing mechanisms, time-dependent phenomenon[81], excited states, and molecular dynamics etc. As the wavefunction for any particular set of coordinates cannot be directly observed, the observable quantity is probability which is given by $\Psi_e^* \Psi_e$. A quantity closely related to probability is electron density, n(r), at a particular position in space. DFT allows the replacement of complicated N-electron wavefunction and associated Schrödinger equation by simpler electron density $n(r)$. The integral of the electron density gives the total number of electrons.

$$\int \mathrm{n(r)dr} = \mathrm{N} \tag{2.11}$$

The relation between $n(r)$ and the many-electron wave-function Ψ_e is

$$n(\vec{r}) = N \iint \dots \int \Psi_e^* (\overrightarrow{r_1}, \overrightarrow{r_2}, \dots, \overrightarrow{r_n}) \Psi_e (\overrightarrow{r_1}, \overrightarrow{r_2}, \dots, \overrightarrow{r_n}) d\overrightarrow{r_1} d\overrightarrow{r_2} \dots d\overrightarrow{r_n} \quad (2.12)$$

The electron density which is a function of only three coordinates contains a great amount of information that is physically observable from the full wavefunction solution to the Schrödinger equation, which is a function of 3N coordinates. Hence the name density functional theory comes from the use of functionals of the electron density.

2.6 Hohenberg - Kohn and Kohn – Sham theorems

2.6.1 Hohenberg and Kohn theorem

The entire field of DFT rests on two fundamental mathematical theorems proved by Kohn and Hohenberg, called HK theorems[74, 75]. These theorems relate the potential and the electronic density in a quantum system.

Theorem 1: The first HK theorem states that the ground-state energy from Schrödinger's equation is a unique functional of electron density i.e. $E_e = E_e[n(r)]$.

According to this theorem there exist one-to-one mapping between the ground-state wavefunction and the ground-state electron density. It implies that ground-state electron density uniquely determines all properties, including the energy and wavefunction of the ground-state. The ground-state wavefunction being a ground state property of the system can be considered to be a functional of the ground state density $\Psi_0[n_0]$ total ground state energy consisted by N interacting electrons of an inhomogeneous system[74] is given by:

$$E_e = \langle\Psi_e|\hat{H}_e|\Psi_e\rangle = \langle\Psi_e|(\hat{T} + \hat{V} + \hat{U}_{ee})|\Psi_e\rangle = \langle\Psi_e|\hat{T}|\Psi_e\rangle +$$

$$\langle\Psi_e|\hat{V}|\Psi_e\rangle + \langle\Psi_e|\hat{U}_{ee}|\Psi_e\rangle = \iint \dots \int \left[-\frac{\hbar^2}{2m}\sum_{i=1}^{N} \Psi_e^* \nabla_i^2 \Psi_e + \right.$$

$$\left. \sum_{i=1}^{N} V(r_i)|\Psi_e^2| + \frac{e^2}{4\pi\varepsilon_0}\sum_{i<j}\frac{|\Psi_e^2|}{|r_i - r_j|} \right] dr_1 dr_2 \dots dr_n \qquad (2.13)$$

Here $|\Psi_e\rangle$ is *N*-electron ground state wavefunction and is a function of each of spatial coordinates of each of *N*-electrons i.e. $|\Psi_e\rangle = |\Psi_e(r_1, r_2, \dots, r_n)\rangle$. This equation isn't separable into single-particle equations because of the interaction internal potential $\hat{U}_{ee}$ the kinetic energy term$\hat{T}$ derivative operator between the wave-functions prevents rewriting the integrand on the form $|\Psi_e|^2$ as needed to turn the kinetic energy term into an expression of the electron density[70]. In the term of the internal potential energy $\hat{U}_{ee}$ the particle positions in the denominator preclude a direct term by term integration.

$$\hat{V} = \iint \dots \int \sum_{i=1}^{N} V(r_i)|\Psi_e^2|\, dr_1 dr_2 \dots dr_n = \frac{1}{N}\sum_{i=1}^{N} \int n(r_i)V(r_i)dr_i =$$

$$\int n(r)V(r)dr \qquad (2.14)$$

From the equation (2.14), external potential energy $\hat{V}$ can write as an explicit functional $V[n]$ of the electron density. This and other functionals with the electron density n(r) as arguments are called density functionals. The other terms in the electronic energy (equation (2.14)) are not in explicit density functional form, but can at least be written as functionals of the many-electron wavefunction Ψ_e :

$$E_e = T[\Psi_e] + U[\Psi_e] + V[n] = F[\Psi_e] + V[n] \qquad (2.15)$$

The next step is to check the possibility to also rewrite the total internal electronic energy $F[\Psi_e]$ as a density functional $F[n]$.

The existence of the total energy functional $E_e[n]$ and an internal electronic energy functional $F[n]$ directly follows as

$$E_e[n] = \langle\Psi_o[n]|H_e|\Psi_o[n]\rangle \;\; and \;\; F[n] = F\big[\Psi_o[n]\big] \qquad (2.16)$$

Above, theorem is used to solve the Schrodinger equation by finding a function of three spatial variables, the electron density, rather than a function of 3N variables. Thus, first HK theorem shows that a functional of electron density can be used to solve the Schrödinger equation, but it does not give any information about the nature of functional.

Theorem 2: The second theorem defines an important property of functional. According to the second HK theorem 'the electron density that minimizes the energy of overall functional is the true electron density corresponding to full solution of the Schrödinger equation'[82]. For a trial density $\tilde{n}(r)$, such that $\tilde{n}(r) \geq 0$, and $\int \tilde{n}(r)\mathrm{dr} = N$,

$$\mathrm{E_o} \leq \mathrm{E}\ [\tilde{\mathrm{n}}]$$

where $E\ [\tilde{n}]$ is the energy functional[75]. This means if some density represents the correct number of electrons N, then the total energy calculated from this density cannot be lower than the true energy of the ground state. The variational principle is used to find ground state density. Thus instead of solving true many body equation (2.12) as the need to find the minimum of functional:

$$E_o = \min_{\Psi} \langle \Psi | \hat{H}_e | \Psi \rangle = \min_{n} (F[n] + V[n]) \qquad (2.17)$$

2.6.2 Kohn-Sham equation

The idea of the Kohn-Sham equations[76] is to achieve the exact ground state density $n_0(r)$ by replacing the real system with another auxiliary system that can be solved more easily. The Kohn-Sham equation is the Schrödinger equation of a many-electron interacting system mapped into a fictitious non-interacting system. Instead, all the many-body terms are put into a local effective potential, called the "Kohn-Sham potential" $v_{eff}(r)$.

The ansatz of the Kohn-Sham method is that the ground state density in a factious non-interacting system is the same ground state density as would be in the real many-electron interacting system. The Kohn-Sham formulations are therefore an exact method (based on the fact that $E_{XC}[n(r)]$ has to be exact), and the method is the most common implementation of the DFT today[83, 84]. As mentioned above, the Kohn-Sham idea is based on electrons in a non-interacting system and therefore it is convenient to start with a Hartree-like many-electron wavefunction, i.e.

$$\psi_k^e(r) = \ \psi_1^e(r_1)\psi_2^e(r_2) \dots \dots \ \psi_N^e(r_N) \tag{2.18}$$

From this one can easily calculate the density as

$$n(r) = \ \sum_{k=0}^{N} |\psi_k^e(r)|^2 \tag{2.19}$$

The Kohn-Sham equations are often represented by the following single-electron eigenvalue equation within the Hartree approximation[85].

$$\left[-\frac{\hbar^2}{2m}\nabla_i^2 + v_{eff}(r)\right]\psi_i^e(r) = \varepsilon_i \psi_i^e(r) \tag{2.20}$$

where the effective potential $v_{eff}(r)$ consists of three different terms

$$v_{eff}(r) = \ V_H(r) + \ V_{XC}(r) + \ V_{en}(r) \tag{2.21}$$

Here, $V_H(r)$ is the Hartree-potential defined, $V_{XC}(r)$ is the exchange-correlation potential which will be described later and $V_{en}(r)$ is a known factor derived from the electron-nucleus interaction, $U_{en}[n(r)] = \int V_{en}(r)\, n(r) dr$ in the many-body Schrödinger equation.

As seen above, the Kohn-Sham equations look similar to the earlier Hartree-Fock equations, but they differ in the underlying theories of how they are achieved. In the HF equations, the variational principle is used to minimize the energy with respect to the single particle wavefunctions to achieve the Slater determinant which in turn describes the full many-

body wavefunction. The KS equations have the same idea, but instead of minimizing with respect to single particle wavefunctions, the minimization is done with respect to the density. The KS equations are also known as a "Beyond Hartree-Fock" method since they include correlation effects. Hohenberg and Kohn[74] stated that the ground-state energy of an interacting inhomogeneous electron gas in an external static potential $V_{en}(r)$ is

$$E[n(r)] = T[n(r)] + U_{ee}[n(r)] + U_{en}[n(r)]$$
$$= F[n(r)] + \int V_{en}(r)\, n(r) dr \quad (2.22)$$

Where $n(r)$ is the electronic density of the system, and $F[n(r)]$ is the universal functional introduced by Hohenberg and Kohn. The universal functional can be divided into two terms;

$$F[n(r)] = T[n(r)] + U_{ee}[n(r)] \quad (2.23)$$

Where the kinetic energy of a system with non-interacting electrons is $T[n(r)]$, $U_{ee}[n(r)]$ is the electron-electron interaction term. All terms are functionals of the electronic density to the system $n(r)$.

The Kohn-Sham is to create another Kohn-Sham system of non-interacting particles to make the calculation easier. Hereby, the expression for the total energy can be rewritten as.

$$E[n(r)] = T_s[n(r)] + U_s[n(r)] + U_{en}[n(r)] + (T[n(r)] - T_s[n(r)])$$
$$+ (U_{ee}[n(r)] - U_{en}[n(r)]) \quad (2.24)$$

Where $T_s[n(r)]$ and $U_s[n(r)]$ are the kinetic and the static potential energy of the Kohn-Sham system, respectively. These can easily be calculated within the Hartree approximation, and are defined by

$$T_s[n(r)] = \sum_{j=1}^{Ne} \int |\psi_i^*(r) \frac{-\hbar^2 \nabla^2}{2m_e} \psi_i(r)\, dr \quad (2.25)$$

$$U_s[n(r)] = \frac{1}{2} \iint \frac{n(r)n(r')}{|r-r'|}\, dr dr' \quad (2.26)$$

The external potential, denoted as $V_{en}(\boldsymbol{r})$, which leads to the $U_{en}[n(r)]$term is unaffected by the change into the Kohn-Sham system. The two parentheses in the expression for the total energy, which are defined as the difference in the kinetic and the potential energy between the real interacting system and the Hartree-like system, are collected into one term defined as the exchange-correlation energy,

$$E_{XC}[n(r)] = (T[n(r)] - T_s[n(r)]) + (U_{ee}[n(r)] - U_s[n(r)]) \quad (2.27)$$

After rewriting, the total energy functional can be expressed as

$$E[n(r)] = T_s[n(r)] + U_s[n(r)] + U_{en}[n(r)] + E_{XC}[n(r)] \quad (2.28)$$

or

$$E[n(r)] = \int \sum_i \psi_i^*(r) \left\{ \frac{-\hbar^2 \nabla^2}{m_e} \right\} \psi_i(r)\, dr + \frac{1}{2} \iint \frac{n(r)n(r')}{|r - r'|}\, drdr' + \int V_{en}(r)\, n(r) dr + E_{XC}[n(r)] \quad (2.29)$$

As the first three terms can be calculated easily within the Hartree approximation, one obtains an exact solution of the total energy if the exchange-correlation energy is known. If the system is non-interacting $E_{XC}[n(r)] = 0$and the system will have the Hartree total energy, which is the total energy based on non-interacting particles**.** In order to find the ground state one obtains the variational method to search for solutions that fulfill the following relation[86]and

$$\frac{\partial E[n(r)]}{\partial \psi_i^*(r)} = 0 \quad (2.30)$$

The reason to take the functional derivative with respect to the complex conjugate wavefunction is to avoid an equation with the complex conjugate in the end. In addition, the solutions need to fulfill an orthonormality requirement defined by

$$g = \sum_i f_i \{ \int \psi_i^*(r) \psi_i(r)\, dr - 1 \} = 0 \quad (2.31)$$

Where f_i is the Lagrange multiplier associated to the normalization condition of $\psi_i(r)$.The two requirements can be summarized in one equation

$$\frac{\partial(E[n(r)]-g)}{\partial\psi_i^*(r)} = 0 \tag{2.32}$$

$$\frac{\partial E[n(r)]}{\partial\psi_i^*(r)} = \frac{\partial g}{\partial\psi_i^*(r)} \tag{2.33}$$

From the equation of the orthonormality requirement one can easily take the functional derivative and obtain an equation for the energy functional.

$$\frac{\partial E[n(r)]}{\partial\psi_i^*(r)} = \frac{\partial g}{\partial\psi_i^*(r)} = f_i\psi_i(r) \tag{2.34}$$

The energy functional can be expressed in terms of a kinetic, an electron-electron interaction, electron-nuclei, and an exchange-correlation part[87]

$$\frac{\partial}{\partial\psi_i^*(r)}\{T_s[n(r)] + U_s[n(r)] + U_{en}[n(r)] + E_{XC}[n(r)]\} = f_i\psi_i(r) \tag{2.35}$$

As the terms are functionals of the electronic density one applies the chain rule to take the functional derivative with respect to density for the last three terms.

$$\frac{\partial}{\partial\psi_i^*(r)} T_s[n(r)] + \frac{\partial}{\partial n(r)}\{U_s[n(r)] + U_{en}[n(r)] + E_{XC}[n(r)]\}\psi_i(r) = f_i\psi_i(r) \tag{2.36}$$

The last factor on the left-hand side is from the chain rule and it is now clear why one should take the functional derivative with respect to the complex conjugate wavefunction. Within the Hartree approximation, the kinetic part and the electron-electron interaction can be calculated and give

$$\left\{\frac{-\hbar^2\nabla^2}{2m_e} + \int \frac{n(r')}{|r-r'|}dr' + V_{en}[n(r)] + V_{XC}[n(r)]\right\}\psi_i = \varepsilon_i\psi_i \qquad (2.37)$$

Which can be recognized the single particle KS equation. f_i is set equal to ε_i to clarify it as an energy term. From classical physics, the potential energy is given as the derivative of the total energy. Therefore the exchange-correlation potential energy is found to be the functional derivative of the exchange-correlation energy [86]

$$V_{XC}[n(r)] = \frac{\partial\, E_{XC}[n(r)]}{\partial n(r)} \qquad (2.38)$$

From the single electron KS equation one multiply by $\sum_i \psi_i^*(r)$ from left to obtain an expression for the single-electron energies.

$$\int \sum_i \psi_i^*(r)\left\{-\frac{\hbar^2\nabla_i^2}{2m_e} + V_H(r) + V_{en}(r) + V_{XC}(r)\right\}\psi_i(r)\,dr = \int \sum_i \psi_i^*(r)\varepsilon_i\psi_i(r)\,dr \qquad (2.39)$$

$$\sum_i \varepsilon_i = \int \sum_i \psi_i^*(r)\left\{\frac{-\hbar^2\nabla^2}{2m_e}\right\}\psi_i(r)\,dr + \iint \frac{n(r)n(r')}{|r-r'|}\,drdr' + \int V_{en}(r)n(r)dr + \int V_{XC}(r)n(r)dr \qquad (2.39a)$$

If one rewrites the latest equation as an expression for the kinetic part and insert it in the expression for the total energy functional one gets a relation between the energy functional and the single-electron energies from the KS equation[87]

$$E[n(r)] = \sum_i^N \varepsilon_i - \frac{1}{2}\iint \frac{n(r)n(r')}{|r-r'|}\,drdr' + E_{XC}[n(r)] - \int V_{XC}(r)n(r)dr \qquad (2.40)$$

The total energy can be generated from the Hartree-like single-electron energies, a self-interacting term and the exchange-correlation functional. The exact energy is therefore generated if the exact form of the exchange-correlation functional is found.

2.7 Approximation

2.7.1 Exchange and correlation functional

DFT Provide a good description of the ground state properties and that DFT are based on so-called exchange-correlation functional. Exchange interaction describes the effect quantum mechanical between identical particles in a system in accordance to Pauli principle. Correlation energy is related the Coulomb interactions between electrons in a system[88]. DFT is difficult of the exact exchange and correlation functionals aren't known except for free electron gas. Some approximations are used to calculate physical quantities with good accuracy[89]. In DFT calculations, there are three types of approximations, first is conceptual with interpretation of eigenvalues and wavefunctions and orbitals as physical energies. The approximation of second is numerical and used to solve the differential equation and a key aspect is choosing the suitable basis functions. The third type of approximation consists of constructing an expression of an unknown function $E_{XC}\,[n]$, which contains all many- electron of the problem[88].

2.7.2 Local Density Approximation (LDA)

In physics the most commonly used approximation is the local density approximation (LDA)[90], where the functional depends only on the density at the point where the functional is calculated. For many decades the LDA has been employed in, i. e. calculations of band structures and total energies in condensed matter physics:

$$E_{XC}^{LDA}[n(r)] = \int \varepsilon_{XC}\,(n(r))n(r)d^3r \qquad (2.41)$$

The most accurate data for $\varepsilon_{XC}(n(r))$ is from Quantum Monte Carlo calculations. The LDA gives very accurate results for systems with

slowly varying charge densities. But it is more useful for homogeneous systems and over-binds molecules and solids. The systems in which geometries are symmetric, bond lengths and angles are accurate to within a few percent, LDA works well.Results for some quantities such as the dielectric and piezoelectric constant are approximately10% large.

The main advantage of LDA-DFT over schemes such as Hartree-Fock is that many experimentally relevant physical properties can be calculated to a significant level of accuracy using LDA. While many ground state properties are well described in the LDA, the dielectric constant is overestimated by up to 10-40% in LDA compared to experimental value. This overestimation results because of the abandoning of a polarization-dependent exchange-correlation field in LDA as compared to DFT.

The local spin-density approximation (LSDA) is a straightforward generalization of the LDA to include electron spin:

$$E_{XC}^{LSDA}[\mathrm{n}\uparrow, \mathrm{n}\downarrow] = \int \varepsilon_{\mathrm{XC}}(\mathrm{n}_{\uparrow}, \mathrm{n}_{\downarrow}) n(r)\, \mathrm{d}^3\mathrm{r} \qquad (2.42)$$

Exact formulae for the exchange-correlation energy density $\varepsilon_{\mathrm{XC}}(\mathrm{n}_{\uparrow}, \mathrm{n}_{\downarrow})$ have been derived from simulations of a free-electron gas.

2.7.3 Generalized Gradient Approximation (GGA)

As LDA determines the electronic density by the energy of a local constant density and improvement form the LDA when taking the gradient of the electron density. This is called Generalized Gradient Approximation (GGA) is a non-local method that depends only on the electronic density[91].

$$E_{XC}^{GGA}[n_{\uparrow}(r), n_{\downarrow}(r)] = \int f(n_{\uparrow}(r), n_{\downarrow}(r), \nabla n_{\uparrow}(r), \nabla n_{\downarrow}(r)) n(r) dr \qquad (2.43)$$

As well as the several systems such as atomic or molecular are often very different from a uniform electron gas and it are not homogeneous. For this reason has been used of the GGA. GGA has shown great improvements of spin-polarized system the accuracy of ground state energies, binding energy, atomization energies, energy barriers, molecular geometries and band structures. In addition, there some GGA functional are the PW91[92], the PBE[91], the RPBE[93]and the WC[94] and the next step in the evaluation of GGA is meta-GGA functional based on the PBE that includes second order derivations of the electronic in its functionals through the use of Laplacian operators. Later there has been introduced the effective parameter U semi-empirical to achieve quantities and properties for the exchange-correlation functionals. This parameter has been shown improvement for electronic ground state and magnetic properties within both the LDA and the GGA[95].

2.8 Basis set

To solve the electronic structure problem in practice either within DFT or within Hartree Fock approaches, a mathematical require representation for electron orbitals. This representation of atomic orbitals in the form of mathematical functions is known as basis set. There are different types of basis sets representations, which are adopted for electronic structure calculations. Based on the LCAO (Linear Combination of Atomic Orbital's) approximation, each one-electron molecular orbital χ_i (basis function) with expansion coefficients C_i is written as

$$\emptyset = C_1\chi_1 + C_2\chi_2 + C_3\chi_3 \ldots\ldots \quad (2.44)$$

Generally the one-electron wavefunction is described by the orbitals|∅α ⟩.In a real space representation these orbital can write $< r|\emptyset_\alpha >= \emptyset_\alpha(r)$. The Kohn Shamor Hartree Fock orbitals are then written as a linear combination of these basis orbitals or basis set:

$$\emptyset_j(r) = \sum_\alpha^M C_{j\alpha}\, \emptyset_\alpha(r) \qquad (2.45)$$

Where j labels the wavefunction, the sum runs over all the basis functions up to the dimension of the basis set M, $C_{j\alpha}$ are the expansion coefficients of the wavefunction j.The choice of basic functions should be such so that it provides a good approximation to the solution of above equation. At the same time want the number of states to bias small as possible because of finite computer resource[96]. In case of effective core potentials core electrons are chemically not so important, but require a large number of basis functions for an accurate description of their orbitals. So an effective core potential (ECP) is a linear combination of specially designed Gaussian functions that model the core electrons, i.e., are represented the core electrons by an effective potential one treats only the valence electrons explicitly.The DFT approach to solve the Schrödinger equation for a system of particles is more efficient and less laborious. As according to this theory do not bother about the wavefunction of individual a particle which is a function on 3N variables, N bring the number of particles in the system. Instead concentrate on the electron density which is a function of only three variables. Now in order to use DFT for practical calculations on genuine systems, to solve the Kohn-Sham equations numerically through a computer, means that the problem must be cast in a finite manner. The solution of the Kohn-Sham equation completely depends on the treatment of electron-nuclear interaction.

The electron-nuclear interaction is generally given by Coulomb potential. But there are two classes of electrons: those that actively participate in chemical bonding, named valence electrons and those tightly bound to the nuclei called core electrons, which do not participate in bonding and can be treated as frozen electrons. Now instead of doing calculation for all electron, the core electrons replace by a fictitious potential. It makes our problem easier. This fictitious potential is known as pseudo potential and is discussed below:

2.9 Pseudopotentials

The physical and chemical properties of the studied systems are generally depending on the valence electrons, as they are responsible for the chemical bonds. By Hans Hellmann in 1934 was first introduced the pseudopotential approach, it aims to obtain the effective potential produced by to replaces the potential of Coulomb interaction of the nuclei and the core electrons that can give a description of the electronic properties and other without taking account the core states[97]. The valence wavefunction so generated is guaranteed to be orthogonal to all the core states. In this method only the chemically active valence electrons are treated explicitly, while the core electrons are 'frozen', taken into account together with the nuclei as rigid non-polarizable ion cores. Norm-conserving pseudopotentials are derived from an atomic state used as reference, with the condition that the pseudo and all-electron valence eigen states have the same energies and amplitude (and thus density) outside a chosen core cutoff radius r_c. A pseudopotential may be formulated for each atomic species which includes effects of the nucleus and core electrons on the grounds that the core electron states may be taken as fixed[98-100]. Thus decreasing the number of plane waves lead to pseudo wavefunctions do not represent the rapid

oscillations of the true wavefunctions corresponding to this modified potential, (See Fig. 2.1). Pseudopotential is formed such that it matches the true potential outside a given radius, termed as the core radius. Similarly, each pseudo wavefunction should match the corresponding true wavefunction beyond this distance. As well as, the charge densities outside the core region must be similar to the true charge density. Therefore, the integration of the squared amplitudes of the pseudo and real wavefunctions over the core region must be identical. The aforementioned condition is known as norm-conservation[101].

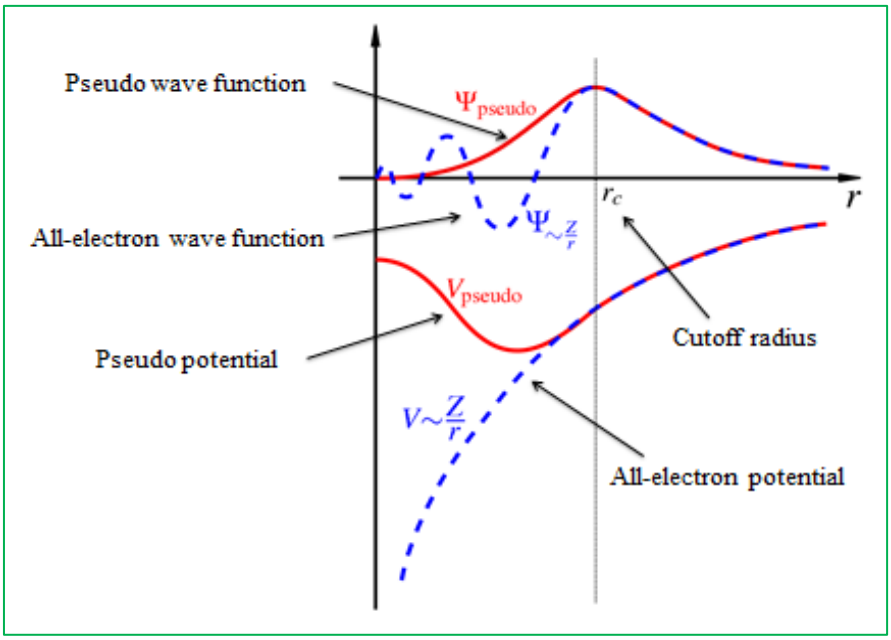

Figure 2.1:Curve which represents the wavefunction of the entire system (all-electron) and the equivalent pseudo-potential[102]. The radius at which all-electron and pseudopotential values meet is termed as r_c.

Pseudopotentials are first calculated for an isolated atom constructed using an *ab-initio* method. The `true' wavefunctions are calculated for an isolated atom using an all-electron DFT approximation. The valence wavefunctions so obtained are then modified in the core region to remove the oscillations while obeying the norm-conservation condition.

The Schrödinger equation is then employed in reverse manner to obtain the pseudopotential which will reproduce the pseudo wavefunctions. This method produces a pseudopotential which may be transferred between widely varying systems in contrast with semi-empirical potentials which are introduced to describe a particular atomic environment.

2.10 Software packages based on DFT

Inside the most recent couple of decades, the first-principles simulations in condensed issue physical science have extended fundamentally, from physics and chemistry into life-science, material science and nanoscale. There are many packages based on DFT which are being extensively used. These include SIESTA, VASP, WIEN2k, CASTEP, CRYSTAL, DMOL, ABINIT, TB-LMTO, GAMESS, QUANTUM-ESPRESSO, and others for calculating different properties. Some codes are better suited for special types of problems and materials than other one, so there are differences in the practical realization of above codes. WIEN2k, CRYSTAL and TB-LMTO use full potential or all-electron methods and take into account the wavefunction of all electrons in each atom. SIESTA, VASP and ABINIT, these codes use pseudopotential methods in which only valance electrons are explicitly included in equation. This properties directly obtained from core electrons for instance isomer sift, electronic filed gradient, hyperfine field at atom cores are not well explained. VASP and ABINIT use plane waves and the basis in WIEN2k is a hybrid one whereas CRYSTAL, SIESTA and TB-LMTO use atoms-centered bases.

2.11 SIESTA

The SIESTA[103] (Spanish Initiative for Electronic Simulation with Thousands of Atoms) is a code which works on (Linux and UNIX), this package is a set independent programs written with Fortran and calculate several physical properties such as electronic structural properties of materials for the study of band structure, the total/projected density of state (TDOS and PDOS), and the total energy of the system and the optimization of structures. This code can calculate the optical and magnetic properties of the materials under consideration.

The computational cost for different *ab initio* quantum mechanical codes scales as 3N, with the number (N) of atoms, while SIESTA is used scale linearly with number of atoms i.e. "order-N methods" scaling, it has an atom centered basis therefore deal with large unit cells and it is considered one of the few codes that use this method[104, 105]. SIESTA uses the standard Kohn-Sham self-consistent density functional theory in the local density (LDA) or generalized gradient (GGA) approximations to describe the various properties and calculate the energies of solid state system[38-39]. It uses normconserving pseudopotential in its fully non local (Kleinman-Bylander) from[106].

2.12 The calculated variables properties

All calculations in this study are carried out by density functional theory based on Generalized Gradient Approximation.

2.12.1 Binding energy (BE)

The Binding energy of ZnONSs can be calculated by Eq. (2.46) as follows while the binding energy of the doped systems has been calculated to evaluate their stability by using eq. (2.47) the expression

$$BE = \{E_{tot}(ZnO) - \ (n_O E_{tot}(O) + n_{Zn} E_{tot}(Zn))\} \quad (2.46)$$

$$BE = [E_{tot}(M_n ZnO) - (n_O \ * E(O) + n_{Zn} \ * E(Zn) + n_i \ * E(M))]/n$$

$$(\mathrm{M} = \ \mathrm{B}, \mathrm{C}, \mathrm{N}, \mathrm{Al}, \mathrm{Si}, \mathrm{P}) \quad (2.47)$$

Where BE is the binding energy per atom of B, C, N, Al, Si and P and $E_{tot}(M_n ZnO)$ is the total energy of the substiutionally ZnO nanosheet doped with n_i is the number of i[th] species present in the configuration, while $E(O),\ E(Zn),\ and\ E(M)$ represent total energies ofsingle Zn, O, and dopant atom of all element respectively and n is the total number of atoms in a supercell (n=84).

2.12.2 Total energy (E_{total})

The total energy is the sum of kinetic energy, Hartree energy, energy of ion-electron, energy of exch.-corr., and energy of ion-ion, at the optimized structure where the total energy of the molecule must be at the lowest value because the molecule is at the equilibrium position, which means, the resultant of the effective forces is zero[107].

2.12.3 Vertical ionization potential (VIP)

VIP is calculated by making M_n-ZnONSs complex one electron deficient computing total energy for M_n-ZnONSs complex and then subtracting from it the total energy of neutral M_n-ZnONSs[108].

$$VIP = ([E(cation) - \ E(neutral)]) \quad (2.48)$$

2.12.4 Vertical electron affinity (VEA)

VEA is calculated by putting one extra electron on neutral M_n-ZnONSs molecule, computing the total energy for the same and then subtracting the same from total energy of neutral M_n-ZnONSs molecule[108, 109]:

$$VEA = \left(\left[E(neulral) - E(anion)\right]\right) \quad (2.49)$$

2.12.5 Electronegativity (EN)

The electronegativity is experimentally related, linear combinations to two known ionization energy and electron affinity, as in the relationship [109]:

$$EN = (VIP + VEA) / 2 \quad (2.50)$$

2.12.6 Hardness (H)

In terms of ionization energies and electron affinities, the hardness is half of the energy gap between two frontier orbitals[109]:

$$H = VIP - VEA \quad (2.51)$$

CHAPTER 3: RESULTS AND DISCUSSION

3.1 Introduction

The current chapter includes the design of zinc oxide nanosheet (ZnONSs) in the SIESTA program, and this chapter is divided into two parts. The first part is enriched by the elements of the second cycle, namely, Boron, carbon and nitrogen. The second part consists of elements of the third cycle aluminum, silicon and phosphor to calculate its structural and electronic properties. The 6 ×7supercell (consisting of 84 atoms) of ZnO nanosheet has been used to simulate the isolated sheet that takes hexagonal structures with a vacuum layer 19Å along the perpendicular direction to avoid interlayer interactions. The effect of doping has been investigated by substitutional O atoms in one to six dopant atoms in 84 atoms host atoms. In years, two dimension are attracting increasing research interest due to their unique properties, such as high surface area, the electron confinement of two dimension materials without interlayer interaction, chemically active exposed surface, high optical transparency the maximum mechanical flexibility and confined thickness[110]. 2D is particularly interesting in developing novel applications in photocatalysts, sensor, ultraviolet photoelectronic device and many application[111]. ZnO can also form two-dimensional nanosheets where it forms a hexagonal structure in which Zn and O atoms are arranged in 3-foldcoordination instead of bulk-like tetrahedral configuration and may have more important advantages because of the large energy gap[112]. Soon, synthesis of high-quality two-monolayer-thick ZnO nanosheet (0001) on Ag(111) substrate has been experimentally achieved, which provided a direct evidence for the presence of planar ZnO sheet[43].

Via most experimental routes, especially the pulsed laser deposition can be produced ZnO thin sheets and it is observed tend to prefer c-axis with a polar morphology[43, 113, 114]. Although ZnO is native n-type semiconductor, using B and N co-doped ZnO the observation stable p-type conductivity has been that the dopant atoms can alter the electronic band structure of ZnO[115]. Nitrogen is regarded as the best candidate to induce p-type doping in ZnO also experimental evidence showing that the B and N codoping results in n-type characteristic instead[116]. The element B, N and C has preferred dopant due to good electron-produces also they donate two electrons per dopant to the conduction band.

3.2 Computational details

Nanosheet is recognized to relax in two dimensions the initial structure of the ZnO sheet cleaved from a (0001) layer of bulk ZnO. To do this analysis, the geometric relaxations and electronic structure calculations have been implemented by using the Spanish Initiative for Electronic Simulation with Thousands of Atoms (SIESTA)[103] code, in which the density functional theory (DFT)[117]. The electronic structure calculation was performed using generalized gradient approximation (GGA) with the exchange-correlation potential in the form of Perdew–Burke-Ernzerhof (PBE)[91, 118]. By pseudopotentials is described the electron-atomic cores interaction and generated within the projector the Troullier–Martins scheme[106]. Pseudopotentials with $3d^{10}\ 4s^2$, $2s^2\ 2p^4$, $2s^2\ 2p^1$, $2s^2\ 2p^2$, $2s^2\ 2p^3$, $3s^2\ 3p^1$, $3s^2\ 3p^2$ and $3s^2\ 3p^3$valence electron configurations were used for Zn, O, B, C, N, Al, Si and P atoms, respectively. Using the conjugate gradient (CG) algorithm are performed optimizations structural to ZnO nanosheet so that the maximum force on each atom in the calculations are less than 0.008eV/Å. The energy cut-

off has been used to 200Ry to define the finite real space grid for numerical integrals. the ZnO nanosheet supercell constructed from a bulk w-ZnO structure with lattice parameters a = 3.29Å and c = 5.3Å these values are both experimental and theoretical results[119, 120].

3.3 First Group

In this part, the structural and electronic properties of pure ZnONSs and doped with B, C, and N atoms have been investigated in density functional theory using the GGA method. Its results are compared with pure ZnONSs.

First of all, the structure of pure ZnO nanosheet (ZnONSs) optimized is shown in Figure 3.1. The atomic structure of the ZnONSs was cut from the initial bulk w-ZnO (0001) plane. A periodic 6×7 supercell of the ZnONSs, which consists of 84 atoms with a vacuum region of 19Å perpendicular to the monolayer plane, is applied to avoid interlayer interactions. Which was found the bond length of Zn-O to be 1.90Å, slightly less than experimental value of 1.92 Å and previously GGA values of 1.90Å and the resulting bond angle Zn-O-Zn or O-Zn-O of pure ZnO nanosheet is120^{o} which in agreement with previous results[42, 43]. Furthermore, the bond length Zn-O is around 2.01Å in bulk ZnO is longer than that of ZnONSs. Interestingly, the contraction of the bond length Zn-O in ZnONSs has attributed the atoms have less number of neighbors then the bulk. The atoms in the ZnONSs reinforce their bonding amongst themselves as compared to the bulk. Also find that the calculated HOMO–LUMO gap is 0.850eV suggests a semiconductor behavior for the ZnO nanosheet which is smaller than the experimental value 3.37eV[6]. Energy gap of the ZnONSs in GGA was obtained equal to 0.95eV [121].This is underestimated due to the

shortcomings of the GGA-PBE approach which does not consider the non-continuity of the exchange correlation[20]and by previous all-electron LDA calculation similar to the value of 0.895eV[122]. Values of vertical ionization potential (VIP) and vertical electron affinity (VEA) of ZnONSs are found 7.33eV, 0.104eV, respectively calculated at the GGA-PBE. these values are in agreement with an experimentally determined value of 7.82eV and 0.12eV reported by Swank[123, 124].

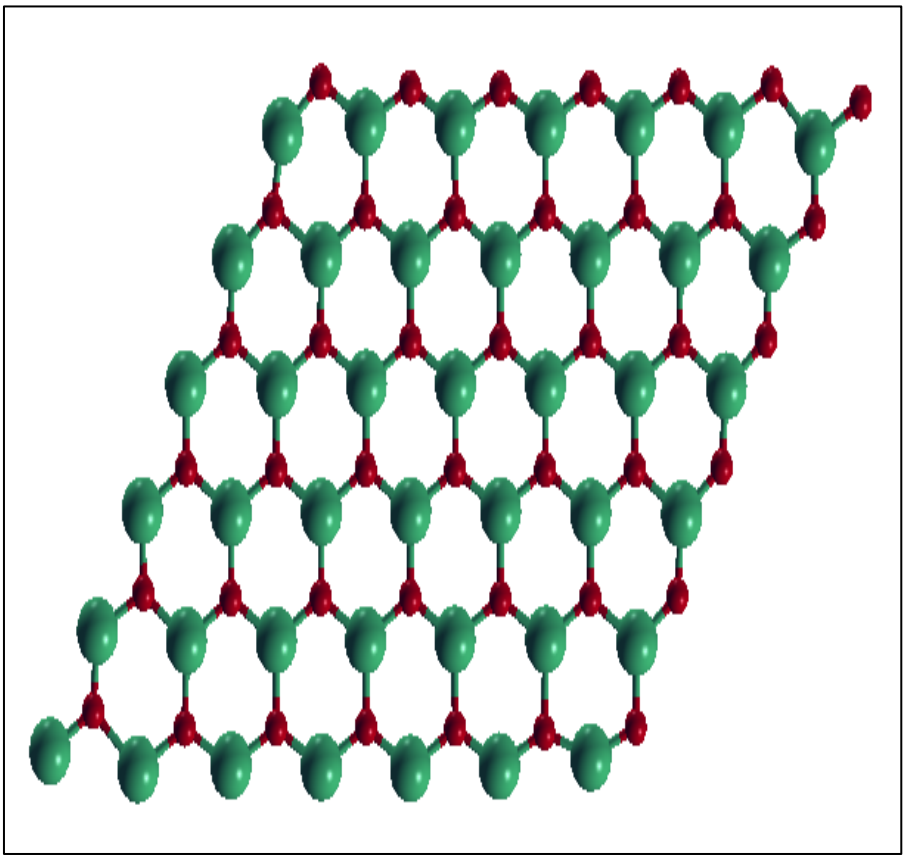

Figure 3.1: Optimized structure of pure ZnO nanosheet.

3.3.1 Structure properties of boron, carbon, and nitrogen-doped zinc oxide nanosheet

The present work includes B, C and N doped ZnONSs in detail. For the structures that are doped, O atoms instead of B, C and N were replaced with a number of atoms from one to six line in the center of ZnONSs this is due to the fact that the space of the nanosheet is insufficient to accommodate a total of more atoms. These atoms are likely to adjust to surrounding Zn atoms of the host. Because of the atomic radius of the O is approaching with B, C and N. When doped ZnONSs with B atoms no significant distortion in the 2D structure of ZnONSs is expected, except for a change in bond length.

In Figure 3.2, the doping of one B atom in the center leads to B_1-$Zn_{42}O_{41}$ stabilizes the bond length between the boron atoms and the nearest neighbor zinc atoms B-Zn is around1.96Å, the bond angle Zn-B-Zn is approximately 122.95^o and there is almost no distortion in the planar structure of nanosheet. While B_2-$Zn_{42}O_{40}$structure was resulting bond length B-B 3.27Å[57].

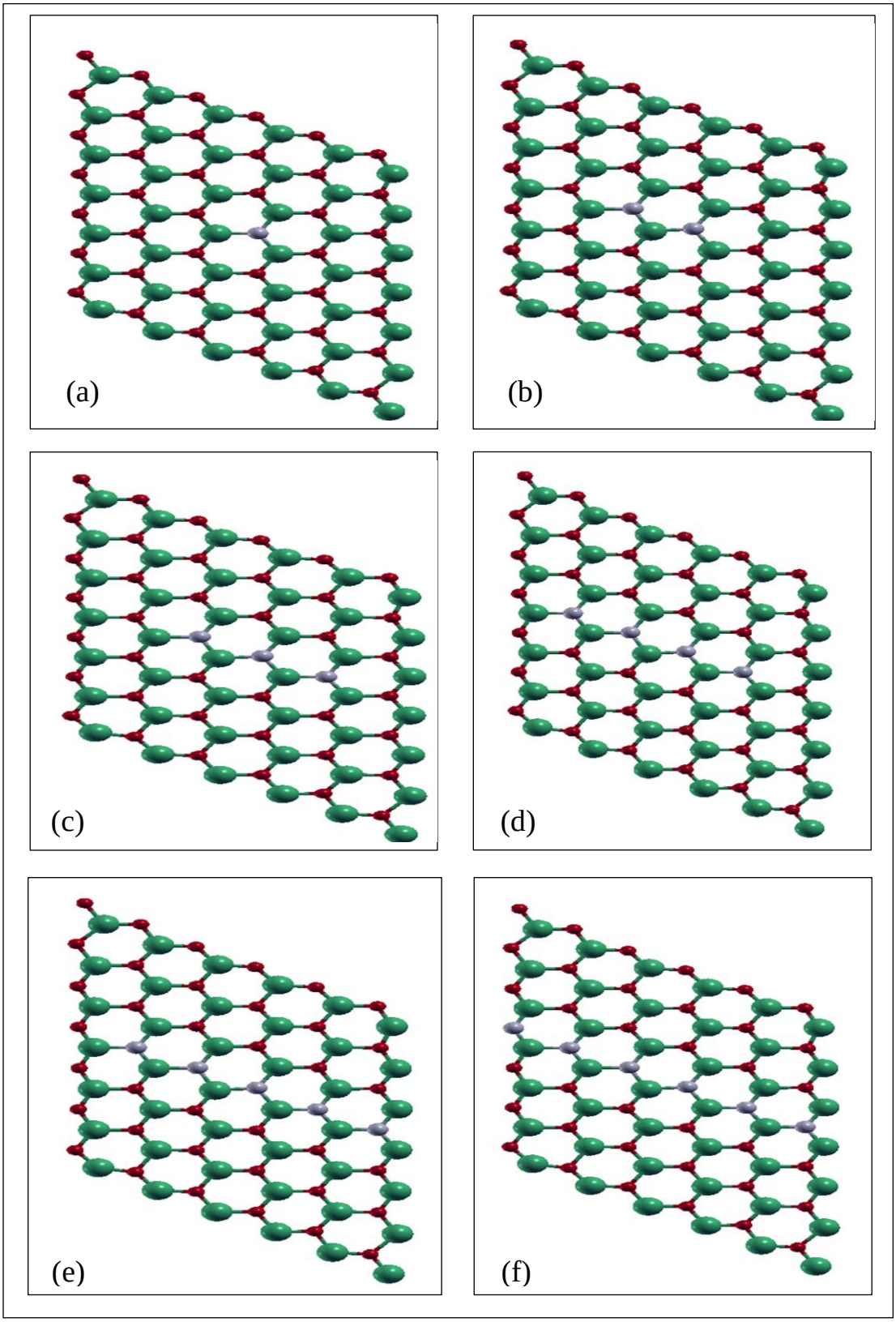

Figure 3.2(a-f): Optimize the structure of B_n-ZnONSs (n=1-6), the red, green and gray spheres refer to oxygen, zinc, and the dopant B atoms, respectively.

The optimized structure for C-doped ZnONSs is shown in Figure 3.3. When an O atom replaced by a C atom in the center as shown in Figure 3.3(a)leads to C_1-$Zn_{42}O_{41}$ structure found the bond length C-Zn for the C atoms to its nearest Zn atom is 1.88Å[23] and the bond angle Zn-C-Zn is 122.56^o. This indicates no deformation compared with pure because of the atomic radius of the C is close to the atomic radius of the O. while doping with two C atoms was resulting in C_2-$Zn_{42}O_{40}$ structure bond length C-C in the optimized structure is 3.27Å.

Moreover, optimize structures for N-doped ZnONSs as shown in Figure 3.4. An O atom replaced by an N atom at the center results N_1-$Zn_{42}O_{41}$ structure as shown in Figure 3.4(a).The bond length N-Zn for the N atom to its nearest Zn is 1.89Å[125] and the Zn-N-Zn bond angle is 121.88^o. As well as doping with two N atoms results N_2- $Zn_{42}O_{40}$ with interatomic distances N-N is 3.29 Å in the optimized structure, as shown in Figure 3.4(b).

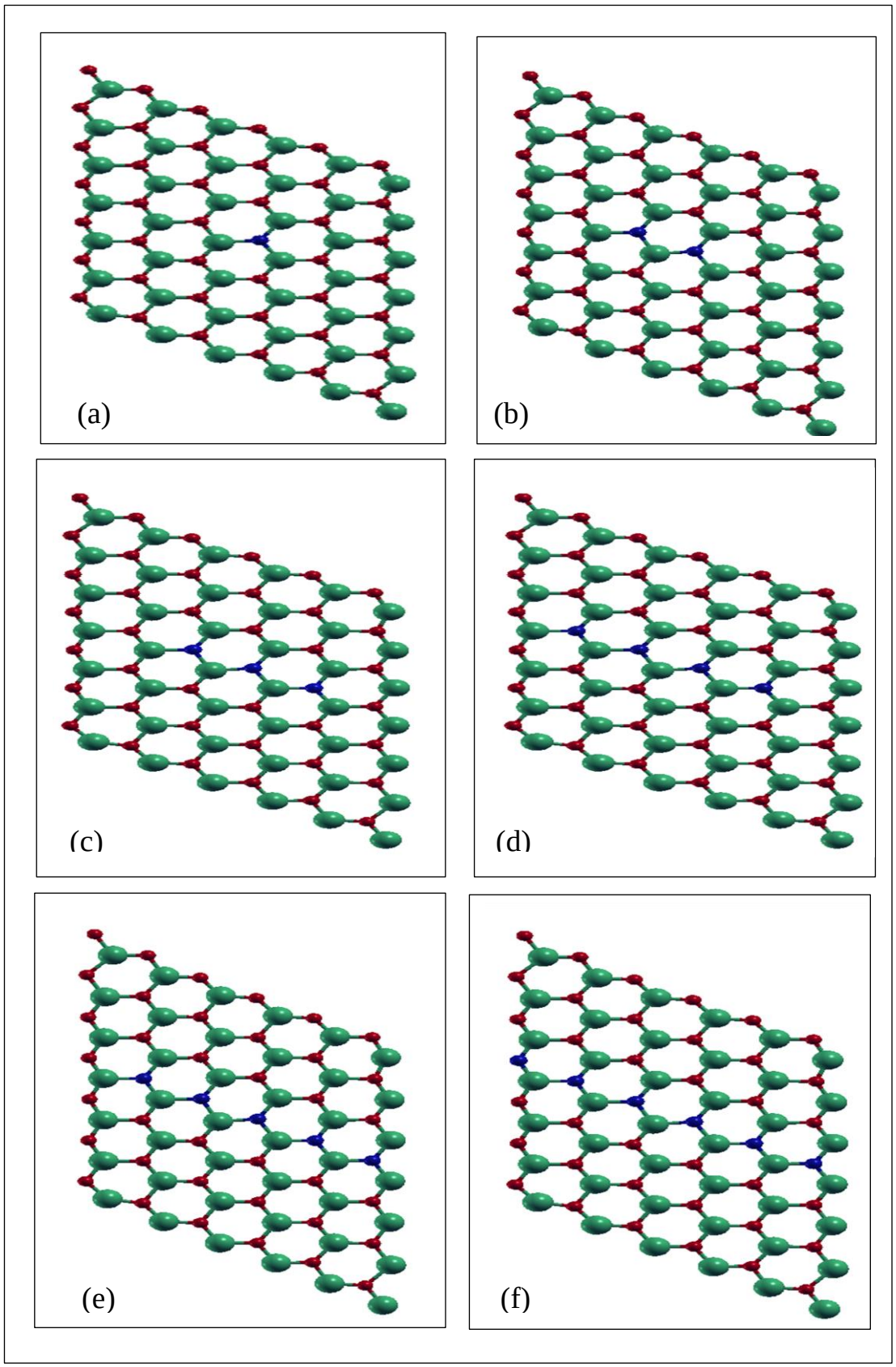

Figure 3.3(a-f): Optimize the structure of C_n-ZnONSs (n=1-6), the red, green, and indigo spheres refer to oxygen, zinc and the dopant C atoms, respectively.

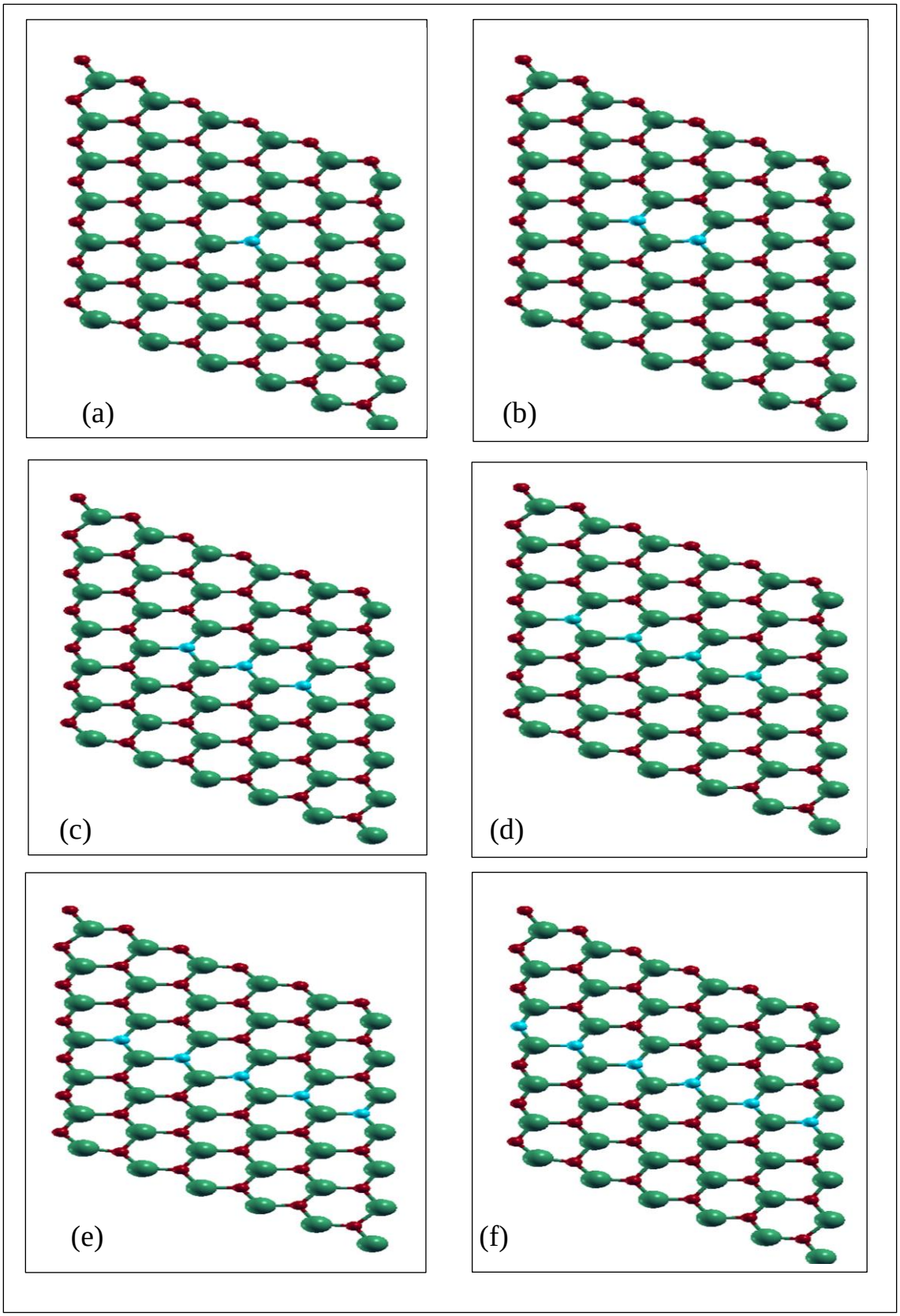

Figure 3.4(a-f): Optimize the structure of N_n-ZnONSs (n=1-6), the red, green and turquoise spheres refer to oxygen, zinc and the dopant C atoms, respectively.

The calculated first neighbour distance of the dopant atoms, d(X-Zn, X = B, C and N), are tabulated in Table 3.1.As seen from Table 3.1, in the B substitution case the B–Zn bond increases and about for B_4-$Zn_{42}O_{38}$, In the C substitution case C–Zn bond increases by about for C_4-$Zn_{42}O_{38}$ and about with respect to the pure case. According to the present results d(X-Zn, X=B, C and N) is relatively larger for B with respect to that of N. The change in bond length with respect to the position and type of dopant is relatively larger in the case of B doping with respect to the N doping case. B doping results are more sensitive to the cell.

Table 3.1: The bond length (d, in Å) 6f B, C and N doped ZnO nanosheet.

Configurations	$d(B_O)$	$d(C_O)$	$d(N_O)$
X_1-$Zn_{42}O_{41}$	1.95	1.90	1. 89
X_2-$Zn_{42}O_{40}$	1.95	1.90	1.90
X_3-$Zn_{42}O_{39}$	1.94	1.88	1.84
X_4-$Zn_{42}O_{38}$	1.97	1.92	1.92
X_5-$Zn_{42}O_{37}$	1.90	1.81	1.78
X_6-$Zn_{42}O_{36}$	1.92	1.89	1.89

3.3.2 Binding energy of boron, carbon and nitrogen-doped zinc oxide nanosheet

For the optimized structures that are doped, the binding energy of the doped systems has been calculated to evaluate their stability by using the equation (2.47). A negative value of binding energy corresponds to a metastable or stable bound dopant when both are present in the system. The value binding energy(BE) for pure ZnONSs is found -6.842 eV in good agreement with the value of -6.82 eV of a graphic sheet of ZnO[126] and -7.52 eV by[112, 127]. The electronic properties observe of substitutional doped ZnONSs with the number, position and type of

dopant atoms and found that B, C and N atoms to give rise stable structure. The variation of binding energy per atom(BE)/dopant atom)of B_n-ZnONSs, C_n-ZnONSs and N_n-ZnONSs with number of dopant atoms as calculated with DFT study is plotted in Figure 3.5. The results indicate that the all structures of B_n-ZnONSs, C_n-ZnONSs, and N_n-ZnONSs (n=1-6) have negative binding energy, these shows that the systems are thermodynamically stable. The binding energies of B and N-doped ZnONSs are larger than those observed in the case of C-doped ZnONSs, which indicates that the doping systems can be more stable, whereas in cases of C-doped ZnONSs decreases linearly with doping dose of BE/atom compared to B and N. The binding energy per atom for single C atom resulted C_1-$Zn_{42}O_{41}$structurehas been found to be -3.864 eV that is more stable in this structure. For B_1-$Zn_{42}O_{41}$ and N_1-$Zn_{42}O_{41}$, the BE/atom values are -3.8366 and -3.839eV, respectively. Doping with two atoms of B and N resulted that B_2-$Zn_{42}O_{40}$ is more stable than N_2-$Zn_{42}O_{40}$.In B_5-$Zn_{42}O_{37}$and N_6-$Zn_{42}O_{36}$the BE/B and BE/N was found to be -3.7851 and -3.7541eV, respectively this implies that structures are in metastable state. These values indicate that B_5 and N_6 are more stable than other dopant. The BE/atom in case of B_6-$Zn_{42}O_{36}$and N_6-$Zn_{42}O_{36}$ are found -3.7929 and -3.7541eV, respectively. From the structure analysis it is found that the stability of ZnONSs strongly depends upon the type, position and number of dopant atoms in the sheet.

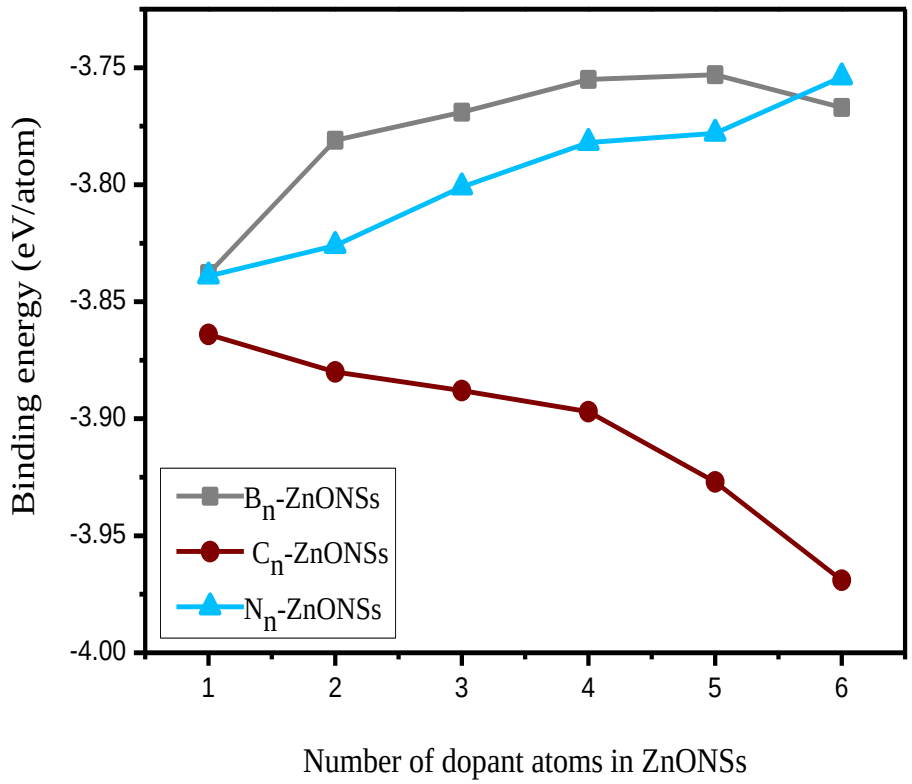

Figure 3.5: Variation of binding energy per atom of B_n-ZnONSs, C_n-ZnONSs, and N_n-ZnONSs with a number of dopants (n=1-6).

3.3.3 Total density of state (TDOS) and projected density of states (PDOS) of pure and doped ZnO nanosheet

After structural optimization, to analyze the distribution of each related orbital associated with the constituent element in doped ZnONSs. The total electronic density of states (TDOS) and projected density of state (PDOS) have studied for pure and doped ZnONSs is shown in Figure 3.6. The hybridization of bulk ZnO is sp^3while it is changed to sp^2 in the ZnONSs (graphene-like) structure, causing the valence and conduction bands to be near. Therefore, ZnONSs can exhibit very different electronic properties, when compared with the bulk ZnO.

In Figure 3.6, TDOS and PDOS from the contributions of different orbital components for each ZnONSs for left (valence band) and right (conduction band) are presented. We can see that the valence band are the distribution of ZnO for a mixture of Zn 3d and O 2p states, it can be seen that the valence band of ZnO can be divided into two regions: the lower part from about −8.5eV to −4.1eV and the upper part from about −4.1 to 0eV. Which the lower valence band is mainly contributed by Zn 3d states, while the upper part of valence band comes from O 2p states, whereas the conduction band of pristine ZnONSs mainly consists from 4s of Zn and 2p O orbitals. The peak of the electronic density of states appearing in -7 eV is provided by the 3d Zn and 2p O orbitals.

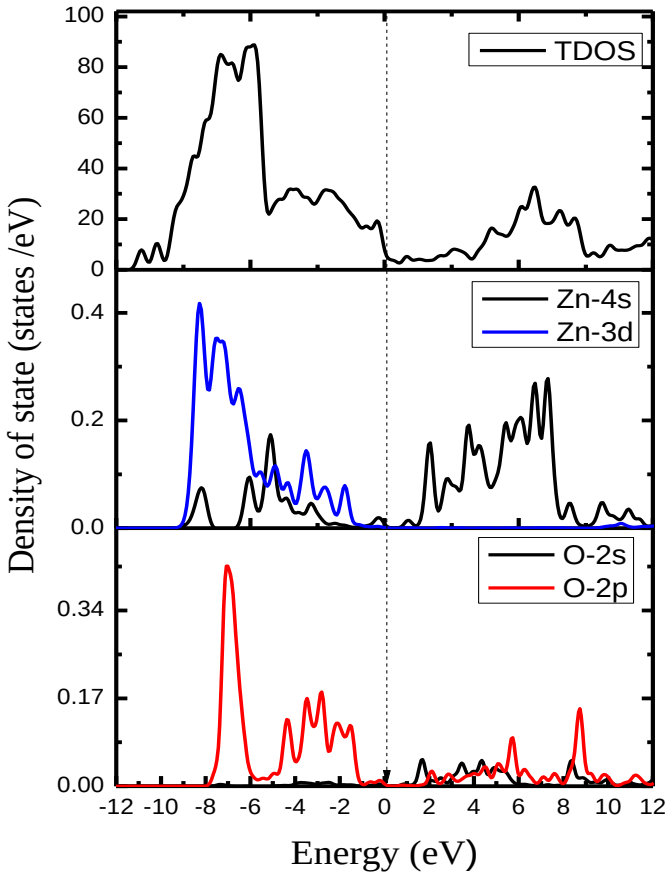

Figure 3.6: Total density of state (TDOS) and projected density of states (PDOS) for pure ZnO nanosheet. Fermi level is set at 0eV.

The total and projected DOS for the B dopant, one can see some differences in the PDOS of Zn atom compared to ZnONSs. Further analysis shows that the B 2p orbitals strongly hybridize with the O 2p orbitals and Zn 3d orbitals, the B 2p orbitals are located in the gap and are very small within the valence band; indicating that they bond more weakly to the Zn atom than O, the states of B atom are determined by 2p orbitals and it is near Fermi energy (E_F) are shown in Figure 3.7. The peak of the electronic density of states appearing in -7 eV is provided by the 3d Zn and 2p O while the peak of the electronic density of states in -8eV is supplied by 2s orbital of B

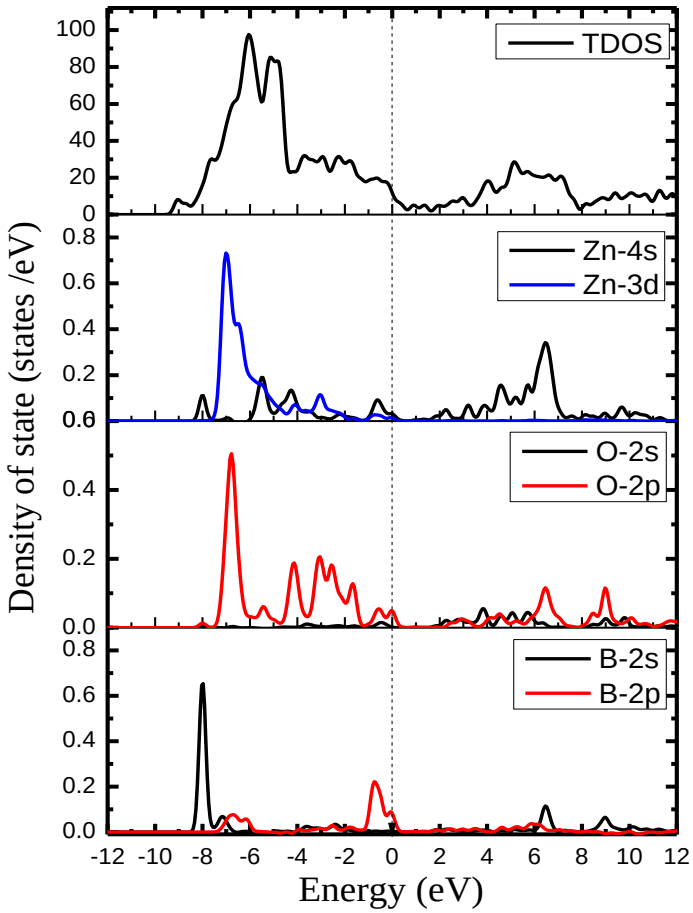

Figure 3.7: TDOS and PDOS for single boron atom doped ZnO nanosheet. Fermi level is set at 0eV.

Figure 3.8 shown TDOS and PDOS of the C 2p orbitals are located in the very small within the valence band, indicating the same p-p interaction and p-d exchange hybridization in C-doped ZnONSs films have been reported[127], therefore C 2p orbitals are relatively localized compared to O indicating a strong interaction between them. The hybridization of C 2p orbitals with the O 2p and Zn 3d orbitals are strongly an interaction between them. This interaction follows in actual fact from quantum mechanical level repulsion, which results in the clear splitting of the energy levels near E_F. The peak of the electronic density of states in -11.5eV is supplied by the 2s orbital of C atom.

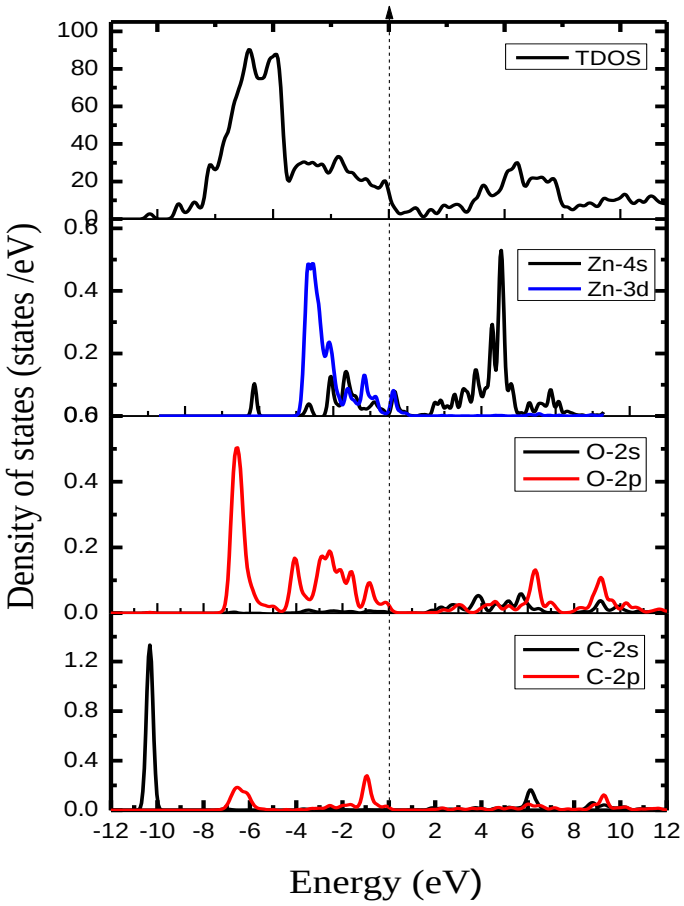

Figure 3.8: TDOS and PDOS for single carbon atom doped ZnO nanosheet. Fermi level is set at 0eV.

In the case N-doped ZnONSs, as shown in Figure 3.9 we found that N2p orbitals is hybridized strongly with the O 2p and Zn 3d orbitals, indicating a strong interaction between them. The hybridization between the N dopant, Zn and O atoms leads to the splitting of the energy level near E_F, as well as N is a deep acceptor with the transition level of 0.19eV that is close to 3.06eV in the former theoretical study. The 3s orbital of N atom in -11.5eV is supplied peak of the electronic density of states.

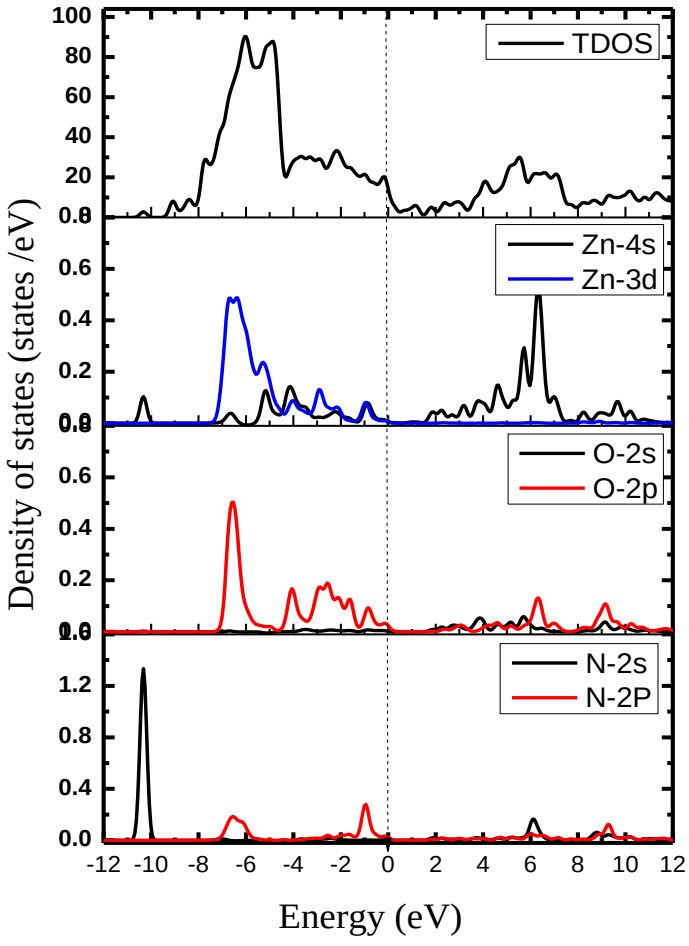

Figure 3.9: TDOS and PDOS for single nitrogen atom doped ZnO nanosheet. Fermi level is set at 0eV.

3.3.4 Total Energy and Energy gap

3.3.4.1 Boron doped Zinc Oxide nanosheet

Results were calculated using density functional theory of the total energy E_{total}; it is observed from Figure 3.10 that the total energy E_{total} of the B_n-ZnONSs structures was decreased with increasing the number of the B atom. Approximately, the E_{total} is linearly increasing with increasing the number of B the replace of O in the ZnONSs, because oxygen has been replaced by small energy boron atom.

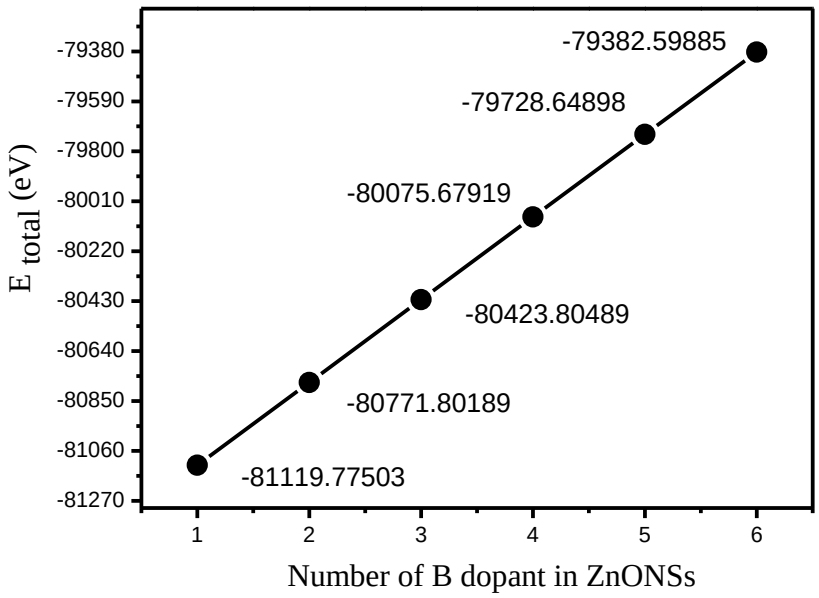

Figure 3.10: E_{total} in eV for boron doped ZnO nanosheet.

In chemical reactions, highest occupied molecular orbital (HOMO) and the lowest unoccupied molecular orbital (LUMO) play a very important role. The gap between HOMO and LUMO energy levels can be used to measure the kinetic stability of complexes. A large HOMO-LUMO gap corresponds to large kinetic stability as it is energetically not favorable to add electrons to a large lying LUMO or to remove electrons from a small lying HOMO.

Figure 3.11 show that the HOMO and LUMO energies of the B atoms doped ZnONSs. The values of the HOMO and LUMO energies depend on the number and position of the B atoms in ZnONSs. The lowest values of HOMO and LUMO energies, which O atoms means the replace of B atoms in ZnONSs changes the HOMO and LUMO energies. These results reflect the linear combination of atomic orbitals in the B and O atoms according to the basis sets that. The energy gap (E_g) gets through the difference between HOMO and LUMO.

In Figure 3.12, B-doped ZnONSs observed that the E_g decreases then increase with doping with an increase in the number of B atoms. This indicates the substitution doping more reactive and HOMO-LUMO gap refers to the stability of the molecule. In case doping with three and six B dopant atoms the less E_g are 0.021eVand 0.039eV, respectively and observed the system in this cases to be conductor.

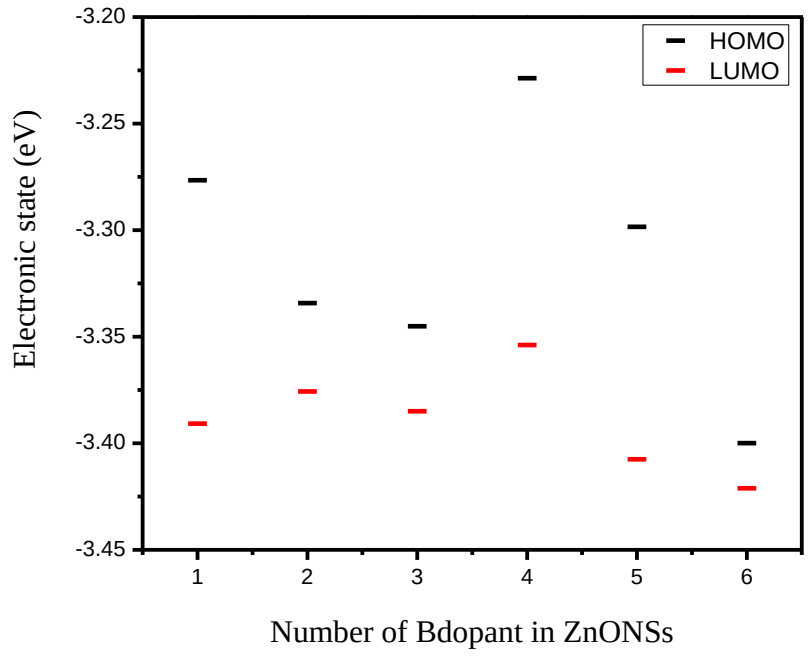

Figure 3.11: HOMO and LUMO in eV for Boron doped ZnO nanosheet.

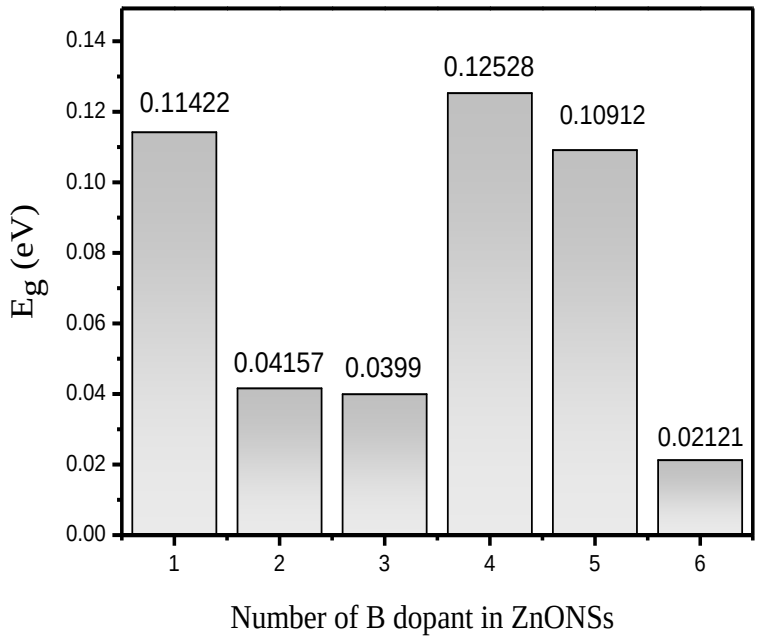

Figure 3.12: E_g in eV for boron doped ZnO nanosheet.

3.3.4.2 Carbon doped zinc oxide nanosheet

Figure 3.13 shows the behavior of E_{total} of a number of C atoms in ZnONSs that, the presence of carbon atoms in the middle of ZnONSs leads to increase the total energy of these structures. On the other hand, it appears that increasing the number of C atoms in the structure increases the total energy of the ZnONSs due to the energy oxygen atom has bigger of carbon atom.

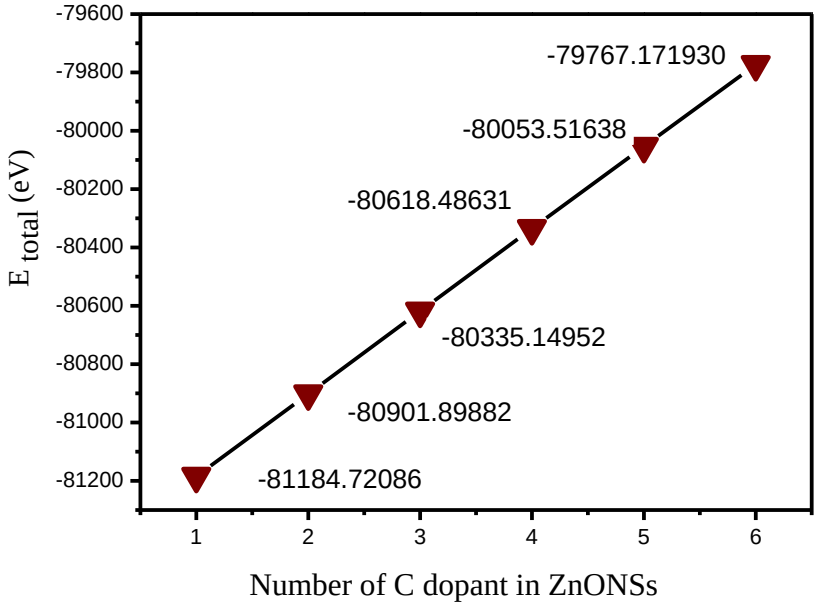

Figure 3.13: E_{total} in eV for Carbon doped ZnO nanosheet.

As shown in Figure 3.14 the energies HOMO and LUMO are affected depending on the number and position of the O atoms replaced with C atoms in ZnONSs, this change is due to the linear combination of atoms orbitals of different atoms in the structure, and therefore, leads to constructing new molecular orbitals in C_n-ZnONSs.

The calculated E_g of C-doped ZnONSs, it observed the bigger value of E_g is 0.051eV while the lowest value of E_g was being 0.021eV that indicates these structures have semiconducting properties. On the other hand, the E_g of the other two and four C atoms structures in ZnONSs have energy gap smaller and have conductor properties the other C in ZnONSs have small values of the energy gap in comparison with the pure ZnONSs, as shown in Figure 4.15.

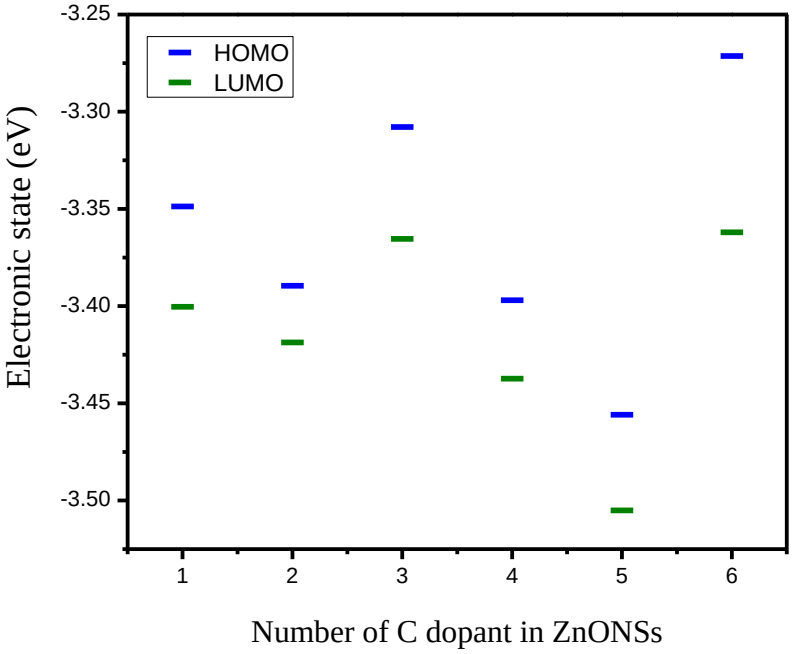

Figure 3.14: HOMO and LUMO in eV for carbon doped ZnO nanosheet.

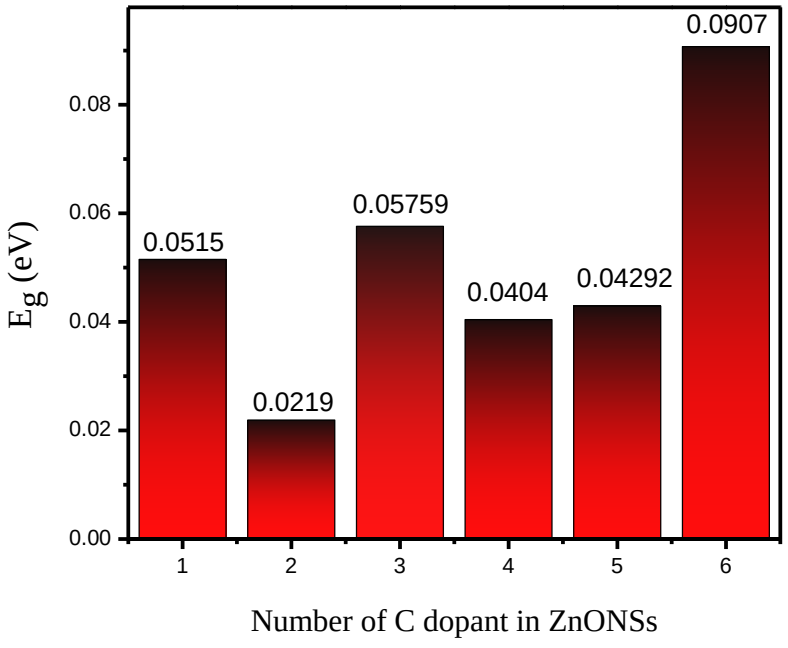

Figure 3.15: Eg in eV for carbon doped ZnO nanosheet.

3.3.4.3 Nitrogen doped zinc oxide nanosheet

Figure 3.16, indicates the E_{total} that increased with increasing the numbers of N atoms replaced in place of O atoms in ZnONSs.

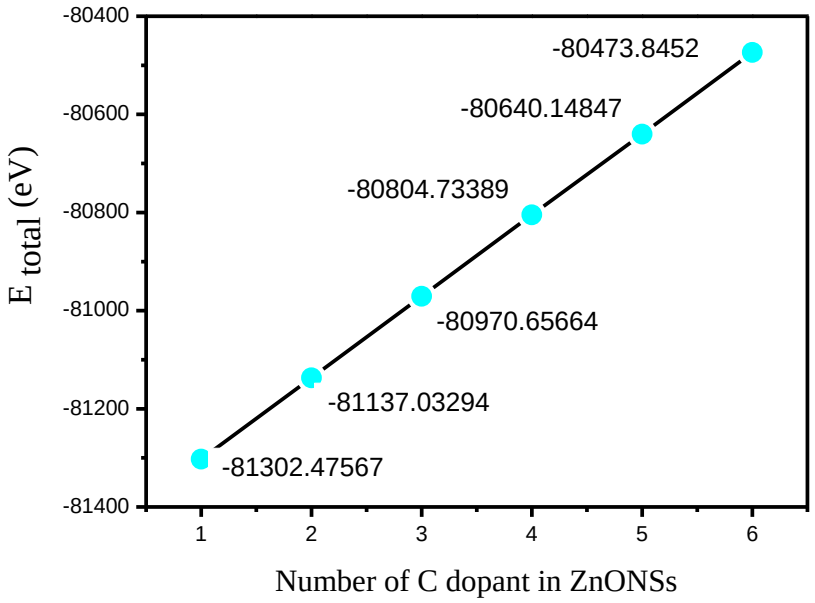

Figure 3.16: E_{total} in eV for nitrogen-doped ZnO nanosheet.

Through the Figures 3.17, the HOMO and LUMO energies are affected depending on the number and position of the N atoms which have been replaced by O atoms in ZnONSs. This change is due to the linear combination of atoms orbitals of different atoms in the structure. Therefore, leads to constructing new molecular orbitals in N_n-ZnONSs. With doping of N changes the energy gap when it was comparing with ZnONSs.

As seen in Figure 4.18.It is clear that the E_g have different values depending on the number and position of the N atoms. With two N atoms doped has a bigger value E_g= 0.087eV. While with three N atoms doped has the lowest value of E_g=0.0061eV that means these structure have conductor properties.

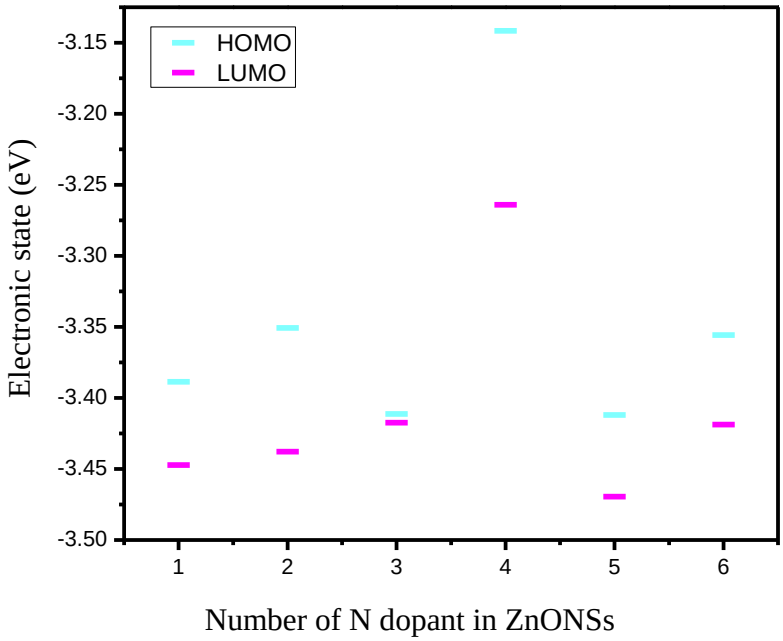

Figure 3.17: HOMO and LUMO in eV for Nitrogen doped ZnO nanosheet.

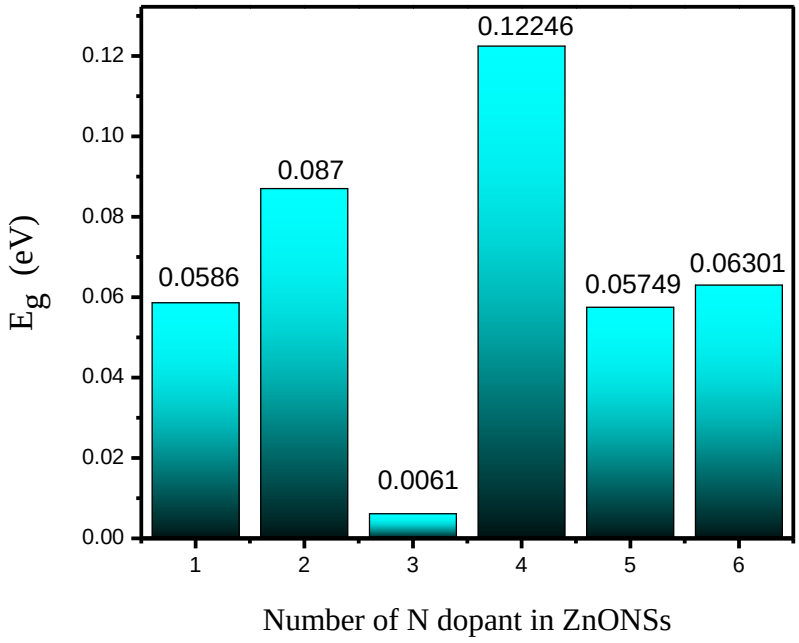

Figure 3.18: E_g in eV for nitrogen doped ZnO nanosheet.

3.3.5 Some Electronic Variables

To investigate the electronic properties, vertical ionization potential (VIP), vertical electron affinity (VEA), electronegativity (EN), and hardness (H) have calculated of doped ZnONSs with dopant atoms.

It is a fundamental property of molecules and is defined as the energy difference between an uncharged species and its negative ion. The anion, or negative ion, results from the addition of an electron from the vacuum to the neutral molecule[128], these parameters help to know the chemical reactivity of doped ZnONSs. Test calculations have performed on the B_2, C_2, and N_2 molecule, for B_2 calculated bond length, VIP and VEA are 1.45Å, 9.07eV, 0.471eV, respectively. While the C_2 molecule was finding bond length, VIP and VEA are1.36Å, 11.29eV, 1.879eV and N_2 molecule calculated bond length, VIP and VEA are 1.40Å, 12.94eV, 1.174eV respectively[109, 129] which are in agreement with reported values.

Variations of VIP and VAE for these complexes are shown in Table3.1. VIP in the begging for the B and C-doped ZnONSs is very close, in case six dopant atoms VIP of B and C decresing that it more reactive to electron donor. N-doped ZnONSs that the VIP upon relaxation changes 3.6718eV to 4.0270eV. Increasing the number of N atoms VIP is lightly increasing in case doped with two and six of N atoms. That means, these structures have high ability to acceptance electrons and becomes anions.

Increasing the number of boron and carbon dopant atoms observed there is an increase in VEA. As well as a bigger VEA for B_6-ZnONSs and C_6-ZnONSs are 3.4716 and 2.9361eV, respectively. For N dopants VEA gradually decrease with increasing number of nitrogen atoms between 2.9781eV and 2.5933eV and shows the similar trend for N

dopants. Broadly, one can say that electron affinity decreases with more substitutional N atoms. In general, the change in VIP and VAE one doping shows the electronic properties of ZnONSs have indeed modified and substitutional doping makes more reactive.

Table 3.2: Calculated vertical ionization potential (VIP) and vertical electron affinity (VAE) in eV for B, C and N doped ZnONSs.

Type of dopant ZnONSs	No. of	VIP(eV)	VAE(eV)
B_n-ZnONSs	**1**	3.7852	2.5925
	2	3.7738	2.6329
	3	3.7002	2.4947
	4	3.6022	2.4571
	5	3.6825	2.7943
	6	3.3456	3.4716
C_n-ZnONSs	**1**	3.7315	2.9007
	2	3.7895	2.7411
	3	3.7377	2.6805
	4	3.7099	2.7851
	5	3.9487	2.8525
	6	2.8444	2.9361
N_n-ZnONSs	**1**	3.6718	2.9781
	2	4.0487	2.7592
	3	3.8599	2.6978
	4	3.6423	2.6753
	5	3.9223	2.6364
	6	4.0270	2.5933

The EN of the B, C, and N are shown in Figure 3.19, the EN of the substitutional structures is bigger of the B and C due to the fact that B, C, N atoms have a smaller values of EN (2.04, 2.55 and 3.04) compression with O atoms have a larger EN (3.44eV) [130]. As well as, the type bond length between B-Zn, C-Zn and N-Zn is covalent bond. In cases of B_6-$Zn_{42}O_{36}$, C_5-$Zn_{42}O_{37}$and N_2-$Zn_{42}O_{40}$ structures have a bigger EN and its chemical effectiveness is very large, the distance between HOMO-LUMO is very small where there are no cases of large irritations.

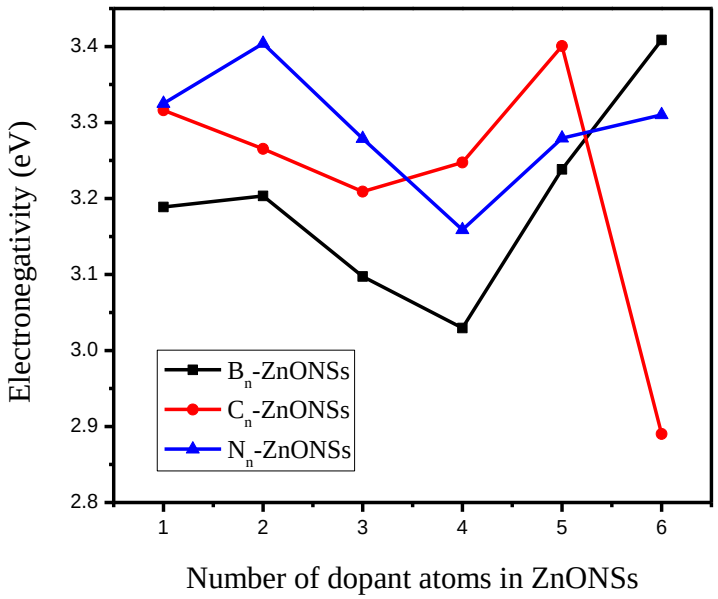

Figure 3.19: Electronegativity in eV for B, C, and N doped ZnO nanosheet.

Figure 3.20 represents the H value of B, C, and N doped in ZnONSs. H values decrease with increasing the number B and C atoms dopant. In cases B_5-$Zn_{42}O_{37}$, C_3-$Zn_{42}O_{39}$ and N_2-$Zn_{42}O_{40}$ structures high hardness due to the high energy gap. Whereas appear oscillates the H with an increasing the number of N atoms dopant, and that the decrease in hardness is due to increased cohesion and convergence between the

atoms and thus will reduce the interior areas and this indicates the characteristics of good mechanics

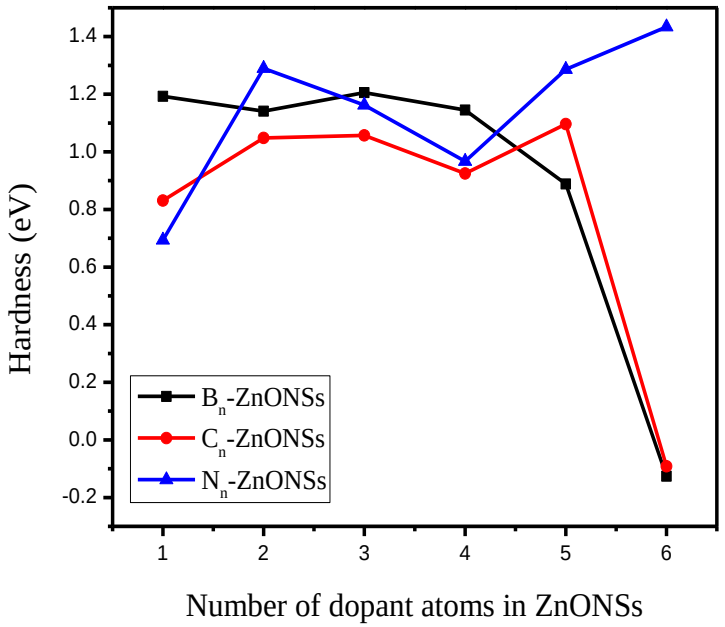

Figure 3.20: Hardness in eV for B, C, and N doped ZnO nanosheet.

3.4 second group

In this part, the results of aluminum, silicon, and phosphor doped Zinc Oxide nanosheet will be presented and discussed. The presence of aluminum, silicon, and phosphor in ZnO nanosheet has been described by earlier published reports.

In this thesis only Al, Si, P with Zn will be considered and geometric optimizations and electronic properties are calculated and evaluated. At first there will be a focus on the doped structures in ZnONSs, after a geometrical optimization of these structures is performed to calculate the bond length, total energy, energy HOMO, energy LUMO, binding energy and energy gap as well as some electronic variables the calculation are performed with a GGA to improve the existing values.

3.4.1 Structure properties of aluminum, silicon and phosphor doped zinc oxide nanosheet

The structural properties of doped ZnONSs have been investigated by DFT calculations. First, a full geometry optimization has performed then the impurities were introduced by substituting Al, Si and P atoms into the O atoms to create the doping atom. In Figure 3.21, shown the ground state structures of Al_n-ZnO (n=1-6). The bond length between the Al and nearest Zn is 2.12Å, it is clear that the Al-Zn is increased compared of the Zn-O bond of the ZnONSs which is in close agreement with the theoretical value 2.38Å[131] frequently quoted in literature. For fully Al doped ZnONSs the bond length Al-Al is 3.29Å in ZnONSs. In Figure 3.22, are shown Si doped ZnONSs, the bond length between the dopant Si and its nearest Zn atom is 2.09Å[132]. Si_2-$Zn_{42}O_{40}$ structure was resulting bond length Si-Si 3.28Å. In the same way, we doped the P atoms the relaxed structures of P_n-ZnO (n=1-6) are presented in Figure 4.3. The bond length of P-Zn in a relaxed structure is 2.10Å this value agreed well with the theoretical value is 2.18Å[23] P-P 3.2. It is clear that the Al-Zn, Si-Zn, P-Zn bond is censored compared to the Zn-O bond of the pristine ZnO. From the bond lengths, it is obvious that Si atom substitution expands the bond length with respect to the Zn-O bond of the pristine ZnO nanosheet. The possible reasons are shown as follows: First, as we know the different atomic radius between doping Al, Si, and P atoms and O atom. Second, due to the electronegativity difference between Al (1.5), P (2.1) and Si (1.9) and O (3.44), the attractive force between Si and O is larger than between O and Zn, so the bond length Zn-Si is larger than the Zn-O bond length.

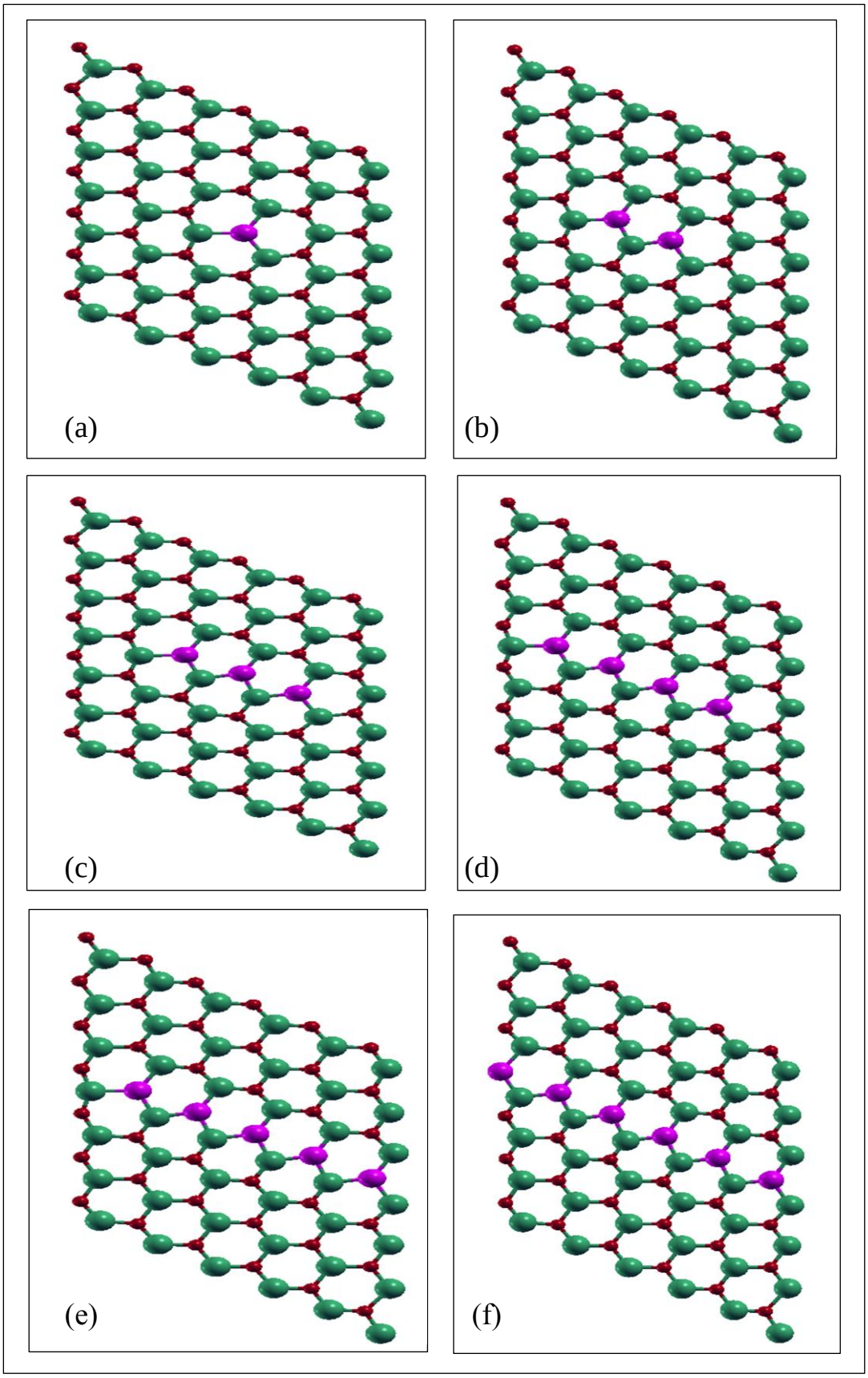

Figure 3.21(a-f): Optimize the structure of Al_n-ZnONSs (n=1-6), the red, green, and purple spheres refer to oxygen, zinc and the dopant Al atoms, respectively.

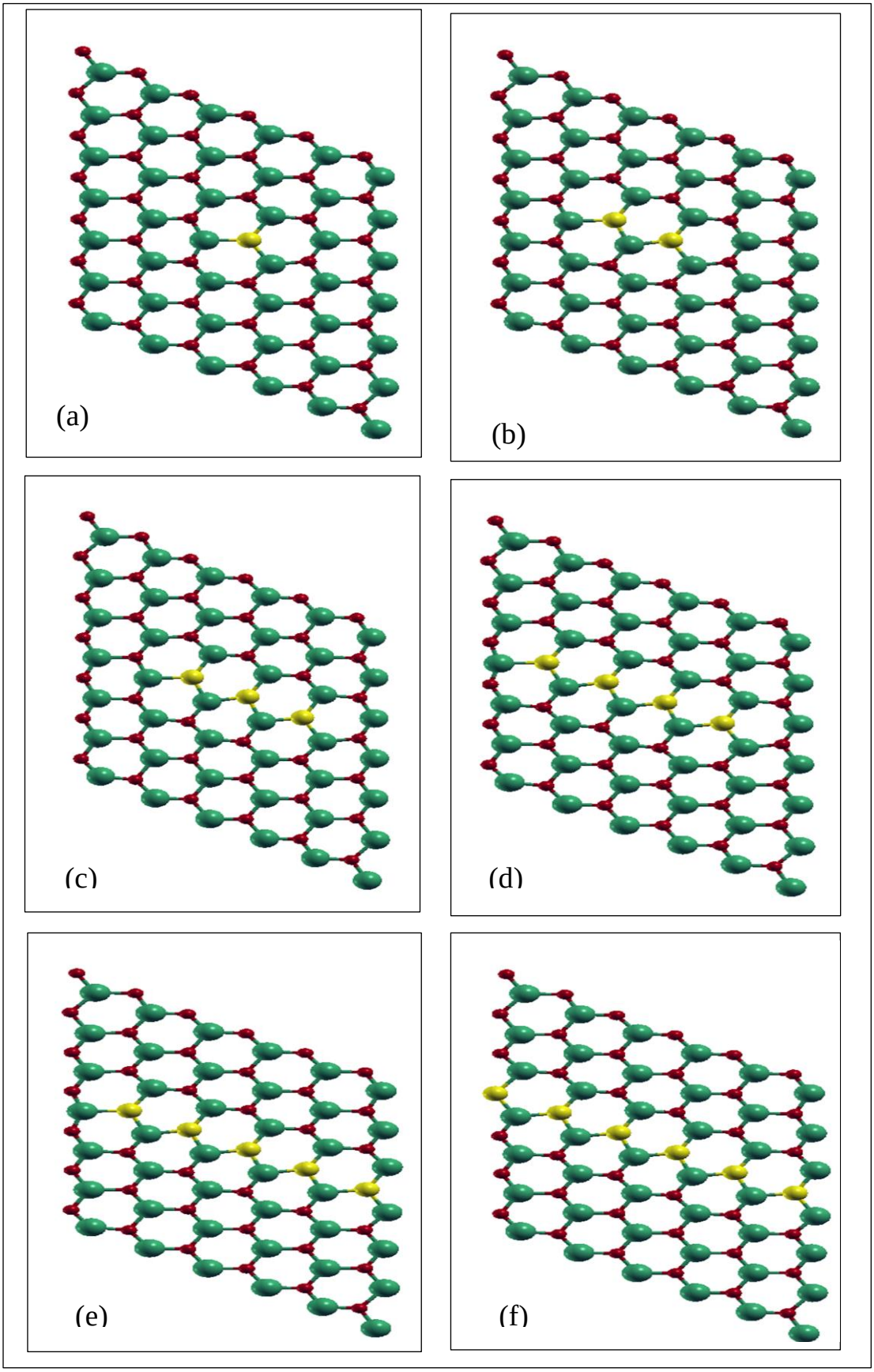

Figure 3.22(a-f): Optimize the structure of Si_n-ZnONSs (n= 1-6), the red, green and yellow spheres refer to oxygen, zinc, and the dopant Si atoms, respectively.

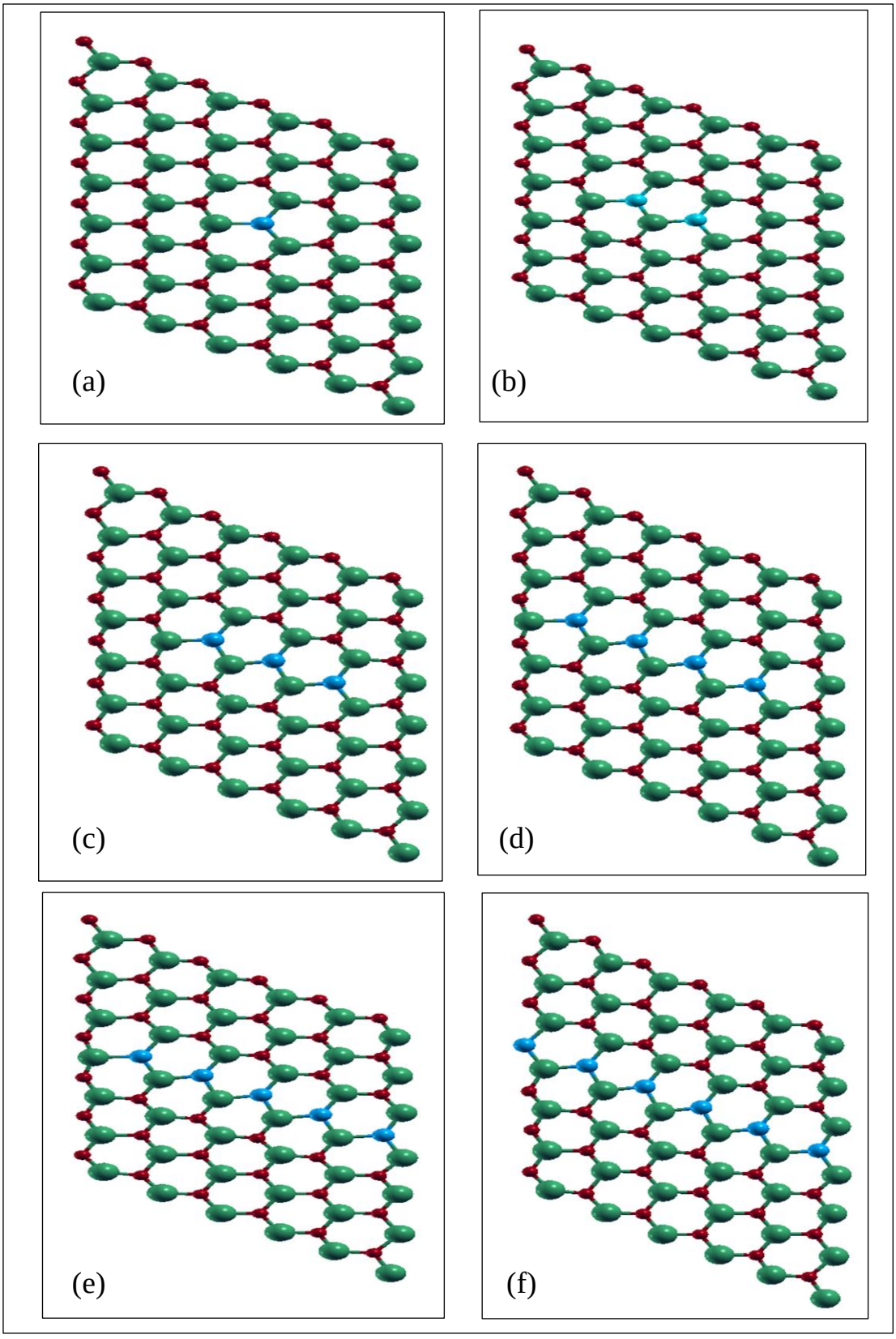

Figure 3.23(a-f): Optimize the structure of P_n-ZnONSs (n=1-6), the red, green, and cyan spheres refer to oxygen, zinc and the dopant P atoms, respectively.

The calculated first neighbour distance of the dopant atoms, d(X-Zn, X = Al, Si and P), are tabulated in Table 3.3.As seen from Table 3.3, in the Al substitution case the Al–Zn bond increases for six dopant atoms. In the Si substitution case Si–Zn bond increases by about for six dopant atoms and about for f6r dopant atoms with respect to the pure case. According to the present results d(X-Zn, X = Al, Si and P) is relatively larger for Al with respect to that of Si and P. The change in bond length with respect to the position and type of dopant is relatively larger. Al doping results are more sensitive to the cell.

Table 3.3: The bond length (d, in Å) of Al, Si and P doped ZnO nanosheet.

Configurations	$d(Al_O)$	$d(Si_O)$	$d(P_O)$
X_1-$Zn_{42}O_{41}$	2.12	2.09	2.10
X_2-$Zn_{42}O_{40}$	2.12	2.11	2.09
X_3-$Zn_{42}O_{39}$	2.10	2.10	2.10
X_4-$Zn_{42}O_{38}$	2.14	2.12	2.12
X_5-$Zn_{42}O_{37}$	2.13	2.12	2.08
X_6-$Zn_{42}O_{36}$	2.32	2.29	2.23

3.4.2 Binding energy of aluminum, silicon and phosphor doped zinc oxide nanosheet

For the optimized structures that are doped, we have studied the variation in binding energy of the doped systems. The binding energy BE per dopant atoms has been calculated to evaluate their stability using the equation (2.47).

Binding energy per dopant atom (BE/atom) has been plotted in Figure 3.24 (no. of Al atoms for green line, no. of Si atoms for blue line and no. of P atoms for black line). BE gives the precise data about the stability of the Al, Si, and P doped ZnONSs.

Hence, the BE observe a gradual increase by increasing the number of Al and Si dopant atoms, indicating that functionalized ZnONSs doped is more stable. While doping of single atom of P in the center of ZnONSs found it more stable compared with dopant Al and Si others.

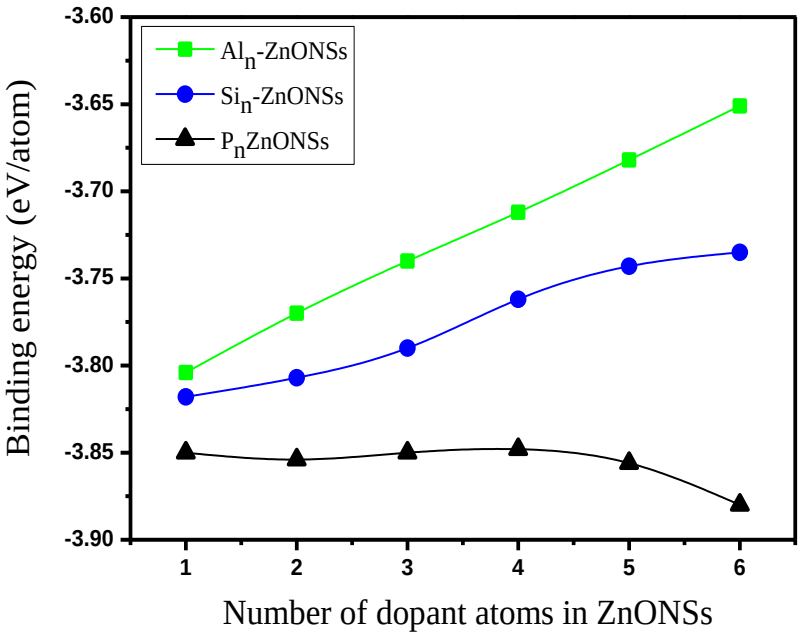

Figure 3.24: Variation of binding energy per atom of Al_n-ZnONSs, Si_n-ZnONSs, and P_n-ZnONSs with a number of dopants (n=1-6).

3.4.3 Total density of state (TDOS) and projected density of states (PDOS) of doped ZnONSs

The TDOS and PDOS for single Al-doped ZnONSs shown in Figure 3.25, can be seen that 3p orbit of Al atoms, the 2p orbit of a second neighboring O atom and 3d of a nearest neighboring Zn atoms calculated by GGA. It can be seen that lower valence band of ZnO is aroused by the 3d orbital of Zn atoms and 3s orbital of Al atom, while the conduction band part is mainly composed of the 3d orbitals and 4s orbital of Zn atoms and less amount of 2p O and 3p Al respectively. The peak of the electronic density of states appearing in -7 eV is provided by the 3d Zn, and 2p O while the peak of the electronic density of states 3s Al orbital in -7.2eV is supplied.

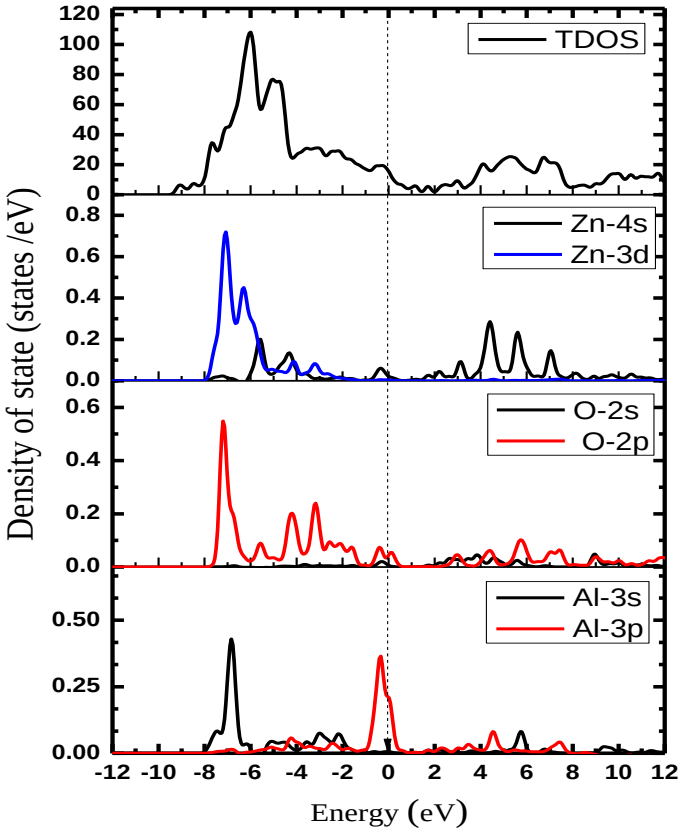

Figure 3.25: TDOS and PDOS for Al-doped ZnO nanosheet. The zero of the energy scale lies at the Fermi energy.

The total and projected DOS for the single Si dopant are shown in Figure 3.26, indicating the same p-p interaction and p-d exchange hybridization in C-doped ZnO films have been reported[26]. Further analysis shows that the Si 3p orbitals strongly hybridize with the O 2p orbitals and Zn 3d orbitals, the Si substitution creates the spin splitting by the Si 3p orbitals just above the top of the valence band, so substitutional Si dopant can induce the ZnO to n-type semiconductor[133], indicating that they bond more weakly to the Zn atom than O. the states of Si atom are determined by 3p orbitals and it is near Femi energy (E_F). The 3d Zn and 2p orbital of O in -7 eV appearing the peak of the electronic density of states while the peak of the electronic density of states is supplied -8.5eV of 3s orbital of Si.

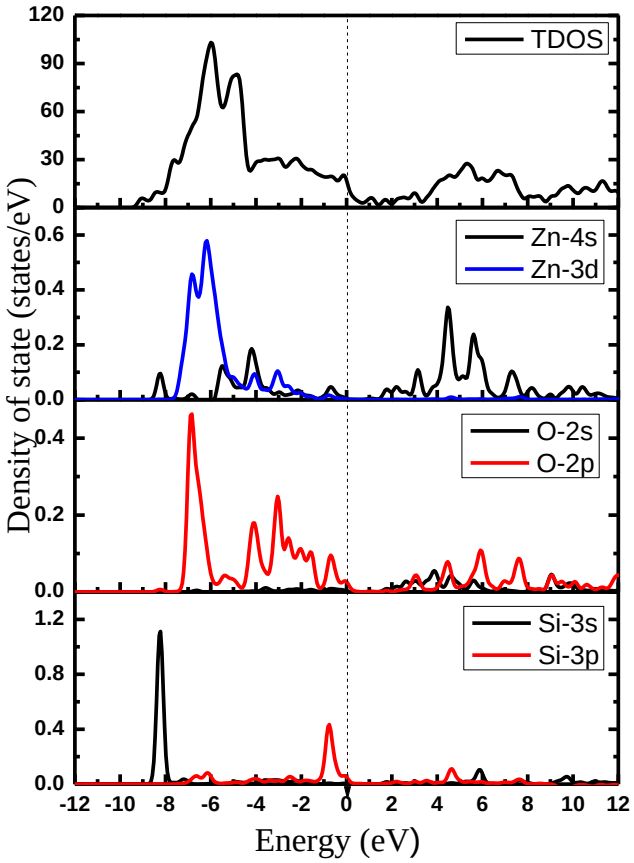

Figure 3.26: TDOS and PDOS for single Si doped ZnO nanosheet. The zero of the energy scale lies at the Fermi energy.

In Figure 3.27 TDOS and PDOS for single P atom doped ZnONSs, it is notable that both the 3p of P and 3d Zn orbitals are located in the Fermi energy level that there exists strong hybridization between the 3p orbital of P and 3d orbital of Zn. The TDOS from -8 to -0eV is derived largely from the 3d Zn, 2p O and 3s P orbitals. It shows a strong d orbital character and comes mostly from the Zn 3d orbital. The broad conduction bands between 0 and 4.5eV are mainly composed of 2p orbital of O which overlaps significantly with those of 3d P orbitals near energy Fermi, suggesting a strong interaction between them. The peak of the electronic density of states acting in -6.5eV is provided by the 3d Zn, and 2p O while 3s of P orbitals is supplied in -10eV.

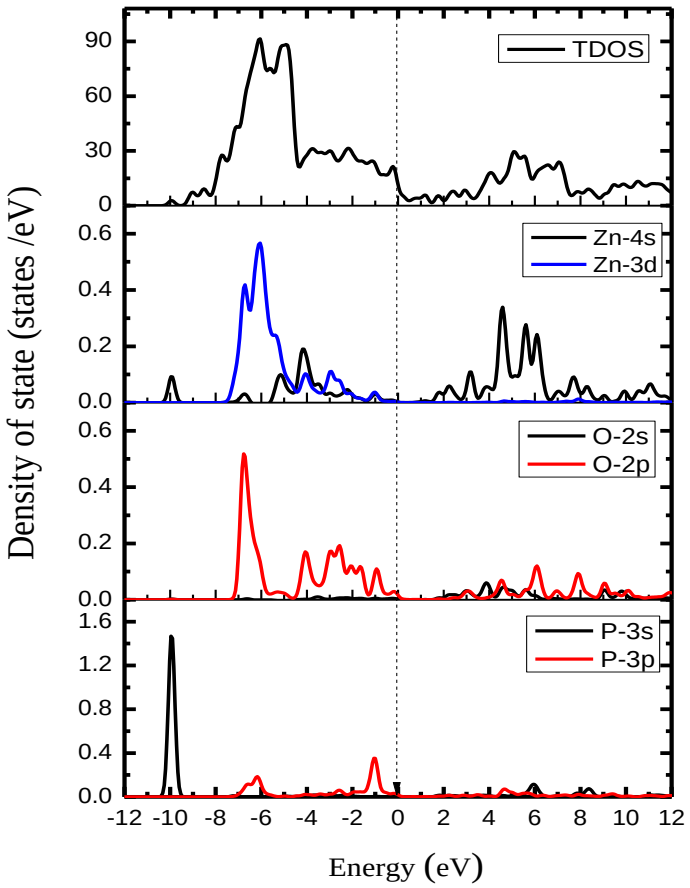

Figure 3.27: TDOS and PDOS for single P atom doped ZnO nanosheet. The zero of the energy scale lies at the Fermi energy.

3.4.4 Total Energy and Energy gap

3.4.4.1 Aluminum doped zinc oxide nanosheet

It is observed from Figure 3.28 that the total energy of Al-doped ZnONSs was increased with increasing the number of Al atom in ZnONSs. On the other hand, the total energy is linearly increasing due to the total energy of Al dopant atom have larger than O atom.

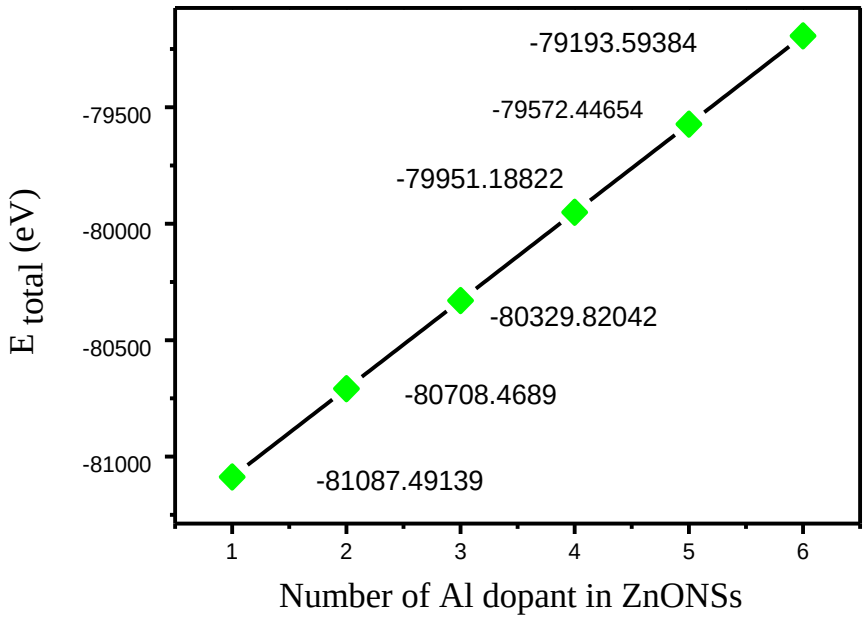

Figure 3.28: E_{total} in eV for Al doped ZnO nanosheet.

Figure 3.29 shows the energies of the HOMO and LUMO in eV of the Al-doped ZnONSs. E_{HOMO} and E_{LUMO} for each Al atoms dopant in ZnONSs change due to the linear combination atomic orbitals molecular orbital LCAO's-MO theory. Increasing the number of Al-doped in ZnONSs leads to change both HOMO and LUMO energies. The behavior of the energy gap (E_g) has been calculated at the GGA-PBE level as a function of the number of Al-doped ZnONSs.

Figure 3.30 shows the order of E_g value of the Al-doped ZnONSs. Increasing the number of Al-doped in the ZnONSs that shows the lowest

energy gap has 0.0657eV in case four atoms of Al. This is due to the fact that the electrons reside in the conduction band of a semiconductor and get full saturation. As well as increasing the energy gap, this global result indicates to obtain new electronic materials.

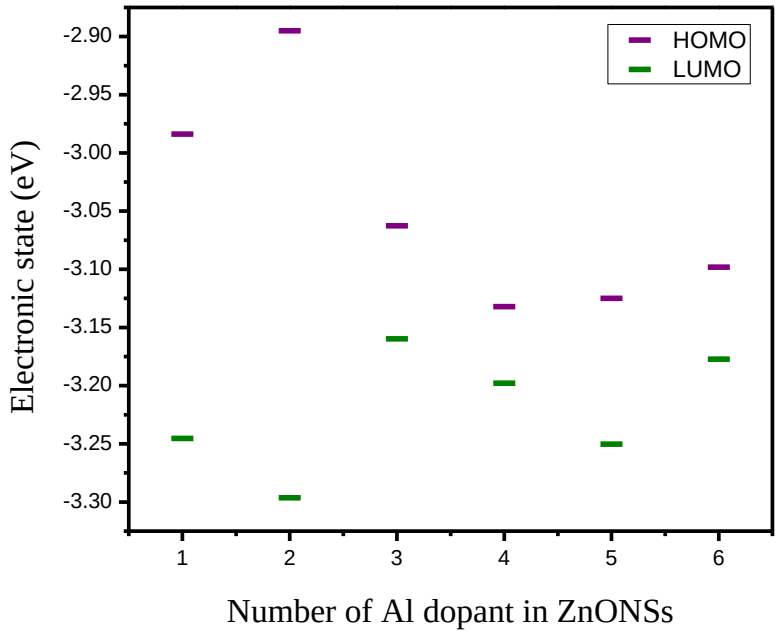

Figure 3.29: HOMO and LUMO in eV for Al doped ZnO nanosheet.

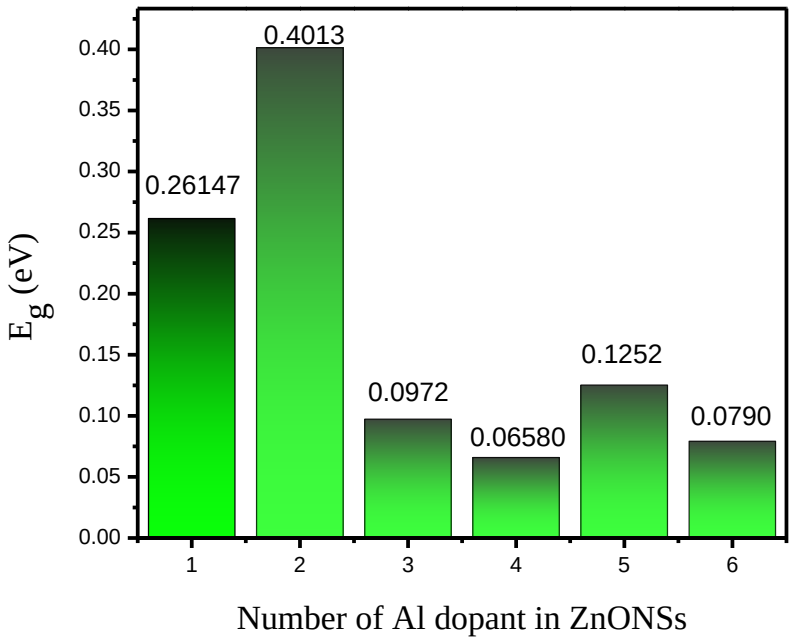

Figure 3.30: E_g in eV for Al doped ZnO nanosheet.

3.4.4.2 Silicon doped zinc oxide nanosheet

Figure 3.31 shows that the presence of silicon atoms doped in ZnONSs leads to a gradual increase in total energy when increased in substitution to the Si dopant. The total energy of the silicon atom is greater than the oxygen atom. On the other hand, it appears that the system is stable during the phases of doping silicon atoms

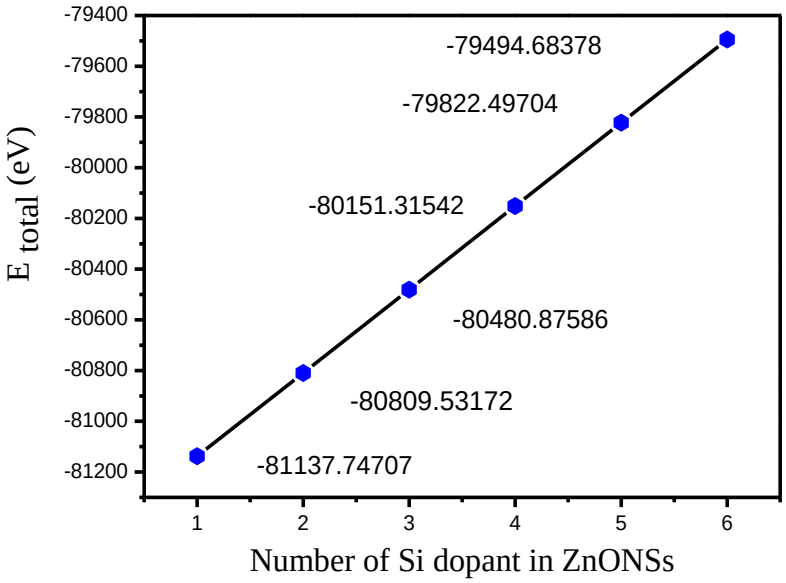

Figure 3.31: E_{total} in eV for Si doped ZnO nanosheet.

Figure 3.32 illustrated the HOMO and LUMO energies of Si-doped ZnONSs. As seen, the HOMO has inversely behavior than the LUMO. In six atoms of Si-doped ZnONSs have the higher HOMO energy and the lower LUMO energy, but the effect of the addition of Si atoms on HOMO is more than on LUMO. These results reflect the linear combination of atomic orbitals in both ZnONSs and Si an atom according to the basis sets that describe the individual components in the structure to construct the molecular orbitals.

The result of the energy gap (E_g) as shown in figure 3.33 observed E_g for one atom of silicon doped ZnONSs decreased while was increasing with adding the two atoms of silicon in ZnO. E_g decreased

from (0.076eV) for the three atoms of silicon to (0.049eV) for four atoms of silicon, and it decreased from (0.079eV) for six atoms of silicon. These results global gave molecular electronics important electronic applications and help to replace some O atoms instead of Si atoms in ZnONSs.

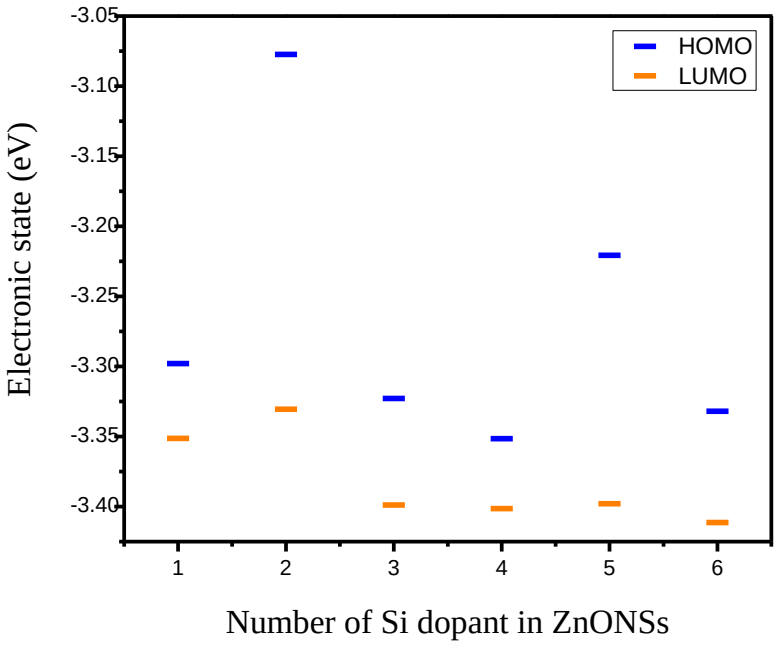

Figure 3.32: HOMO and LUMO in eV for Si doped ZnO nanosheet.

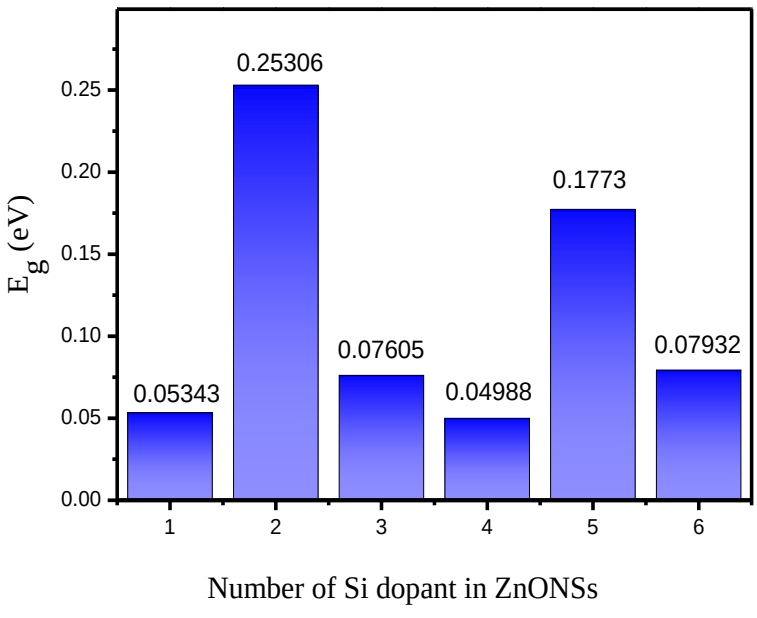

Figure 3.33: Eg in eV for Si doped ZnO nanosheet.

3.4.4.3 Phosphor doped zinc oxide nanosheet

As a general trend from the present results, the dopant atoms bigger total energy with increasing the numbers of P atoms replaced in place of O atoms in ZnONSs, the total energy is linearly increasing due to the total energy of Al dopant atom have larger than oxygen atom. as seen in Figure 3.34.

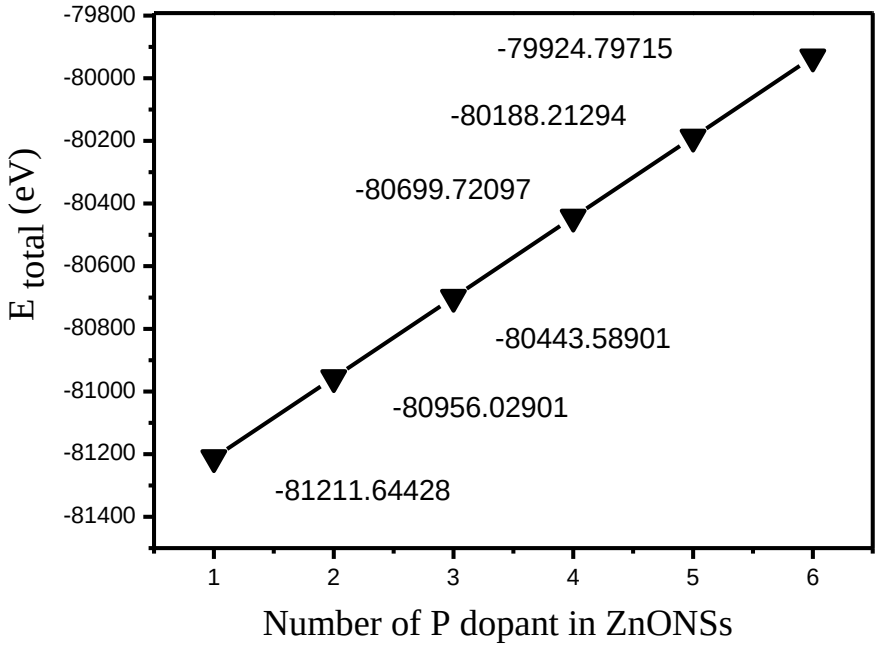

Figure 3.34: E_{total} in eV for P doped ZnO nanosheet.

Figure 3.35 shows that HOMO and LUMO energies are affected depending on the number of the P atoms in ZnONSs, and the presence of the P atoms in ZnONSs leads to change the electronic states of the structure. This change is due to construct new molecular orbitals result to the linear combination of atoms orbitals of different atoms in the structure.

The energy gap changes with doping of P, as seen in Figure 3.36. It is observed that the E_g indicates an increase from the doped two and five atoms of P-doped ZnONSs, and then decreases three after that it increases up six atoms of P. In both cases, note a sharp descent.

The reason for this is the results of addition dopant atoms obtain re-distribution of electrons in energy levels.

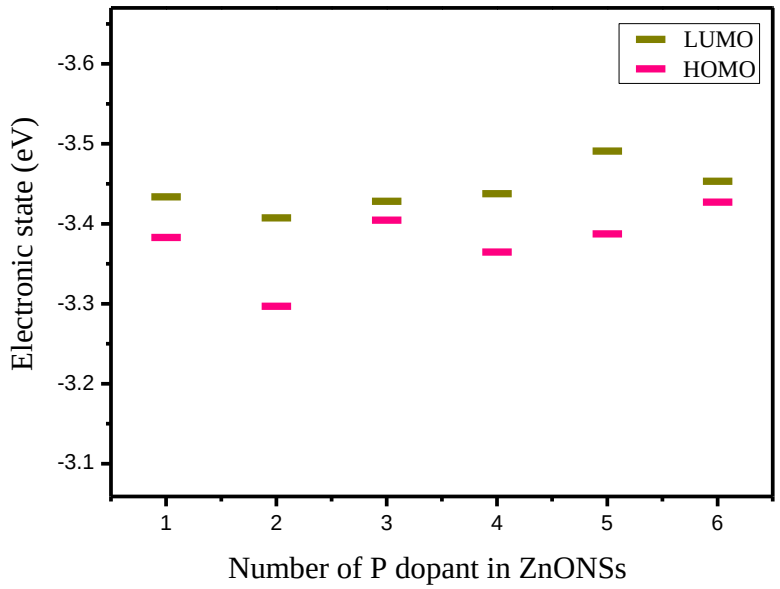

Figure 3.35: HOMO and LUMO in eV for P doped ZnO nanosheet.

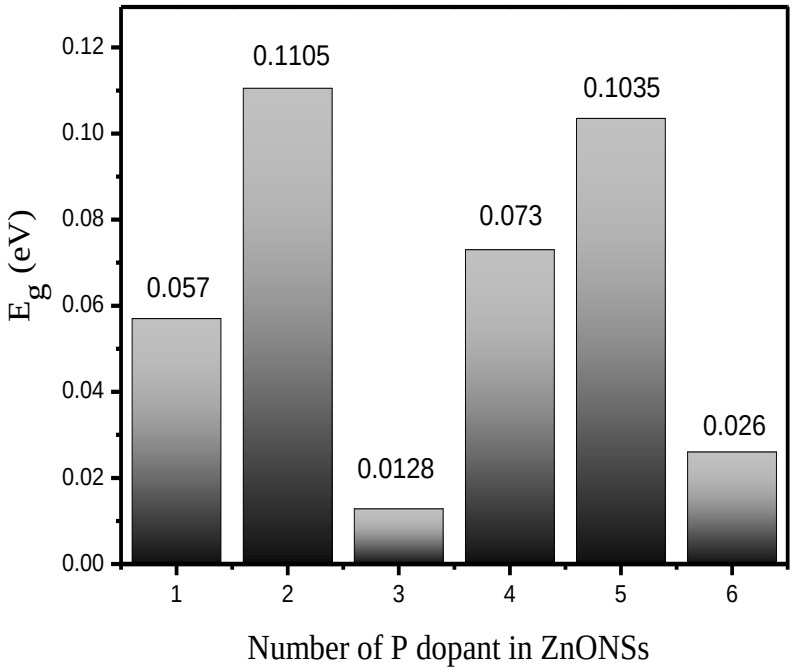

Figure 3.36: E_{total} in eV for P doped ZnO nanosheet.

3.4.5 Some Electronic Variables

Some electronic variables for aluminum, silicon and Phosphor doped zinc oxide nanosheet. These variables are calculated by gradient general approximation (GGA) according to the Kohn-Sham theorem. These variables include VIP, VEA, EN and H. bond length, VIP and VEA calculated for Al_2, Si_2, and P_2 molecules. For the Al_2 molecule the bond length Al-Al, VIP, and VEA were 1.45Å, 9.07eV and 0.471eV, respectively, while Si_2 molecule was finding bond length, VIP and VEA are 2.23Å, 7.55eV and 2.29eV, respectively[134-137] and P_2 molecule calculated P-P bond length, VIP, and VEA are 1.29Å, 10.465eV and 1.998eV, respectively[129] which are in agreement with reported values. The Vertical ionization potential (VIP) is illustrated in Table 3.4; the calculated values of VIP of the Al, Si, and P doped ZnONSs are smaller than that of the pure ZnONSs. These results indicate that the presence of Al, Si, and P in the middle of the ZnONSs rings gave the constructed ZnONSs the donor or acceptor of electrons to/from surrounding media. In the cases of Si and P observed that there is a slight stability with the increase of doping and then get decrease in Si_4-$Zn_{42}O_{38}$ and P_4-$Zn_{42}O_{38}$ then returns in increase. The VIP decreases due to the fact that the Si and P contain two and three electron in the secondary casing p, which facilitates the loss of this electron. In the case of Al the VIP was found to vary between 2.7096eV and 3.1408eV and take a form oscillatory. The VIP for p higher for Al and Si this is due to the secondary casing for P is saturated with more than that in the Al and Si.

Table (3.4) shows calculated VEA of doped ZnONSs for different Al, Si and P atoms. The VEA for Al and P dopant increasing with increased and takes oscillator for Si dopants that the dopant atom depends on type, position and number dopant. The lowest value of VEA at Al_1-$Zn_{42}O_{41}$, Si_3-$Zn_{42}O_{37}$ and P_2-$Zn_{42}O_{40}$ due to this structures a high

ability to acceptance electrons and becomes anions. The bigger VEA for Al_6-$Zn_{42}O_{36}$, Si_4-$Zn_{42}O_{38}$ and P_6-$Zn_{42}O_{36}$ structures is found to very 3.1519eV, 3.4051eV and 3.2586eV this indicates that ZnONSs is likely to be a good electron acceptor. So it can be used in applications such as photovoltaics as well as charge mobility and re-regulation energy.

Table 3.4: Calculated vertical ionization potential (VIP) and vertical electron affinity (VEA) in eV for aluminum, silicon and phosphor doped zinc oxide nanosheet.

Type of dopant ZnONSs	No. of	VIP(eV)	VAE(eV)
Al_n-ZnONSs	**1**	2.7096	2.5971
	2	3.0156	2.8871
	3	0.0072	2.9236
	4	3.2966	3.1010
	5	3.3406	3.0941
	6	3.1408	3.1519
Si_n-ZnONSs	**1**	3.3640	3.1239
	2	3.3437	3.0328
	3	3.3162	2.1056
	4	2.9617	3.4051
	5	3.5841	2.9646
	6	3.8580	2.613
P_n-ZnONSs	**1**	3.7262	3.0911
	2	3.8835	2.8300
	3	3.8054	2.9088
	4	3.5327	3.1790
	5	3.9349	3.1101
	6	3.9496	3.2586

In Figure 3.37 are shown the EN of the Al, Si and P, The values EN of Al and Si doped take an oscillating behavior. In cases Al_3-$Zn_{42}O_{39}$ and Si_3-$Zn_{42}O_{39}$ small values in EN due to the distance between HOMO-LUMO is very small and covalent bond is very exile between Zinc and dopant. the fact that Al, Si and P atoms have a smaller values of EN (1.61, 1.90 and 2.19) compression with O atoms have a larger EN (3.44eV)[130]. While the EN of P gradually increases during doping stages as well as, the type bond length between Al-Zn, Si-Zn and P-Zn is covalent bond. In cases of Al_4-$Zn_{42}O_{38}$, Si_4-$Zn_{42}O_{38}$ and P_6-$Zn_{42}O_{36}$, N_2-$Zn_{42}O_{40}$ structures have bigger values of EN and its chemical effectiveness is very large.

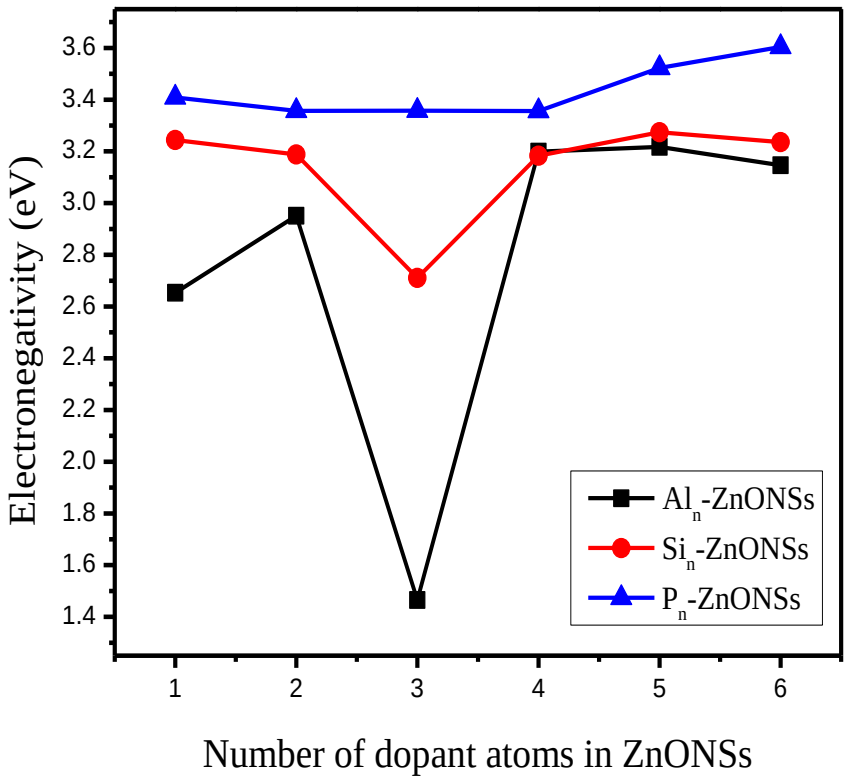

Figure 3.37: Electronegativity in eV for Al, Si, and P doped ZnO nanosheet.

The influences of the presence of M-doped (M= Al, Si, P) atoms in replace of O atoms on the hardness (H) a plot of the variation of H with number of atoms is shown in Figure 3.38. When Al_3, Si_4 and P_4 atoms are doped, there is smaller H these results agree with small energy gap and excitation energy. In case atoms of Al_2-$Zn_{42}O_{40}$, Si_6-$Zn_{42}O_{36}$ and P_2-$Zn_{42}O_{40}$ observed bigger values of H, this is due to reduce the coherence and convergence between the atoms and thus will increase interior spaces

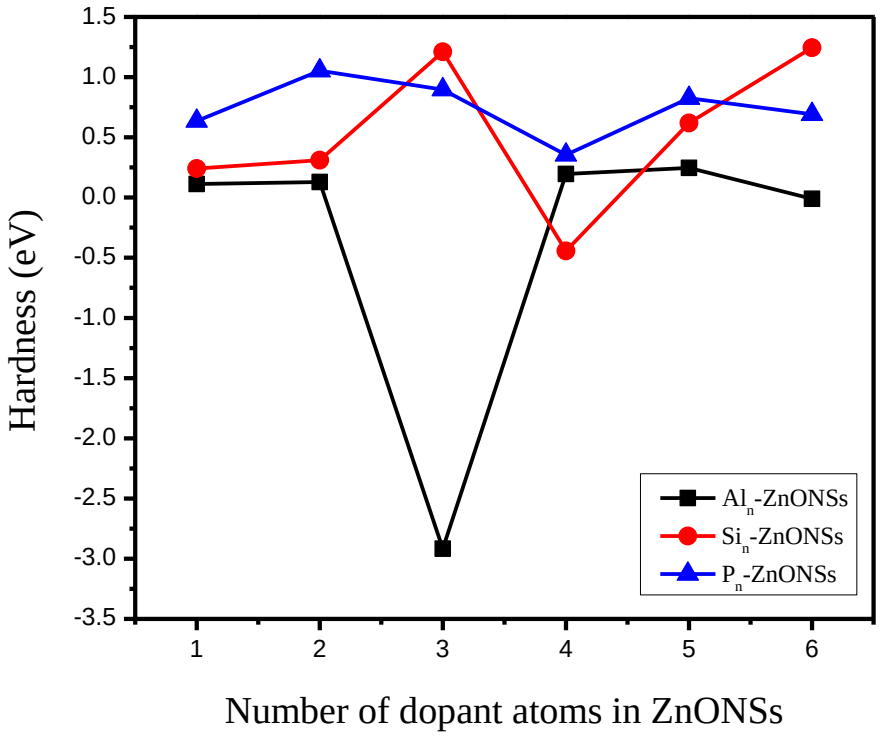

Figure 3.38: Hardness in eV for Al, Si, and P doped ZnO nanosheet.

CHAPTER 4: CONCLUSION

4.1 Conclusion

In this study, all calculations are carried out and analysis by using the SIESTA program based on density functional theory. SIESTA program which is allowed standard calculation for systems with a large number of atoms and it uses norm-conserving pseudopotentials. A study of various modifications in ZnONSs focused by chemical doping (substitutional) of two horizontal series of periodic table elements are B, C, N, Al, Si, and P atoms. The structural and electronic properties have been investigated of pure ZnONSs and the effect of substitutionally doping with a different number of atoms in ZnONSs based on the *ab-intio* calculation in a detail. The electronic properties included vertical ionization potential (VIP), vertical electron affinity (VAE), HOMO-LUMO energies, energy gap, electronegativity (EN), and hardness (H) for doped ZnONSs have been calculated in this study.

From the results, one can be concluded the following

1. Good relax done for the pure ZnONSs, the geometrical parameters bond lengths and bond angles calculated from DFT. It has been found that B and P atom substitution expands the bond length with respect to pristine sheets good agreement with experimental data.
2. The substitution atoms have been replaced on the oxygen site; all the calculations have been repeated for different dopant atoms. The binding energy per atom of B and Al atoms is more stable than other doped.
3. The DFT calculations presented the good result of total energies of all studied systems calculated from the summation of the total

energies of the components for each structure. The total energy of the ZnONSs increased with increasing number of dopant atoms.

4. The energy gap of ZnO nanosheets decreases gradually along with dopant ions occupying O sites; these structures have different values of energy gap depending on the number and position of the dopant atoms in the structure of ZnONSs. Some of these structures have conducting applications.

5. Ionization potential and vertical electron affinity for B and Al doping and has donor level at 3.3eV. On the other hand, for the N and P doped ZnO nanosheet has acceptor level at 4.0eV. The electronegativity increased for N and P doped and hardness decreased for B, C and Al doped that is shown more energetic favorable.

4.2 Suggestions for future works

When working on a project within a limited time period one isn't able to perform all the calculations but the presented topics in this thesis have to a large extent been studied comprehensively. The topics which are suggested to be considered further:

1. Study of the structural and electronic properties of ZnONSs doped B, C, N, Al, Si, and P with replacing Zn atoms by considering different doping locations for the same concentration of dopant and with different widths: DFT.

2. Study of the electrical and thermal properties of the pure and doped ZnONSs

3. Study of the optical and spectrum properties of pure and doped ZnONSs.

References

[1] Z. Fan, J.G. Lu, Zinc oxide nanostructures: synthesis and properties, Journal of nanoscience and nanotechnology, **5** (2005) 1561.
[2] A. Janotti, C.G. Van de Walle, Fundamentals of zinc oxide as a semiconductor, Reports on progress in physics, **72** (2009) 126501.
[3] D. Wu, Z. Bai, K. Jiang, Temperature induced hierarchical growth of ZnO microcrystal, Materials Letters, **63** (2009) 1057.
[4] A. Sekar, S. Kim, A. Umar, Y. Hahn, Catalyst-free synthesis of ZnO nanowires on Si by oxidation of Zn powders, Journal of crystal growth, **277** (2005) 471.
[5] Z.L. Wang, Zinc oxide nanostructures: growth, properties and applications, Journal of Physics: Condensed Matter, **16** (2004) R829.
[6] Ü. Özgür, Y.I. Alivov, C. Liu, A. Teke, M. Reshchikov, S. Doğan, V. Avrutin, S.-J. Cho, H. Morkoc, A comprehensive review of ZnO materials and devices, Journal of Applied Physics, **98** (2005) 11.
[7] Z.L. Wang, Nanostructures of zinc oxide, Materials today, 7 (2004) 26.
[8] S. Kishwar, K.u. Hasan, G. Tzamalis, O. Nur, M. Willander, H. Kwack, D.L.S. Dang, Electro-optical and cathodoluminescence properties of low temperature grown ZnO nanorods/p-GaN white light emitting diodes, physica status solidi (a), **207** (2010) 67.
[9] K. Ul Hasan, N. Alvi, J. Lu, O. Nur, M. Willander, Single nanowire-based UV photodetectors for fast switching, Nanoscale research letters, **6** (2011) 348.
[10] U. Rössler, Energy bands of hexagonal II-VI semiconductors, Physical review, **184** (1969) 733.
[11] B. Meyer, Alves, H, D. Hofmann, W. Kriegseis, D. Forster, F. Bertram, J. Christen, A. Hoffmann, M. Straßburg, M. Dworzak, Bound exciton and donor–acceptor pair recombinations in ZnO, physica status solidi (b), **241** (2004) 231.
[12] D. Vogel, P. Krüger, J. Pollmann, Ab initio electronic-structure calculations for II-VI semiconductors using self-interaction-corrected pseudopotentials, Physical Review B, **52** (1995) R14316.
[13] V. Coleman, C. Jagadish, Basic properties and applications of ZnO, in: Zinc oxide bulk, thin films and nanostructures, Elsevier, 2006, p. 1.
[14] S.Y. Zhou, G.-H. Gweon, A. Fedorov, P. First, de, W. De Heer, D.-H. Lee, F. Guinea, A.C. Neto, A. Lanzara, Substrate-induced bandgap opening in epitaxial graphene, Nature materials, **6** (2007) 770.
[15] K. Matsubara, P. Fons, K. Iwata, A. Yamada, K. Sakurai, H. Tampo, S. Niki, ZnO transparent conducting films deposited by pulsed laser deposition for solar cell applications, Thin Solid Films, **431** (2003) 369.

[16] B. Paul, B. Singh, S. Ghosh, A. Roy, A comparative study on electrical and optical properties of group III (Al, Ga, In) doped ZnO, Thin Solid Films, **603** (2016) 21.
[17] M. Mazilu, N. Tigau, V. Musat, Optical properties of undoped and Al-doped ZnO nanostructures grown from aqueous solution on glass substrate, Optical materials, **34** (2012) 1833.
[18] Y.-C. Peng, C.-C. Chen, H.-C. Wu, J.-H. Lu, First-principles calculations of electronic structure and optical properties of Boron-doped ZnO with intrinsic defects, Optical materials, **39** (2015) 34.
[19] D. Sun, C. Tan, X. Tian, Y. Huang, Comparative Study on ZnO Monolayer Doped with Al, Ga and In Atoms as Transparent Electrodes, Materials, **10** (2017) 703.
[20] X.-Y. Feng, Z. Wang, C.-W. Zhang, P.-J. Wang, Electronic structure and energy band of IIIA doped group ZnO nanosheets, Journal of Nanomaterials, **2013** (2013) 61.
[21] F.-b. Zheng, C.-w. Zhang, P.-j. Wang, H.-x. Luan, First-principles prediction of the electronic and magnetic properties of nitrogen-doped ZnO nanosheets, Solid State Communications, **152** (2012) 1199.
[22] U. Wahl, E. Rita, J. Correia, A. Marques, E. Alves, J. Soares, I. collaboration, Direct evidence for As as a Zn-site impurity in ZnO, Physical review letters, **95** (2005) 215503.
[23] H. Kökten, Ş. Erkoç, X-Doped (X= C, N, F, P) ZnO Sheet: Density Functional Theory Calculations, Journal of Computational and Theoretical Nanoscience, **12** (2015) 395.
[24] Y. Xue, X. Yang, L. Li, Q. Song, First-principles calculations of electronic structure and optical properties of boron–phosphorus co-doped zinc oxide, Materials Science in Semiconductor Processing, **30** (2015) 406.
[25] H.J. Fan, B. Fuhrmann, R. Scholz, C. Himcinschi, A. Berger, H. Leipner, A. Dadgar, A. Krost, S. Christiansen, U. Gösele, Vapour-transport-deposition growth of ZnO nanostructures: switch between c-axial wires and a-axial belts by indium doping, Nanotechnology, **17** (2006) S231.
[26] M.C. Roco, C.A. Mirkin, M.C. Hersam, Nanotechnology research directions for societal needs in 2020: summary of international study, in, Springer, 2011.
[27] I.P. Kaur, V. Kakkar, P.K. Deol, M. Yadav, M. Singh, I. Sharma, Issues and concerns in nanotech product development and its commercialization, Journal of Controlled Release, **193** (2014) 51.
[28] L.A. DeLouise, Applications of nanotechnology in dermatology, Journal of Investigative Dermatology, **132** (2012) 964.
[29] S.K. Arora, R.W. Foley, J. Youtie, P. Shapira, A. Wiek, Drivers of technology adoption—the case of nanomaterials in building

construction, Technological Forecasting and Social Change, **87** (2014) 232.
[30] S. Chattopadhyay, L.-C. Chen, K.-H. Chen, Energy production and conversion applications of one-dimensional semiconductor nanostructures, NPG Asia Materials, **3** (2011) 74.
[31] A.P. Alivisatos, Perspectives on the physical chemistry of semiconductor nanocrystals, The Journal of Physical Chemistry, **100** (1996) 13226.
[32] Y. Zhang, M.K. Ram, E.K. Stefanakos, D.Y. Goswami, Synthesis, characterization, and applications of ZnO nanowires, Journal of Nanomaterials, **2012** (2012) 20.
[33] W. Zhao, X. Song, Z. Yin, C. Fan, G. Chen, S. Sun, Self-assembly of ZnO nanosheets into nanoflowers at room temperature, Materials Research Bulletin, **43** (2008) 3171.
[34] D. Liu, W. Wu, Y. Qiu, S. Yang, S. Xiao, Q.-Q. Wang, L. Ding, J. Wang, Surface functionalization of ZnO nanotetrapods with photoactive and electroactive organic monolayers, Langmuir, **24** (2008) 5052.
[35] Z.L. Wang, ZnO nanowire and nanobelt platform for nanotechnology, Materials Science and Engineering: R: Reports, **64** (2009) 33.
[36] L. Schmidt-Mende, J.L. MacManus-Driscoll, ZnO–nanostructures, defects, and devices, Materials today, **10** (2007) 40.
[37] T. Sahoo, S.K. Nayak, P. Chelliah, M.K. Rath, B. Parida, Observations of two-dimensional monolayer zinc oxide, Materials Research Bulletin, **75** (2016) 134.
[38] A. He, X. Wang, R. Wu, Y. Lu, Y. Feng, Adsorption of an Mn atom on a ZnO sheet and nanotube: A density functional theory study, Journal of Physics: Condensed Matter, **22** (2010) 175501.
[39] S.Z. Butler, S.M. Hollen, L. Cao, Y. Cui, J.A. Gupta, H.R. Gutiérrez, T.F. Heinz, S.S. Hong, J. Huang, A.F. Ismach, Progress, challenges, and opportunities in two-dimensional materials beyond graphene, ACS nano, **7** (2013) 2898.
[40] T. Sasaki, M. Watanabe, H. Hashizume, H. Yamada, H. Nakazawa, Macromolecule-like aspects for a colloidal suspension of an exfoliated titanate. Pairwise association of nanosheets and dynamic reassembling process initiated from it, Journal of the American Chemical Society, **118** (1996) 8329.
[41] V. Nicolosi, M. Chhowalla, M.G. Kanatzidis, M.S. Strano, J.N. Coleman, Liquid exfoliation of layered materials, Science, **340** (2013) 1226419.
[42] F. Claeyssens, C.L. Freeman, N.L. Allan, Y. Sun, M.N. Ashfold, J.H. Harding, Growth of ZnO thin films—experiment and theory, Journal of Materials Chemistry, **15** (2005) 139.

[43] C. Tusche, H. Meyerheim, J. Kirschner, Observation of depolarized ZnO (0001) monolayers: formation of unreconstructed planar sheets, Physical review letters, **99** (2007) 026102.
[44] G. Weirum, G. Barcaro, A. Fortunelli, F. Weber, R. Schennach, S. Surnev, F. Netzer, Growth and surface structure of zinc oxide layers on a Pd (111) surface, The Journal of Physical Chemistry C, **114** (2010) 15432.
[45] A. Tsukazaki, M. Kubota, A. Ohtomo, T. Onuma, K. Ohtani, H. Ohno, S.F. Chichibu, M. Kawasaki, Blue light-emitting diode based on ZnO, Japanese Journal of Applied Physics, **44** (2005) L643.
[46] M. Law, L.E. Greene, J.C. Johnson, R. Saykally, P. Yang, Nanowire dye-sensitized solar cells, Nature materials, **4** (2005) 455.
[47] K. Maeda, T. Takata, M. Hara, N. Saito, Y. Inoue, H. Kobayashi, K. Domen, GaN: ZnO solid solution as a photocatalyst for visible-light-driven overall water splitting, Journal of the American Chemical Society, **127** (2005) 8286.
[48] L. Irimpan, V. Nampoori, P. Radhakrishnan, Spectral and nonlinear optical characteristics of ZnO nanocomposites, Science of Advanced Materials, **2** (2010) 117.
[49] H. Wang, H. Huang, B. Wang, Effect of Mn substitution for Fe in multiferroic BiFeO3: a first-principles study, Science of Advanced Materials, **2** (2010) 184.
[50] A. Seif, A. Boshra, Single-Wall GaN Nanotubes: A Density Functional Theory Study of Ga-69 and N-14 Quadrupole Coupling Constants, Journal of Computational and Theoretical Nanoscience, **6** (2009) 732.
[51] X. Wang, J. Song, P. Li, J.H. Ryou, R.D. Dupuis, C.J. Summers, Z.L. Wang, Growth of uniformly aligned ZnO nanowire heterojunction arrays on GaN, AlN, and Al0. 5Ga0. 5N substrates, Journal of the American Chemical Society, **127** (2005) 7920.
[52] B. Zhang, N. Binh, K. Wakatsuki, Y. Segawa, Y. Yamada, N. Usami, M. Kawasaki, H. Koinuma, Formation of highly aligned ZnO tubes on sapphire (0001) substrates, Applied Physics Letters, **84** (2004) 4098.
[53] M. Yin, Y. Gu, I.L. Kuskovsky, T. Andelman, Y. Zhu, G. Neumark, S. O'Brien, Zinc oxide quantum rods, Journal of the American Chemical Society, **126** (2004) 6206.
[54] J. Lao, J. Huang, D. Wang, Z. Ren, ZnO nanobridges and nanonails, Nano letters, **3** (2003) 235.
[55] K. Govender, D.S. Boyle, P.B. Kenway, P. O'Brien, Understanding the factors that govern the deposition and morphology of thin films of ZnO from aqueous solution, Journal of Materials Chemistry, **14** (2004) 2575.

[56] X.Y. Kong, Y. Ding, R. Yang, Z.L. Wang, Single-crystal nanorings formed by epitaxial self-coiling of polar nanobelts, Science, **303** (2004) 1348.
[57] C.-W. Zhang, F.-b. Zheng, P.-j. Wang, F. Li, P. Li, First-principles study on ferromagnetism in two-dimensional ZnO nanosheet, Chemical Physics Letters, **548** (2012) 60.
[58] F. Li, C. Zhang, M. Zhao, Magnetic and optical properties of Cu-doped ZnO nanosheet: First-principles calculations, Physica E: Low-dimensional Systems and Nanostructures, **53** (2013) 101.
[59] J. Ren, H. Zhang, X. Cheng, Electronic and magnetic properties of all 3d transition-metal-doped ZnO monolayers, International Journal of Quantum Chemistry, **113** (2013) 2243.
[60] G. Qin, X. Wang, J. Zheng, C. Kong, B. Zeng, First-principles investigation of the electronic and magnetic properties of ZnO nanosheet with intrinsic defects, Computational Materials Science, **81** (2014) 259.
[61] Y.-H. Zhang, M.-L. Zhang, Y.-C. Zhou, J.-H. Zhao, S.-M. Fang, F. Li, Tunable electronic and magnetic properties of graphene-like ZnO monolayer upon doping and CO adsorption: a first-principles study, Journal of Materials Chemistry A, **2** (2014) 13129.
[62] S. Datta, G.C. Kaphle, S. Baral, A. Mookerjee, Study of morphology effects on magnetic interactions and band gap variations for 3 d late transition metal bi-doped ZnO nanostructures by hybrid DFT calculations, The Journal of chemical physics, **143** (2015) 084309.
[63] D. Ma, Q. Wang, T. Li, Z. Tang, G. Yang, C. He, Z. Lu, CO catalytic oxidation on Al-doped graphene-like ZnO monolayer sheets: a first-principles study, Journal of Materials Chemistry C, **3** (2015) 9964.
[64] C. Tan, D. Sun, D. Xu, X. Tian, Y. Huang, Tuning electronic structure and optical properties of ZnO monolayer by Cd doping, Ceramics International, **42** (2016) 10997.
[65] C. Supatutkul, S. Pramchu, A.P. Jareonjittichai, Y. Laosiritaworn, First principle study of the conductive type stability in Sn, Li and Li-Ni doped ZnO nanosheet, Ceramics International, **43** (2017) S525.
[66] S.A. Khan, S. Azam, M.B. Kanoun, G. Murtaza, M. Rani, S. Goumri-Said, Tailoring the electronic structure and optical properties of cadmium-doped zinc oxides nanosheet, Cogent Physics, **4** (2017) 1391734.
[67] Z. Luan, D. Sun, C. Tan, X. Tian, Y. Huang, First-principles calculations of electronic structure and optical properties of Be-doped ZnO monolayer, Integrated Ferroelectrics, **179** (2017) 84.
[68] L.H. Thomas, The calculation of atomic fields, in: Mathematical Proceedings of the Cambridge Philosophical Society, Cambridge University Press, 1927, p. 542.

[69] P.A. Cox, Introduction to quantum theory and atomic structure, Oxford University Press, 1996.
[70] D.W. Rogers, Computational Chemistry using the PC, John Wiley & Sons, 2003.
[71] M. Born, R. Oppenheimer, Zur quantentheorie der molekeln, Annalen der physik, **389** (1927) 457.
[72] P. Kiréev, La physique des semiconducteurs, (1975).
[73] D.R. Hartree, The wave mechanics of an atom with a non-Coulomb central field. Part I. Theory and methods, in: Mathematical Proceedings of the Cambridge Philosophical Society, Cambridge University Press, 1928, p. 89.
[74] P. Hohenberg, W. Kohn, Inhomogeneous electron gas, Physical review, **136** (1964) B864.
[75] W. Kohn, L.J. Sham, Self-consistent equations including exchange and correlation effects, Physical review, **140** (1965) A1133.
[76] L. Sham, W. Kohn, One-particle properties of an inhomogeneous interacting electron gas, Physical review, **145** (1966) 561.
[77] W. Yang, P.W. Ayers, Density-functional theory, in: Computational Medicinal Chemistry for Drug Discovery, CRC Press, 2003, p. 103.
[78] K. Burke, J. Werschnik, E. Gross, Time-dependent density functional theory: Past, present, and future, The Journal of chemical physics, **123** (2005) 062206.
[79] W. Kohn, Nobel Lecture: Electronic structure of matter—wave functions and density functionals, Reviews of Modern Physics, **71** (1999) 1253.
[80] R.G. Parr, W. Yang, Density-Functional Theory of Atoms and Molecules, vol. 16 of International series of monographs on chemistry, in, Oxford University Press, New York, 1989.
[81] E. Runge, E.K. Gross, Density-functional theory for time-dependent systems, Physical review letters, **52** (1984) 997.
[82] V. Fock, Näherungsmethode zur Lösung des quantenmechanischen Mehrkörperproblems, Zeitschrift für Physik, **61** (1930) 126-148.
[83] R.M. Martin, Electronic structure: basic theory and practical methods, Cambridge university press, 2004.
[84] J.N. Lalena, D.A. Cleary, Principles of inorganic materials design, John Wiley & Sons, 2010.
[85] D. Sholl, J.A. Steckel, Density functional theory: a practical introduction, John Wiley & Sons, 2011.
[86] J. Toulouse, Introduction to density-functional theory, (2015).
[87] J. Thijssen, Computational physics, Cambridge university press, 2007.

[88] K. Capelle, A bird's-eye view of density-functional theory, Brazilian Journal of Physics, **36** (2006) 1318.
[89] J. Joutsensaari, Aerosol synthesis of nanostructured, ultrafine fullerene particles, Technical Research Centre of Finland, 1999.
[90] J.P. Perdew, A. Zunger, Self-interaction correction to density-functional approximations for many-electron systems, Physical Review B, **23** (1981) 5048.
[91] J.P. Perdew, K. Burke, M. Ernzerhof, Generalized gradient approximation made simple, Physical review letters, **77** (1996) 3865.
[92] J.P. Perdew, J.A. Chevary, S.H. Vosko, K.A. Jackson, M.R. Pederson, D.J. Singh, C. Fiolhais, Atoms, molecules, solids, and surfaces: Applications of the generalized gradient approximation for exchange and correlation, Physical Review B, **46** (1992) 6671.
[93] B. Hammer, L.B. Hansen, J.K. Nørskov, Improved adsorption energetics within density-functional theory using revised Perdew-Burke-Ernzerhof functionals, Physical Review B, **59** (1999) 7413.
[94] Z. Wu, R.E. Cohen, More accurate generalized gradient approximation for solids, Physical Review B, **73** (2006) 235116.
[95] B. Himmetoglu, A. Floris, S. Gironcoli, M. Cococcioni, Hubbard-corrected DFT energy functionals: The LDA+ U description of correlated systems, International Journal of Quantum Chemistry, **114** (2014) 14.
[96] J. Kohanoff, Electronic structure calculations for solids and molecules: theory and computational methods, Cambridge University Press, 2006.
[97] H. Hellmann, A new approximation method in the problem of many electrons, The Journal of chemical physics, **3** (1935) 61.
[98] J.C. Phillips, Energy-band interpolation scheme based on a pseudopotential, Physical review, **112** (1958) 685.
[99] M.L. Cohen, V. Heine, The fitting of pseudopotentials to experimental data and their subsequent application, in: Solid state physics, Elsevier, 1970, p. 37.
[100] M. Yin, M.L. Cohen, Theory of ab initio pseudopotential calculations, Physical Review B, **25** (1982) 7403.
[101] D. Hamann, M. Schlüter, C. Chiang, Norm-conserving pseudopotentials, Physical review letters, **43** (1979) 1494.
[102] M.C. Payne, M.P. Teter, D.C. Allan, T. Arias, a.J. Joannopoulos, Iterative minimization techniques for ab initio total-energy calculations: molecular dynamics and conjugate gradients, Reviews of Modern Physics, **64** (1992) 1045.
[103] J.M. Soler, E. Artacho, J.D. Gale, A. García, J. Junquera, P. Ordejón, D. Sánchez-Portal, The SIESTA method for ab initio order-N

materials simulation, Journal of Physics: Condensed Matter, **14** (2002) 2745.
[104] P. Ordejón, D.A. Drabold, M.P. Grumbach, R.M. Martin, Unconstrained minimization approach for electronic computations that scales linearly with system size, Physical Review B, **48** (1993) 14646.
[105] E. Artacho, D. Sánchez-Portal, P. Ordejón, A. Garcia, J.M. Soler, Linear-scaling ab-initio calculations for large and complex systems, physica status solidi (b), **215** (1999) 809.
[106] N. Troullier, J.L. Martins, Efficient pseudopotentials for plane-wave calculations, Physical Review B, **43** (1991) 1993.
[107] C.D. Sherrill, Introduction to Electronic Structure Theory, (2002).
[108] J.A. Santana, J.T. Krogel, J. Kim, P.R. Kent, F.A. Reboredo, Structural stability and defect energetics of ZnO from diffusion quantum Monte Carlo, The Journal of chemical physics, **142** (2015) 164705.
[109] R. Shankar, K. Senthilkumar, P. Kolandaivel, Calculation of ionization potential and chemical hardness: A comparative study of different methods, International Journal of Quantum Chemistry, **109** (2009) 764.
[110] A.K. Geim, K.S. Novoselov, The rise of graphene, Nature materials, **6** (2007) 183.
[111] J.N. Tiwari, R.N. Tiwari, K.S. Kim, Zero-dimensional, one-dimensional, two-dimensional and three-dimensional nanostructured materials for advanced electrochemical energy devices, Progress in Materials Science, **57** (2012) 724.
[112] M. Topsakal, S. Cahangirov, E. Bekaroglu, S. Ciraci, First-principles study of zinc oxide honeycomb structures, Physical Review B, **80** (2009) 235119.
[113] X. Sun, H.S. Kwok, Optical properties of epitaxially grown zinc oxide films on sapphire by pulsed laser deposition, Journal of Applied Physics, **86** (1999) 408.
[114] G. Wei, W. Qin, L. Ning, R. Kim, G. Wang, D. Zhang, P. Zhu, K. Zheng, L. Wang, Synthesis of ZnO nanosheets by microwave thermal vapor method, Journal of nanoscience and nanotechnology, **10** (2010) 2065.
[115] R. Sahu, H.B. Gholap, G. Mounika, K. Dileep, B. Vishal, S. Ghara, R. Datta, Stable p-type conductivity in B and N co-doped ZnO epitaxial thin film, physica status solidi (b), **253** (2016) 504.
[116] G. Liu, F. Shan, W. Lee, B. Shin, H. Kim, J. Kim, Boron and nitrogen co-doped ZnO thin films for opto-electronic applications, Ceramics International, **34** (2008) 1011.
[117] P. Giannozzi, S. Baroni, N. Bonini, M. Calandra, R. Car, C. Cavazzoni, D. Ceresoli, G.L. Chiarotti, M. Cococcioni, I. Dabo, QUANTUM ESPRESSO: a modular and open-source software project

for quantum simulations of materials, Journal of Physics: Condensed Matter, **21** (2009) 395502.
[118] J. Junquera, Ó. Paz, D. Sánchez-Portal, E. Artacho, Numerical atomic orbitals for linear-scaling calculations, Physical Review B, **64** (2001) 235111.
[119] M. Benali Kanoun, S. Goumri-Said, A. Manchon, U. Schwingenschlögl, Ferromagnetism carried by highly delocalized hybrid states in Sc-doped ZnO thin films, Applied Physics Letters, **100** (2012) 222406.
[120] M. Catti, Y. Noel, R. Dovesi, Full piezoelectric tensors of wurtzite and zinc blende ZnO and ZnS by first-principles calculations, Journal of Physics and Chemistry of Solids, **64** (2003) 2183.
[121] H. Nejatipour, M. Dadsetani, Electronic structures of ZnX (X= O and S) nanosheets from first-principles energy loss near edge structure studies, Journal of Electron Spectroscopy and Related Phenomena, **203** (2015) 14.
[122] M. Usuda, N. Hamada, T. Kotani, M. van Schilfgaarde, All-electron GW calculation based on the LAPW method: Application to wurtzite ZnO, Physical Review B, **66** (2002) 125101.
[123] R.K. Swank, Surface properties of II-VI compounds, Physical review, **153** (1967) 844.
[124] D. Mora-Fonz, J. Buckeridge, A.J. Logsdail, D.O. Scanlon, A.A. Sokol, S. Woodley, C.R.A. Catlow, Morphological Features and Band Bending at Nonpolar Surfaces of ZnO, The Journal of Physical Chemistry C, **119** (2015) 11598.
[125] W. Zhang, T. Li, C. He, X. Wu, L. Duan, H. Li, L. Xu, S. Gong, First-principle study on Ag-2N heavy codoped of p-type graphene-like ZnO nanosheet, Solid State Communications, **204** (2015) 47.
[126] B. Wang, S. Nagase, J. Zhao, G. Wang, The stability and electronic structure of single-walled ZnO nanotubes by density functional theory, Nanotechnology, **18** (2007) 345706.
[127] X. Wang, X. Chen, R. Dong, Y. Huang, W. Lu, Ferromagnetism in carbon-doped ZnO films from first-principle study, Physics Letters A, **373** (2009) 309.
[128] J.C. Rienstra-Kiracofe, G.S. Tschumper, H.F. Schaefer, S. Nandi, G.B. Ellison, Atomic and molecular electron affinities: photoelectron experiments and theoretical computations, Chemical reviews, **102** (2002) 231.
[129] A.D. Becke, A new inhomogeneity parameter in density-functional theory, The Journal of chemical physics, **109** (1998) 2092.
[130] L.C. Allen, E.T. Knight, Electronegativity: why has it been so difficult to define?, Journal of Molecular Structure: THEOCHEM, **261** (1992) 313.

[131] N.L. Hadipour, A. Ahmadi Peyghan, H. Soleymanabadi, Theoretical study on the Al-doped ZnO nanoclusters for CO chemical sensors, The Journal of Physical Chemistry C, **119** (2015) 6398.
[132] M. Houssa, B. van den Broek, E. Scalise, G. Pourtois, V. Afanas' Ev, A. Stesmans, An electric field tunable energy band gap at silicene/(0001) ZnS interfaces, Physical Chemistry Chemical Physics, **15** (2013) 3702.
[133] H.-C. Wu, Y.-C. Peng, T.-P. Shen, Electronic and optical properties of substitutional and interstitial Si-doped ZnO, Materials, **5** (2012) 2088.
[134] X. Jing, N. Troullier, D. Dean, N. Binggeli, J.R. Chelikowsky, K. Wu, Y. Saad, Ab initio molecular-dynamics simulations of Si clusters using the higher-order finite-difference-pseudopotential method, Physical Review B, **50** (1994) 12234.
[135] J. Zhao, X. Chen, Q. Sun, F. Liu, G. Wang, Tight-binding calculation of ionization potentials of small silicon clusters, Physics Letters A, **198** (1995) 243.
[136] K. Fuke, K. Tsukamoto, F. Misaizu, Photoionization of small silicon clusters: ionization potentials for Si 2 to Si 40, Zeitschrift für Physik D Atoms, Molecules and Clusters, **26** (1993) 204.
[137] D.-S. Hao, J.-R. Liu, W.-G. Wu, J.-C. Yang, Study on structures and electron affinities of small potassium–silicon clusters Si n K (n= 2–8) and their anions with Gaussian-3 theory, Theoretical Chemistry Accounts, **124** (2009) 431.

الخلاصة

تصف الرسالة الخواص الهيكلية والإلكترونية لطبقة ZnO النانوية المشوبة بـ B و C و N و Alو Si و P وتم التحقيق فيها عن طريق إجراء حسابات نظرية داله الكثافة. الهدف من هذه الدراسة هو التعرف على تأثيرات الاستبدال من واحد إلى ست ذرات من الأكسجين مع شوائب مختلفة في وحده خلية ZnO المكونة من 84 ذرة مستضيفة مع الأخذ بعين الاعتبار مواقع الشوائب وتأثيراتها على الخصائص الهيكلية والإلكترونية لطبقة ZnO النانوية باستخدام برنامج SIESTA. يمكن السيطرة على الخصائص الإلكترونية بالتأكيد الخطوة الأكثر أهمية في تطوير الأجهزة الإلكترونية عن طريق تناول التشويب. تم تحسين جميع الأنظمة قيد النظر بالكامل. طول الاصرة، وزاوية الرابط، والطاقة الربط لكل ذره ،الكثافة الكلية والجزيئية، الطاقة الكلية، الحالات الإلكترونية، فجوة الطاقة، بعض المتغيرات الإلكترونية (جهد التأين العمودي (VIP) ، الآلفة الإلكترونية العمودية (VAE)، الكهروسلبية (EN) والصلابة (H) قد تم حسابها ومقارنتها مع بعضها البعض. وتبين النتائج أن استبدال ذرات B و P يوسع طول الاصرة فيما يتعلق بالزنك النقي. لذلك، يوضح التحليل لدالة الكثافة أن الاستقرار العالي لطبقة ZnO النانوية يمكن تحقيقه لكل من الشوائب تبعاً لحالة النمو المصممة ونوع الشائبة. إن مركبات ذرات B و Al التي تحل محل ذرات O أكثر استقرارًا من الذرات الأخرى. يختلف كل من HOMO و LUMO اختلافًا طفيفًا، وهذا يشير إلى أنه وفقًا للعدد، نوع والموقع الشائبة في التركيب دورًا مهمًا في الخصائص الإلكترونية وتحسين قدرة القبول بالإلكترونات. وقد وجد أن فجوة الطاقة في طبقة النانوية ZnO تتناقص تدريجياً مع B، C، N، Al، Si و P في الحالات B_2، C_2، N_3، P_3، Al_4 و Si_4 تحتل مواقع O كمركبات لها الفجوات في الطاقة للمواد موصل. بالإضافة إلى الاختلاط القوي للمدارات بين p، C، N و Zn هذه النتائج من المحتمل أن تكون مفيدة للتطبيقات .أوضحت النتائج أن جهد التأين العمودي الآلفة الإلكترونية العمودية لـ B و Al المشوب لها مستوى مانح عندeV 3.3 .من ناحية أخرى ،ان ل N و P لديها مستوى متقبل فيeV 4.0 . في حين زادت الكهروسلبية لـ N و P الشوبة وقلت الصلابة لـ B ، C و Al المشوب الذي يظهر أكثر حيوية مواتية.

جمهورية العراق
وزارة التعليم العالي والبحث العلمي
جامعة كربلاء/كلية العلوم
قسم الفيزياء

دراسة نظرية لخواص التركيب الإلكتروني لطبقة نانوية من اوكسيد الزنك المشوبة

رسالة مقدمة إلى قسم الفيزياء – كلية العلوم – جامعة كربلاء
وهي جزء من متطلبات نيل درجة الماجستير في علوم الفيزياء

من قبل

حنين علي راشد النصراوي
بكالوريوس علوم في الفيزياء جامعة بابل 2016

بإشراف

أ.م.د. نبراس موسى عمران

2019م 1440 هـ